AD-A040 653 STANFORD UNIV CALIF INST FOR PLASMA RESEARCH F/G 3/2
LARGE-SCALE PERIODIC SOLAR VELOCITIES: AN OBSERVATIONAL STUDY.(U)
MAR 77 P H DITTMER N00014-76-C-0207
UNCLASSIFIED SU-IPR-686 NL

1 OF 3
AD
A040653

LARGE-SCALE PERIODIC SOLAR VELOCITIES: AN OBSERVATIONAL STUDY

by

Phil Howard Dittmer

Office of Naval Research
Contract N00014-76-C-0207

National Aeronautics and Space Administration
Grant NGR 05-020-559

National Science Foundation
Grant ATM74-19007
Grant DES75-15664

and

The Max C. Fleischmann Foundation

SUIPR Report No. 686

March 1977

INSTITUTE FOR PLASMA RESEARCH
STANFORD UNIVERSITY, STANFORD, CALIFORNIA

UNCLASSIFIED

SECURITY CLASSIFICATION OF THIS PAGE (When Data Entered)

REPORT DOCUMENTATION PAGE

READ INSTRUCTIONS BEFORE COMPLETING FORM

1. REPORT NUMBER: SUIPR Report No. 686
2. GOVT ACCESSION NO.
3. RECIPIENT'S CATALOG NUMBER
4. TITLE (and Subtitle): Large-Scale Periodic Solar Velocities: An Observational Study
5. TYPE OF REPORT & PERIOD COVERED: Scientific, Technical rept.
6. PERFORMING ORG. REPORT NUMBER
7. AUTHOR(s): Phil Howard Dittmer
8. CONTRACT OR GRANT NUMBER(s): N00014-76-C-0207; NASA-NGR-05-020-559
9. PERFORMING ORGANIZATION NAME AND ADDRESS:
Institute for Plasma Research
Stanford University
Stanford, California 94305
10. PROGRAM ELEMENT, PROJECT, TASK AREA & WORK UNIT NUMBERS
11. CONTROLLING OFFICE NAME AND ADDRESS:
Office of Naval Research
Electronics Program Office
Arlington, Virginia 22217
12. REPORT DATE: March 1977
13. NO. OF PAGES: 211
14. MONITORING AGENCY NAME & ADDRESS (if diff. from Controlling Office): 215p.
15. SECURITY CLASS. (of this report): Unclassified
15a. DECLASSIFICATION/DOWNGRADING SCHEDULE

16. DISTRIBUTION STATEMENT (of this report)

This document has been approved for public release and sale; its distribution is unlimited.

17. DISTRIBUTION STATEMENT (of the abstract entered in Block 20, if different from report)

18. SUPPLEMENTARY NOTES

TECH: OTHER

19. KEY WORDS (Continue on reverse side if necessary and identify by block number)

solar pulsations
five-minute oscillations
large-scale solar velocities

20. ABSTRACT (Continue on reverse side if necessary and identify by block number)

Observations of large-scale solar velocities have been made using the mean field telescope and Babcock magnetograph of the Stanford Solar Observatory. Observations were made in the magnetically insensitive iron line at 5124 Å, with light from the center (limb) of the disk right (left) circularly polarized, so that the magnetograph measures the difference in wavelength between center and limb. Computer calculations are made of the wavelength difference produced by global pulsations for spherical harmonics up to second order. Computations are also made of the signal produced by displacing the solar image relative →

next page

DD FORM 1 JAN 73 1473

EDITION OF 1 NOV 65 IS OBSOLETE

UNCLASSIFIED

SECURITY CLASSIFICATION OF THIS PAGE (When Data Entered)

332 630

19. KEY WORDS (Continued)

20 ABSTRACT (Continued)

cont → to polarizing optics or diffraction grating. Such displacements are the probable source of slow drifts in the observed signal. Individual observations clearly show the five-minute oscillations. From power spectra, the amplitude is 2.0 meters/second, and the period is 312.9 ± 0.9 seconds. The amplitude gives evidence for a horizontal wavelength greater than 20000 kilometers, and the period is larger than reported for smaller apertures. Six months of almost daily observations have been examined for changes in oscillatory power or period that might be associated with large-scale coronal and solar wind structures as identified by solar sector boundaries, the amplitude of the mean magnetic field, or the C9 index. No evidence for large-scale organization of the oscillations has been found.

The average power spectrum has no statistically significant features at periods between seven and seventy minutes. Independent calculations support Hill's claim that the presence of a large portion of the downward propagating solution would give his technique added sensitivity at these periods. However, this explanation is unlikely to explain differences between Hill's observations and those presently reported beacuse (1) radiative damping greatly reduces the downward propagating solution, (2) the observed increase in five-minute amplitude with height is too small, and (3) the observed ratio of five- to ten-minute power is too large. Questions are also raised concerning the statistical significance of the peaks in the power spectra of Hill and Brown.

Using analysis similar to that used in the Crimea, no 160 minute oscillation is observed. Calculations show that the absence of signal cannot be explained by vignetting, different polarization dimensions, incorrect choice of period, or subtraction of a parabolic fit. As a result of a data exchange with the Crimea, it was found that (1) twelve-hour period drifts in the Stanford data can produce a signal at 160 minutes, (2) integer fractions of a day other than 160 minutes are favored in the Crimea data, and (3) editing can produce a 160 minute signal in the Stanford data, though it is of small amplitude and present only in the final one-third of the data.

LARGE-SCALE PERIODIC SOLAR VELOCITIES: AN OBSERVATIONAL STUDY

by

Phil Howard Dittmer

Office of Naval Research
Contract N00014-76-C-0207

National Aeronautics and Space Administration
Grant NGR 05-020-559

National Science Foundation
Grant ATM74-19007
Grant DES75-15664

and

The Max C. Fleischmann Foundation

SUIPR Report No. 686

March 1977

Institute for Plasma Research
Stanford University
Stanford, California

Ph.D. Dissertation
March 1977

ACKNOWLEDGMENTS

The author would first like to thank those most responsible for the length and breadth of this study. His adviser, John M. Wilcox, first directed his interest to the area of periodic solar velocities. He made available financial support and the use of telescope and computer facilities which enabled this study to be undertaken. His careful and thorough approach to research has extended the time and effort required to obtain the results obtained herein, but with greater confidence therefore justified in these results. This study could not have been conducted without the velocity subtraction technique developed by Valeri A. Kotov. He and A. B. Severny are also thanked for exchanging data and for causing this investigation to be extended to the two-hour forty-minute range. The work of Henry A. Hill and collaborators has led to a much more thorough investigation of oscillations at periods from five to seventy minutes than would otherwise have been undertaken. Financial support for this investigation has been provided by the Office of Naval Research through Contract N00014-76-C-0207, by the National Aeronautics and Space Administration through Grant NGR 05-020-559, by the National Science Foundation through Grant ATM74-19007 and Grant DES75-15664, and by the Max C. Fleishman Foundation.

Appreciation should next be expressed to those who aided in the accomplishment of this study. The assistance of Philip H. Scherrer has been conspicuous at all stages of this investigation, from putting the

telescope into operation and keeping it operating to data analysis and interpretation. He read the entire manuscript and gave many helpful suggestions, especially on the second chapter. John M. Wilcox, A. B. C. Walker, Jr., and Peter A. Sturrock are also thanked as readers of the dissertation. Eric K. Gustafson, assisted by Steven D. Bryan, performed most of the actual observations. Thomas L. Duvall, Jr. helped improve operation of the telescope, and he, Eric Fossat, Robert Howard, and Leif Svalgaard provided helpful discussions. George A. Kotler helped prepare optics and Gerard H. Dewerk helped machine mounts for the polarizing aperture. Marguerite F. Dearborn did an excellent job of typing the final manuscript.

Last, but not least, the author wishes to thank those whose contributions were more personal than scientific. He thanks his wife and sweetheart, Janet, for her constant love, her insistent encouragement, and her efforts which succeeded in making the author's residence a home. She also did an excellent job of proof-reading the second and final drafts of the manuscript. The author thanks his parents for love and support, for planting the seed of this project in his initials, and for encouraging attitudes toward education and work which enabled the seed to bear fruit. He also thanks his boys, Andrew and Peter, for being ever loyal but totally unimpressed with this accomplishment.

TABLE OF CONTENTS

ABSTRACT

Observations of large-scale solar velocities have been made using the mean field telescope and Babcock magnetograph of the Stanford Solar Observatory. Observations were made in the magnetically insensitive iron line at 5124 Angstroms, with light from the center (limb) of the disk right (left) circularly polarized, so that the magnetograph measures the difference in wavelength between center and limb. Computer calculations are made of the wavelength difference produced by global pulsations for spherical harmonics up to second order. Computations are also made of the signal produced by displacing the solar image relative to polarizing optics or diffraction grating. Such displacements are the probable source of slow drifts in the observed signal.

Individual observations clearly show the five-minute oscillations. From power spectra, the amplitude is 2.0 meters/second, and the period is 312.9 $\pm$ 0.9 seconds. The amplitude gives evidence for a horizontal wavelength greater than 20000 kilometers, and the period is larger than reported for smaller apertures. Six months of almost daily observations have been examined for changes in oscillatory power or period that might be associated with large-scale coronal and solar wind structures as identified by solar sector boundaries, the amplitude of the mean magnetic field, or the C9 index. No evidence for large-scale organization of the oscillations has been found.

The average power spectrum has no statistically significant features at periods between seven and seventy minutes. Independent calculations support Hill's claim that the presence of a large portion of the downward propagating solution would give his technique added sensitivity at these periods. However, this explanation is unlikely to explain differences between Hill's observations and those presently reported because (1) radiative damping greatly reduces the downward propagating solution, (2) the observed increase in five-minute amplitude with height is too small, and (3) the observed ratio of five- to ten-minute power is too large. Questions are also raised concerning the statistical significance of the peaks in the power spectra of Hill and Brown.

Using analysis similar to that used in the Crimea, no 160 minute oscillation is observed. Calculations show that the absence of signal cannot be explained by vignetting, different polarizer dimensions, incorrect choice of period, or subtraction of a parabolic fit. As a result of a data exchange with the Crimea, it was found that (1) twelve-hour period drifts in the Stanford data can produce a signal at 160 minutes, (2) integer fractions of a day other than 160 minutes are favored in the Crimean data, and (3) editing can produce a 160 minute signal in the Stanford data, though it is of small amplitude and present only in the final one-third of the data.

CHAPTER I

INTRODUCTION AND HISTORICAL BACKGROUND

> And God said, Let there be lights in the firmament of the heaven to divide the day from the night; and let them be for signs, and for seasons, and for days, and years; and let them be for lights in the firmament of the heaven to give light upon the earth: and it was so. And God made two great lights; the greater light to rule the day, and the lesser light to rule the night: he made the stars also. And God set them in the firmament of the heaven to give light upon the earth, and to rule over the night, and to divide the light from the darkness: and God saw that it was good. Genesis 1:14-18.

Even in today's world of diverse and contending philosophies and ideologies, most men would agree with the statement in Genesis that the sun is good. Not only is it the ultimate source of terrestrial light and energy, but also in its apparent motion across the sky it divides day from night and separates the year into seasons. It is widely agreed today that this motion is an illusion produced by the earth's rotation and the inclination of its axis of rotation relative to the ecliptic. However, developments in astronomy have improved the sensitivity of observations to such an extent that the question of the nature and magnitude of the sun's motions has become one of considerable current interest and of some disagreement. This dissertation will not attempt to answer all questions related to the sun's motions, but only to contribute a few observational results to the discussion.

The first change in man's ideas of the sun's motion was part of the Copernican revolution in astronomy, which replaced the idea of the sun as part of a rotating universe with that of the earth as part of a

heliocentric solar system. It is interesting to notice that this conclusion was more the result of careful observation and analysis than the result of any technological breakthrough, and that it was the result of the study of the other planets rather than of the sun itself. Even while the rotating earth explanation of the sun's transit across the sky was still a matter of controversy, the development of telescopes made possible the systematic observation and study of sunspots, enabling Galileo in 1610 to deduce that the sun has a rotation of its own. Christoph Scheiner, one of Galileo's contemporaries, measured a different rotation rate for sunspots at different solar latitudes, but the sun's differential rotation was not widely known until the careful observations of Carrington were made in 1853-1861. Fraunhofer's discovery of absorption lines in the sun's spectrum added a valuable tool to astronomers, which enabled Vogel to confirm solar rotation from the Doppler shift of spectral lines in 1871 (Meadows, 1970, p. 28). Further work by Dúner and later by Halm showed that the differential rotation of the photosphere measured by spectral techniques was substantially the same as inferred from sunspot motions. The accumulation of extensive spectral observations of solar rotation led Halm (1922) to believe that there were significant variations in the rotation rate on the time scale of a solar cycle, while J. S. Plaskett (1915) concluded that yearly averages of rotation were essentially constant but that there existed significant variations on a much shorter time scale indicative of local movements or eddy currents of a transitory character. Rotational variations and large-scale horizontal motions have recently been given new attention, in part due to the extensive observations at the Mount Wilson Observatory

(Howard and Harvèy, 1970; Howard, 1971) and partly because of current theories relating large-scale horizontal motions to differential rotation (Starr and Gilman, 1965; Busse, 1970; Durney, 1970; Yoshimura and Kato, 1971), to large scale organization of solar activity (Bumba, 1970), and the sun's magnetic sector structure (Yoshimura, 1971; Wolff, 1974a and b); and by the fact that differential rotation is the energy source in the popular Babcock-Leighton model of the solar cycle (Babcock, 1961; Leighton, 1964) and recent investigations (Eddy, 1976) indicate that changes in the differential rotation may be related to very long-term variation in solar activity. The present work is concerned principally with radial rather than horizontal motions, but it is important to remember that these may be hard to separate, especially when spectral techniques are employed to measure velocities on a spherical sun.

The existence of solar radial motions was first revealed through progress in the observation and interpretation of solar granulation, which is well recounted by Bray and Loughhead (1967). Sir William Herschel first noticed "corrugations" in the solar surface in 1801. This discovery was not pursued until the early 1860's when Nasmyth and Huggins established the existence of small bright grains separated by dark lanes, which were named "granules" by Dawes. In 1877 the French astronomer Pierre Jules Janssen announced that he had successfully photographed granulation. A convective origin for granulation was first suggested by Unsöld in 1930, and Plaskett in 1936 recognized the similarity to cellular convection in thin liquid films as studied in the laboratory by Bénard. Confirmation of the radial velocities expected for cellular convection was made by Richardson in 1949 from high resolution spectra made possible by the

improved gratings of H. D. Babcock at Mt. Wilson. The cellular character was, however, made uncertain by an unexpectedly low correlation between velocity and brightness. Stuart and Rush explained this discrepancy by recognizing the existence of large-scale velocity fluctuations uncorrelated with brightness. Though this explanation proved correct, there remained sufficient controversy to launch Project Stratoscope by which Richardson and Schwarzschild obtained granulation photographs of unsurpassed resolution from a balloon at 80,000 feet (24.4 km). These photographs as well as those of Leighton at Mt. Wilson confirmed that granules were convective cells rather than turbulent eddies.

In order to further understand the velocity fields associated with convection, Leighton and co-workers (Leighton et al., 1962) devised ingenious photographic techniques which exposed two solar velocity fields which previously had been little noticed, and by so doing, opened up a new era in the study of motions on the sun. One velocity feature was observed especially toward the limb and therefore primarily horizontal. Large cells of $\sim$ 30,000 km in diameter were recognized with the velocity pattern one of radial outflow from the center of the cell at a velocity of about 0.5 km/s. A periodic horizontal velocity pattern had previously been recognized by Hart (1954, 1956), but it was Leighton's work which established its extent and cellular character and which gave the phenomenon the name of supergranulation. Further investigation (Simon and Leighton, 1964) showed that the intercellular regions corresponded to stronger magnetic fields, to downflows seen in the H_α line, and to the chromospheric network as measured by enhanced emission in the Ca-K line. Tanenbaum et al., (1969) found evidence that the downflows persisted down to photospheric levels.

Five-Minute Oscillations

The other velocity field recognized was of smaller scale and especially distinguished by a temporal periodicity of five minutes. H. H. Plaskett (1954) had already concluded that the limited correlation between granular brightness and velocities could be explained by the existence of a large-scale oscillatory velocity field, but did not measure the period. This period, by which the five-minute oscillations are known, has made them a favorite of observers since the existence of such a resonant period makes possible or tempting the identification of a solar origin for a signal even when signal-to-noise conditions may be poor. It has also been a challenge for theorists who have been able to devise a surprising variety of physical models which might produce such a periodicity. Fortunately, these models vary in other predictions, especially related to spatial scale size and vertical distribution of power, which greatly limit the ability of all but a few to match all of the details of the extensive observations. The different observational techniques that have been used to study the five-minute oscillations will now be discussed, followed by a description of the observational details which have been assembled and the different theories proposed to match these details.

Observational Techniques

The technique employed by Leighton has previously been mentioned. A solar image was formed by the 150 foot tower telescope in the usual manner, but instead of allowing light from this image to pass directly through the spectrograph entrance slit, a beam splitter and reflecting

optics were used to replace the light which would normally pass through half of the slit with a duplicate of the light passing through the other half of the slit. Glass plates tilted in opposite directions before the exit slit gave the two pieces of spectrum formed from the identical positions on the sun shifts in wavelength in the opposite directions. The exit slit was positioned on an absorption line so that with the tilt of the glass plates, light from the opposite wings of the absorption line would pass through the slit onto photographic film. The image was scanned past the entrance slit and the film simultaneously scanned past the exit slit so that two spectroheliograms were produced of the same portion of the disk in wavelengths corresponding to the line wings. These two plates were subtracted photographically so that intensity fluctuations would cancel, but since Doppler shifts of the absorption line would change the intensity on the two wings in the opposite direction, these differences were enhanced by subtraction. The result was a map of the sun with velocity toward or away from the observer recorded as bright or dark places on film. To obtain information about changes in the velocity field with time, a scan was made in one direction, the film changed, and the scan repeated in the opposite direction. The two velocity maps were then subtracted and the result was a map of velocity change as a function of time. This enabled the discovery of the five-minute periodicity since it was found that the velocity difference was large after two and one-half minutes and small after five.

This technique has the advantage of producing a detailed two-dimensional velocity map which immediately made clear the cellular nature of supergranulation. It also had several disadvantages which have limited

its use in the study of five-minute oscillations since then. The photographic subtraction itself (three subtractions in the case of the Doppler difference plate) was difficult and time consuming, especially because of the necessity of closely aligning plates before subtraction. Calibration of velocity amplitude in terms of film exposure was also difficult, and information about the time development of an oscillation was very limited. Video techniques have now been developed which greatly simplify the subtraction procedure (Fister and Hill, 1971) and the addition or subtraction of "Dopplergrams" separated by half an oscillatory period has been used (Sheeley and Bhatnagar, 1971a and b; Lynch and Chapman, 1975) to separate five-minute oscillations from lower frequency velocity changes due to granulation.

A second technique to study velocity fields is the use of spectrograms, which had been used by Plaskett (1954) to discover a large-scale oscillatory field before the better known finding of Leighton. Spectra are limited to one spatial dimension, but also can sample a wider range of the spectrum than the spectroheliogram. This enabled Evans and collaborators (Evans and Michard, 1962a and b; Evans, Michard, and Servajean, 1963 and 1965) at the Sacramento Peak Observatory to study velocities over an extended vertical range in the atmosphere by using lines formed at different heights, and at the same time to record changes in continuum intensity. The Ca-K line has been especially useful (Jensen and Orrall, 1963; Orrall, 1966; Cha and Orrall, 1966; Liu, 1974) since different wavelengths are formed over a wide vertical range in the upper photosphere and lower chromosphere and there is a weaker line (FeIλ3931.122) formed in the wing which allows simultaneous measurement of velocity lower in

the photosphere. The temporal resolution which Plaskett lacked was obtained by taking spectra repeatedly at regular intervals and at the same position on the disk. Besides the limitation to one spatial dimension, this technique has been limited by difficulties in precise measurement of line shifts, though these have been largely overcome by the development of special equipment for this purpose (e.g., Evans, 1963).

A third device widely used to measure velocities has been the solar magnetograph (Howard, 1962; Deubner, 1967; Severny, 1967; Tanenbaum et al., 1969). As in the Leighton method, exit slits are positioned to pass the light from the wings of an absorption line, though the intensity is measured by photomultipliers rather than on film. In order to measure magnetic as well as velocity fields, the difference in intensity is not itself recorded but instead is nulled by a servo mechanism to keep the slits on the line wings. The position of the device which aligns slit and line then gives a measure of the wavelength of the line. This technique has the advantage of easy calibration and of producing data in digital form. It is limited in spatial resolution by the size of the entrance aperture. It is often used in scanning mode to measure velocities over an extended portion of the disk, but the extent is limited by the need for finite exposure time at each scan position and the need for temporal resolution much less than the five-minute period.

A fourth technique involves the use of an atomic beam (Roddier, 1965, 1966, and 1967; Gonczi and Roddier, 1969) or a heated vapor cell (Fossat and Roddier, 1971; Snider et al., 1974) which utilize resonant scattering of sunlight by atoms to select solar photons of the desired wavelength. If a magnetic field is applied, Zeeman splitting causes

the light to be scattered from the wings of the absorption line, which can be distinguished since light scattered from opposite wings will be of opposite circular polarization. This technique has the advantages of great sensitivity, of an absolute wavelength reference, and of not needing a spectrograph with its instabilities due to atmospheric variations or turbulence. It has the disadvantage of being limited to the lines of elements for which cells or beams are available (alkali metals have usually been used in the past) and to magnetically sensitive lines. Its great sensitivity has made it an especially useful technique for observing oscillations with large apertures for which amplitudes are very small.

Observed Characteristics

The first detail of the observations to be considered is the period. Although Leighton's technique enables measurement of the period only by visual estimation of the point of minimum contrast on velocity difference plates, he used many observations and independent determinations to reduce errors and measured a period of 296.1 $\pm$ 1.3 sec for the low-lying Caλ6103 line (Noyes and Leighton, 1963). Spectrograms (Evans et al., 1963), magnetographs (Howard, 1962), and resonant scattering devices (Roddier, 1967; Fossat and Ricort, 1975a) have all confirmed this result with rare exceptions (Mel'nikov et al., 1973). Evans and Michard (1962b), using spectrograms, estimated the dispersion of periods to be less than 15% of the mean, indicating a strong resonance. Evans, Michard, and Servajean (1963) found a shorter period by measuring individual wave trains (250 sec) than from power spectra (295 sec) and suggested the difference might be due to the largest amplitude oscillations having a shorter period, but later observers (Orrall, 1965; Howard, 1967) have not confirmed such a relationship.

Variations in period for different heights in the atmosphere were recognized early by Evans and Michard (1962b) and by Noyes and Leighton (1963), who reported a decrease in period from 296.1 $\pm$ 1.3 sec at the height of Caλ6103 to 285 $\pm$ 1.5 sec for Naλ5896. The range of height sampled has been extended, especially using intensity fluctuations in the calcium-K line (CaIIλ3933) (Jensen and Orrall, 1963; Noyes and Leighton, 1963; Liu, 1974), and the period is observed to drop to 180 sec at the height of formation of the K_3 core. As higher frequency power increases with height, the resonant peak is broadened and the periodicity becomes less marked (see also Evans and Michard, 1962b; Evans et al., 1963; Noyes, 1967).

A complication in the picture of a single resonant period was suggested by Frazier (1966, 1968a and b) who found distinct 265 sec and 345 sec peaks in power spectra made from spectrograms. His observations indicated that the decrease in period with height was due to an increase in amplitude of the shorter period (265 sec) peak relative to the longer zone. A different multi-peak character with a central peak and two smaller sidelobes has been reported by Gonczi and Roddier (1969) and Snider et al. (1974) from resonant scattering devices, which they suggest might be the signature of modulated wave trains. Modulation or interference of wave trains was further suggested by phase shifts near π observed by Musman and Rust (1970) and by observations with high spatial resolution performed by Reif and Musman (1971). Observations using longer time periods and larger apertures have not shown such a multipeaked structure. A careful study of the waveform from an information theory viewpoint (White and Cha, 1973; Cha and White, 1973) identifies the oscillation as a

narrow-band Gaussian random process and gives convincing argument that the multiple peaks reported are not statistically significant. The report of Frazier has nevertheless been very important in terms of encouragement given theorists seeking a modal description of the oscillation.

Power spectra have also been used as one of many methods of estimating a lifetime for the oscillations. White and Cha (1973) measure a bandwidth of 0.9 mHz about a peak of 3.4 mHz giving a lifetime of ~ 20 min, which compares well with a 23 min value obtained from examining individual bursts. This agrees well with the results obtained by Deubner (1967), Gonczi and Roddier (1969), and Bhattacharyya (1972) who estimate burst lengths from magnetographs, a resonance cell, and spectrograms respectively. The latter observer also reported shorter bursts (14.2 min) for chromospheric than for photospheric lines (31.4 min), consistent with the broadening of the resonance mentioned above. Howard et al. (1968) report a shorter lifetime of 630 ± 120 sec from the autocorrelation matrix created from a magnetograph observation, but the apparent factor of two disagreement may be easily resolved since oscillatory bursts have been shown to have a symmetrical rise and fall in time (Deubner, 1967; Tanenbaum, 1971). A greater discrepancy in lifetime arises if estimates using photographic subtraction are included--Leighton et al. (1962) give a lifetime $\tau \sim 380$ sec, and Sheeley and Bhatnager (1971a) report that oscillatory features usually last ≤ 2 cycles. Such short lifetimes seem unlikely, especially in view of the examples of very long phase coherence (up to 100 min) reported by other observers (Howard et al., 1968).

The horizontal scale of the oscillatory velocity field has been the object of much wider disagreement than the period. Leighton et al. (1962)

reported a scale size of 1700 km (or about 2".5 since 1" = 725.3 km) for lower lines increasing to 3500 km for lines formed higher. Evans and Michard (1962b) obtained a somewhat larger value (2000-3000 km) from spectrograms, though Frazier (1968b) estimated a wavelength of about 5000 km from the same method. Magnetograph measurements have generally given values in the 5"-10" range as at first estimated by Howard (1967) and later measured by Deubner (6".6, 1967; 7"-8", 1969; 10".5, Deubner and Hayashi, 1973; 9"-15", 1974) and Howard et al. (7700 ± 2300 km, 1968). Photographic separation of oscillatory and slowly varying components has given estimates of 3000 km (Sheeley and Bhatnager, 1971a) or 6".9 ± 2".1 (Lynch and Chapman, 1975) from a more sophisticated fit to a random spatial signal. Thomas (1972) has suggested that the larger spatial scales indicated by recent measurements are due to smaller elements being blurred by seeing, an effect demonstrated by computer simulation. In contrast, Wolff (1973) has argued that the smaller scales seen by Leighton and by Sheeley and Bhatnagar are due to incomplete removal of granular velocity fields which are known to be of smaller spatial extent. This suggestion is supported by the increase of scale size measured for higher lines (Leighton et al., 1962) and in magnetic regions (Sheeley and Bhatnagar, 1971a) since granulation is less important in both cases.

Observational evidence for a larger scale size has also been reported. Deubner (1972b) and Musman and Rust (1970) have reported a much larger coherence length (20" for Deubner, 46000 km for Musman and Rust) for phase than for amplitude, though Deubner and Hayashi (1973) argue that this is due to the high-phase stability and random alignment of independent regions. There have also been reports of phase coherence up to

100" (Musman and Rust, 1970) and of well-defined oscillations for an aperture 25" in diameter (Gonczi and Roddier, 1969). Tanenbaum et al. (1969) have shown that such a result is to be expected for cells oscillating independently at the same period but at random phases. They show that the amplitude should be proportional to $(\text{area})^{-1/2}$ or $(d)^{-1}$ where d is the diameter of a circular aperture or length of a square aperture. This relation is confirmed and a cell size of 3000 km deduced by simulating large apertures from one-dimensional magnetrograph scans. Snider et al. (1974) use a resonance cell and obtain agreement with amplitude $\propto (\text{area})^{-0.86}$ and cell size < 8". From similar resonance techniques, Fossat and Ricort (1973) reported amplitude $\propto (\text{area})^{-0.71}$ in disagreement with Tanenbaum et al. Later work (Fossat and Ricort, 1975a) with much more extensive observations showed better agreement with the amplitude $\propto (\text{area})^{-1}$ relation if larger apertures were used, and a cell size of about 20000 km. Fossat further argues (Fossat, 1975) that this value for the wavelength is in agreement with the coherence length of $\sim$ 5000 km reported by earlier observers because of different mathematical definitions of the characteristic horizontal scale. The wavelength he obtains is much longer than that estimated by Tanenbaum et al., and would seem to confirm the report of substantial oscillatory power found for $\lambda \sim 30"$ to 60" by Deubner (1972a).

One weakness in the use of statistical arguments from large apertures to determine the spatial wavelength is that these arguments are based on independent cells, which are not observed. Deubner (1969, 1971) has reported that zero lines in the velocity move irregularly within a fraction of a period and do not return to the original position after

one period, which shows that well-defined cells do not exist. Another possible weakness in the statistical argument would be the existence of large regions where oscillations are not present. Observations are in agreement that this is not the case--oscillations are usually present (Deubner, 1969) even at the level of the K_3 core (Liu, 1974), though the percentage of area with oscillations present drops as the threshold used to define an oscillating region is increased (Howard et al., 1968; Bhattacharyya, 1972).

There has also been some scatter in values reported for the amplitude of the oscillations, but this is largely explained by the use of different observing apertures and different definitions, since a sinusoid has a peak-to-peak amplitude a factor of $2\sqrt{2} = 2.8$ times larger than its rms amplitude. Any differences have also been much less closely watched than differences in horizontal scale since the latter have been used to distinguish between different models, as will be explained below. Some difference in measured amplitudes are of physical interest. For example, the amplitude increases monotonically with height in the atmosphere, from 0.25 km/s near the continuum to 0.4 - 0.6 km/s for the upper photosphere where medium-strength Fraunhofer lines are formed, to 1.6 km/s at the height of formation of H_α (Noyes, 1967). Some increase in amplitude is expected from energy conservation since the density drops off rapidly, and details of the vertical amplitude dependence and extent of penetration help to distinguish between different models and to determine the amount of energy transported or dissipated. Observers have generally agreed (Evans and Michard, 1962b; Howard, 1967) that the amplitude decreases toward the limb in a manner consistent with vertical motion.

(For an exception, see Gopasyuk and Tsap (1973), who claim a significant horizontal component from a questionable definition of oscillatory power.)

A reduced amplitude in plage areas was noticed by Leighton et al. (1962) and estimated by Howard (1967) to be a decrease of about 25%. Howard et al. (1968) reported a strong decrease in the amplitude of oscillations over penumbrae and their absence over umbrae of spots. Other observers using other lines have found oscillations in umbral photospheres at 310-448 sec (Bhatnagar et al., 1972) and chromospheres, especially near 180 sec (Bhatnagar and Tanaka, 1972; Beckers and Schultz, 1972). Umbral flashes (Beckers and Tallant, 1969) repeating every ~ 145 sec and penumbral waves (Moore and Tang, 1975) may also be related to the resonant oscillations in a sunspot region, and it has even been suggested (Glencross and Craig, 1972; Mullan, 1973) that oscillations could be a trigger or energy source for flares. Reports of different periods in plage regions have also been made (Orrall, 1965) and not confirmed (Howard, 1967), and a report (Sheeley and Bhatnagar, 1971a) of an increase in cell size by a factor of three in magnetic regions was previously mentioned. However, attempts to detect a change in character of the photospheric oscillations due to magnetic fields at supergranule boundaries has proven unsuccessful (Tanenbaum, 1971). Some interaction of oscillations with magnetic fields even in quite regions is suggested by the observation of oscillations in the magnetic field by Severny (1967) and Tanenbaum et al. (1971), though the former report was at a period of nine minutes and could not easily be the result of coupling with five-minute velocity oscillations.

In addition to the decrease in period and increase of amplitude with height, much observational information has been gathered regarding the vertical range and propagation of the oscillations. Though granulation becomes increasingly predominant deeper in the photosphere, the five-minute oscillation has been recognized in the deepest photospheric lines (Evans et al., 1965; Deubner, 1971) and even in continuum intensity fluctuations (Edmonds, 1966; Frazier, 1968a; Mehltretter, 1971; Tanenbaum et al., 1969).

Attempts to extend the observations of oscillations radially outward from the photosphere have involved observations at wavelengths longer or shorter than the visible and results from different techniques have not yet established a clear and consistent picture. Noyes and Hall (1972) report 7% amplitude fluctuations in the line core of a CO line k = 4142.7 cm^{-1} (λ = 4.667 μ) found near the temperature minimum, which they calculate correspond to peak-to-peak oscillations of 225°K in temperature or 1.3 km/s in velocity. Simon and Shimabukuro (1971) report 180 sec oscillations at 3.3 mm and 3.5 mm due to free-free emission above the temperature minimum. Yudin (1968) and Durasova et al. (1971) report peaks at 280 sec and 400 sec from power spectra of 3.3 cm observations. Sentman and Shawhan (1974) took 285 hours of data at λ = 2 cm and found no significant peaks. In addition, they claim an upper limit well below the observation of Noyes and Hall, and question the statistical significance of the results of Simon and Shimabukuro. A negative result is also obtained by Shuter and McCutcheon (1973) from observations at λ = 9.6 mm, along with argument for a possible atmospheric origin of the Yudin result. Longer periods reported from radio observations will be discussed below.

Observations at shorter than visible wavelengths have only begun to realize their potential for determining the vertical range of oscillations. Jones and Rense (1970) matched high resolution profiles of the OI triplet at 1302-1306 Å from rocket spectrograms to a model indicating rms velocities of V_{rms} = 7 km/s. The first claimed observation of a periodicity near 300 sec was the result of Chapman et al., in which three EUV lines measured from OSO-7 all had a peak in the power spectrum at 262 $\pm$ 25 sec. Sentman and Shawhan (1974) questioned the statistical significance of these peaks, and Huber et al. (1973) failed to confirm them, though perhaps in part due to lower resolution (35" x 35" versus 10" x 20" for Chapman et al.). Recent observations from OSO-8 have shown oscillations in velocity ($\pm$ 2 km/s) and intensity (present perhaps 50% of the time) for the upper chromospheric line CIIλ1336 (Chipman et al., 1976) though only rarely visible in the transition zone (Bruner et al., 1976). At higher frequencies, 90 sec and 35 sec periods also seem to be favored (Athay et al., 1976). Semi-periodic fluctuations have also been reported in the corona (Billings, 1959; Noxon, 1966), and the interplanetary magnetic field (Ness et al., 1966), and a possible solar origin has even been mentioned for semi-periodic structure observed in cosmic ray fluctuations at the earth (Dhanju and Sarabhai, 1970) and in the terrestrial atmospheric spectrum at 8 cm^{-1} (Baluteau et al., 1973). Such connections have been challenged stiffly (Gebbie et al., 1974), and are far from being well established.

Propagation of the oscillations through the upper photosphere has been readily accessible for examination by comparative studies of absorption lines formed there. Since Leighton's photographic subtraction

technique did not permit simultaneous velocity measurements in two different lines, early comparative work was done by Evans and co-workers from Sacramento Peak Observatory spectrograms (Evans and Michard, 1962b; Evans et al., 1962, 1963, and 1965). They found small but measurable lags between the low-lying Tiλ5173.75 line and the higher Mgλ5172.70 (b_2) line. It was also found that somewhat longer lags, perhaps indicative of progressive rather than standing waves, could be found for larger wave trains, early in a wave burst, and at slightly higher frequencies. The vertical range of studies has been extended using the Ca-K line and the weak iron line (FeIλ3931.122) in its wing (Jensen and Orrall, 1963; Cha and Orrall, 1973) and lags of $\leq$ 30 sec have been found for a 700 km separation. This gives a phase velocity well above the $\sim$ 7 km/s sound velocity, indicating evanescent waves. Even higher phase velocities near 100 km/s have been reported (Musman and Rust, 1970; Canfield and Musman, 1973) from comparisons of photospheric lines.

Possible horizontal propagation of the oscillations was first suggested (Mein, 1965) by an asymmetry in the two-dimensional power spectrum, which identifies periodicities in the spatial as well as the temporal domains. Observations further suggesting horizontal propagation include hyperbolic patterns suggesting an expanding radial front intersecting a slit (Musman and Rust, 1970), a phase difference in oscillatory bursts observed at adjacent points (Howard et al., 1968), and the visual impression from movies made from H_α wing filtergrams (Sawyer, 1974). However, Lynch (1975) has challenged the interpretation of the two-dimensional power spectrum as indicative of horizontal propagation, Deubner (1975) has argued that the apparent horizontal propagation is consistent with

random phase changes, and Deubner and Hayashi (1973) did not confirm the hyperbolic patterns of Musman and Rust in an experiment designed to do so. The existence of appreciable horizontal propagation is therefore left in doubt.

Oscillatory intensity fluctuations have also been studied for clues regarding the character of the waves. Maximum intensity corresponds to maximum temperature which occurs at maximum compression, which corresponds to the time of maximum upward velocity for progressive waves and 90° earlier for standing waves. If the radiative relaxation time is shorter than the compression time (period/ 2π), the maximum temperature will be advanced in phase compared with the maximum compression. Observers have found the maximum brightness leads the maximum upward velocity by approximately 90° (120°, Frazier, 1968a; 120°, Holweger and Testerman, 1975; 93.5°, Sivaraman, 1973; 10[illegible] to 135°, Cha and Orrall, 1973), which would indicate waves of a primarily standing character. Tanenbaum et al. (1969), however, record a value less than 90° for lower lines which they believe requires a progressive wave nature in view of the substantial effect of a short radiative relaxation time at these levels. A clear distinction between standing and progressive waves cannot be made since observations agree that some energy in the wave travels upward and some energy is lost. Attempts to determine the flux of energy delivered higher into the atmosphere (e.g. Canfield and Musman, 1973) are especially significant as a test of the importance of five-minute oscillations in heating the chromosphere and/or corona. It should also be mentioned that broad contribution functions make the determination of phase velocities from phase lags between lines somewhat hazardous (Athay, 1976, pp. 29-30).

The interpretation of intensity oscillations is complicated by differences in model atmospheres or thermodynamics which lead to widely varying estimates of the temperature fluctuations involved. Hudson and Lindsey (1974) calculate $\Delta T_{rms} \sim 3°K$ at $\tau_{5000} = 3.5 \times 10^{-2}$ using the infrared continuum at 22 μ, Holweger and Testerman (1975) calculate $\Delta T_{rms} \sim 20°K$ at $\tau_{5000} = 10^{-2}$ from changes in line optical depths, and Noyes and Hall (1972) obtain $\Delta T_{pk\text{-}to\text{-}pk} = 225°K$ ($\sim 80°K$ rms) at the temperature minimum from intensity fluctuations in the core of a CO line (2142.7 cm^{-1}). This range in values is in the right direction but much too large to be explained by longer radiative relaxation times--theoretical and experimental uncertainties clearly remain.

Theories

The five-minute resonance in the solar atmosphere was not anticipated by theory, but several models have been proposed since its discovery. These models may be described by the answers given to three questions about the oscillations: 1) what type of waves are involved, 2) how are the waves generated, and 3) how is the resonant period selected.

Before considering the models and comparing them with the observations, the types of waves present in a gravitationally stratified atmosphere will be described. The linearized equations of motion, state, and mass conservation for a plane, isothermal atmosphere in the presence of a constant gravitational field are: (taken from Hines, 1960; see also Whitaker, 1963, and Worrall, 1972)

$$\rho_o \frac{\partial \underline{u}}{\partial t} = \rho \underline{g} - \underline{\nabla} P$$

$$\frac{\partial P}{\partial t} + \underline{u} \cdot \underline{\nabla} P_o = c^2 \left(\frac{\partial \rho}{\partial t} + \underline{u} \cdot \underline{\nabla} \rho_o \right)$$

$$\frac{\partial \rho}{\partial t} + \underline{u} \cdot \underline{\nabla} \rho_o + \rho_o \underline{\nabla} \cdot \underline{u} = 0$$

where ρ is the perturbed and ρ_o the unperturbed density, P is the perturbed and P_o the unperturbed atmospheric pressure, $\underline{u}$ is the perturbation velocity, $\underline{g} = -g\,\hat{z}$ is the acceleration of gravity, and c is the unperturbed sound velocity ($c^2 = \gamma P_o/\rho_o$). Viscous effects, radiative damping, and magnetic fields are neglected. For an unperturbed atmosphere, the first equation becomes

$$\rho_o \underline{g} - \underline{\nabla} P_o = 0$$

which gives the barometric law,

$$P_o,\ \rho_o \propto \exp\left(\frac{-\gamma g z}{c^2}\right) = \exp\,(-z/H)$$

where $H \equiv c^2/\gamma g$ is the scale height. The temporal and spatial dependence of the variable may be specified by assuming

$$\frac{P-P_o}{P_o \Pi} = \frac{\rho-\rho_o}{\rho_o R} = \frac{u_x}{X} = \frac{u_z}{Z} = Ae^{i(\omega t - K_x x - K_z z)}$$

where x is the horizontal and z the vertical direction. Substitution into the three equations yields two component equations

$$(-\omega^2 + K_x^2 c^2)\, u_x + c^2\,(K_x K_z - iK_x g)\, u_z = 0 \quad (\hat{x} \text{ equation})$$

$$(-iK_x(\gamma-1)g + c^2 K_x K_z)\, u_x + (-\omega^2 - iK_z\gamma_g + c^2 K_z^2)\, u_z = 0 \quad (\hat{z} \text{ equation})$$

A solution exists only if the determinant of the coefficients vanishes, which gives the dispersion relation:

$$\omega^4 - \omega^2 c^2\,(K_x^2 + K_z^2) + K_x^2 g^2\,(\gamma-1) + \omega^2\, iK_z\gamma g = 0$$

An exponential horizontal dependence is excluded by setting $K_x = k_x$ where k_x is real. Solution of the dispersion relation using the quadratic formula shows that real ω^2 can be obtained for K_z pure imaginary or $K_z = k_z + i\gamma g/2c^2$ for k_z real. The second form is chosen since a growth

of amplitude is expected from energy considerations, and the dispersion relation becomes

$$\omega^4 - \left[c^2(k_x^2 + k_z^2) + \omega_a^2\right]\omega^2 + \omega_g^2 k_x^2 c^2 = 0$$

where

$$\omega_a \equiv \gamma g/2c \text{ and } \omega_g \equiv \frac{g}{c}\sqrt{\gamma-1}$$

The meaning of this dispersion relation is clarified by solving for k_z^2

$$k_z^2 = \frac{\omega^2-\omega_a^2}{c^2} - k_x^2\left(1-\frac{\omega_g^2}{\omega^2}\right)$$

and plotting the $k_z^2 = 0$ lines in the $k_x - \omega$ plane, referred to as the diagnostic diagram (Figure 1). In regions I and III, $k_z^2 > 0$ so k_z is real and the waves will propagate, and in region II, k_z is imaginary and the waves are evanescent or standing waves. The physical character of waves in the propagating regions may be further clarified by mathematically eliminating either of the two forces acting on an element of gas. If $g = 0$, gravity forces are eliminated and ω_a and ω_g go to zero, thus eliminating the waves in region III, which are seen to be gravity waves. Similarly, if the compressibility (γ^{-1}) vanishes, both ω_a and ω_g become large, eliminating the waves of region I, which are acoustic waves. For the conditions present in the solar atmosphere the two critical frequencies ω_a and ω_g both correspond to periods near 300 sec (Tanenbaum, 1971) and theorists have proposed several ways in which such periods might be selected.

Some theories would explain the existence of five-minute oscillations in terms of the distinctive properties of the plane-parallel, isothermal atmosphere. These models generally assume that a broad spectrum of waves

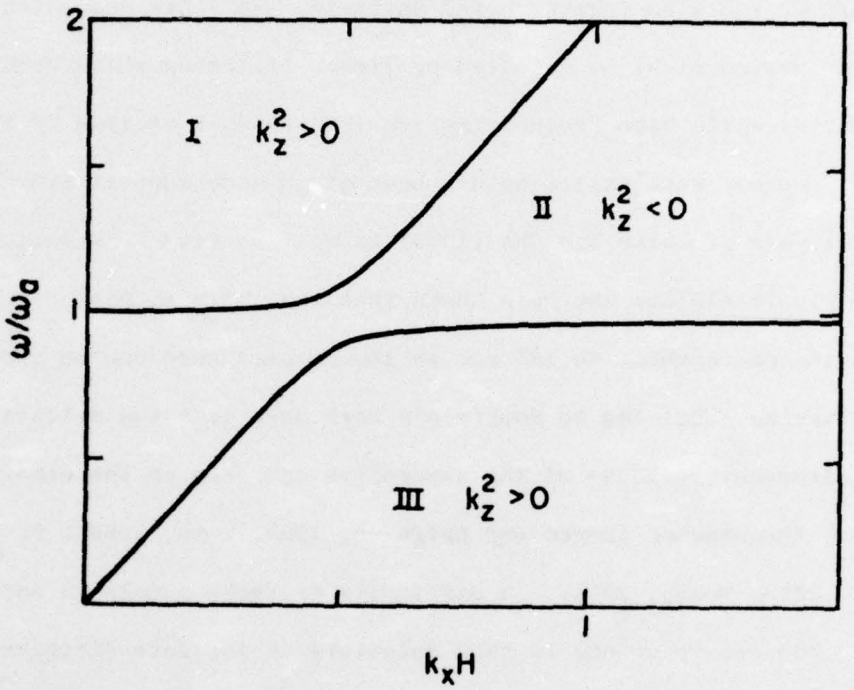

Figure 1. Diagnostic diagram for adiabatic propagation in an isothermal, gravitationally stratified atmosphere with $\gamma = 5/3$.

extending over a large portion of the diagnostic diagram may be produced by turbulent motions in the convective zone (the Lighthill mechanism). Souffrin (1966, see also Schatzman and Souffrin, 1967) has suggested that the resonant period might be selected by linear filtering which removes low frequencies while high frequencies are less readily excited by the convective source. Such filtering has been given some support from the waveform analysis of White and Cha (1973) as well as from observations of Fossat and Ricort (1975b) who have shown that the shift in period from 300 sec in the photosphere to 180 sec in the chromosphere can be produced by such filtering. Related to Souffrin's work have been the calculations showing a divergent response of the atmosphere near one or the other of the critical frequencies (Noyes and Leighton, 1963; Kato, 1966a, b, and c; Worrall, 1972; Moore, 1974). A difficulty of these models in accounting for the 300 sec resonance is that calculations indicate (Leibacher, 1973) that the waves generated by convective turbulence are strongest at periods shorter than 85 sec. An early proposal which overcomes this difficulty is the suggestion by Moore and Spiegel (1964, see also Zhugzhda, 1972) that a thermal overstability might force excitation of non-propagating modes. Excitation by overstability will be discussed in greater detail below in relation to trapping models. A more fundamental weakness of the atmospheric filtering model is that a high-pass filter can account for the shift of the resonant peak to shorter periods higher up in the atmosphere, but cannot account for the observation of the 300 sec period at the upper boundary of the convective zone before the filtering occurs (Schatzman and Souffrin, 1967).

Another explanation for the oscillations was prompted by the observation by Evans and Michard (1962b) of a wave train beginning 40 sec after the upward motion of a granule. This was further indicated by the observation that upper lines lag lower lines appreciably ($\sim$ 35 sec) early in a wave train and much less later on, suggesting that the granular disturbance propagates upward but that as higher lines with their shorter periods "catch up" to the lower line, the oscillation takes on a standing wave character. Two observational difficulties with this model recognized early included the larger scale size of oscillations compared with granules (Schmidt and Zirker, 1963) and the symmetric rise and fall of a wave train (Deubner, 1967; Tanenbaum, 1971). Computer modelling of a piston source of the oscillations (Stix, 1970) showed a spatial extent 2-3 times that of the granular disturbance and a less abrupt onset, but led to the conclusion that radiative damping would cause lifetimes to peak in the 0.75-1.5 period range as contrasted with the observation of Deubner (1967) of a most common lifetime of 15 min. Holweger and Testerman (1975) support this conclusion on the basis of a radiation damping time deduced from observed equivalent width oscillations, while Souffrin (1972) concludes that radiative damping does not exclude this mechanism but instead argues that granular excitation would be too isolated to produce the oscillations observed. Stix and Wöhl (1974) have also found that horizontal Lamb waves prediced for oscillations excited by convective overshoot are not present. The simplest and strongest observational evidence against this model is the determination by Musman (1974) that granules and oscillations are essentially uncorrelated.

It is widely agreed that the solar atmosphere is not isothermal, and several theories have been advanced proposing that the five-minute

resonance could result from trapping of waves produced by temperature or pressure changes. The first such proposal was that of Kahn (1961, 1962) who suggested that acoustic waves might be refracted about the temperature minimum. For a sound velocity $c(z) = (\gamma kT(z)/m)^{1/2}$ and an assumed parabolic temperature profile $T(z) = T_o + \frac{1}{2} T_o'' z^2$, he calculated that the increase in sound velocity about the temperature minimum would refract obliquely propagating waves in much the same way that shortwave radio waves are bounced off of the ionosphere. A wave packet produced by convective turbulence would be refocused by this refraction 285 sec after its original passage through the temperature minimum, at a horizontal distance of $\sim$ 2250 km. Observations have shown neither the large horizontal component of motion nor the successive horizontal displacement of oscillating centers predicted by this model.

Another proposal for producing the observed resonance by trapping was suggested by Bahng and Schwarzschild (1963) and later reworked by other authors (Stein and Leibacher, 1969; McKenzie, 1971). The basic idea was that acoustic waves would be trapped by the sharp pressure gradient at the base of the photosphere and reflected at the high temperature, low pressure corona, which would act as a free surface. Temperature profiles with a chromosphere at 8 to 15 x 10^3°K between a 6 x 10^3°K photosphere and a corona with $T > 10^5$°K gave solutions resembling observations. The predicted damping was too small to match observed lifetimes, though lateral energy losses were invoked to correct this difficulty. A more serious difficulty was the prediction of a sharp drop in amplitude going down into the photosphere, which is at variance with later observations.

Gravity waves trapped about the temperature minimum were suggested

by Uchida (1965, 1967) and later using a different mathematical formulation and atmospheric model by Thomas et al. (1971). Gravity waves would be more susceptible than acoustic waves to generation by turbulence in the convective zone (Stein, 1967). Uchida described trapping in terms of a region in the k-ω plane where propagation would be possible at lower temperatures but not at higher temperatures, due to a shift in the $k_z^2 = 0$ line defining the cutoff for gravity wave propagation. Thomas et al. instead showed by calculations using the Bilderberg Continuum Atmosphere (Gingerich and de Jager, 1968) that a broad maximum existed in the Brunt-Vaisala frequency $\omega_{BV} = (\omega_g^2 + (g/T)\ dT/dz)^{1/2}$, which is the cutoff frequency for gravity waves generalized to a non-isothermal atmosphere. Uchida calculated eigenfrequencies corresponding to 266 sec, 313 sec, and 347 sec using $k_x = 3 \times 10^{-8}$ cm^{-1} ($\lambda_x \simeq 2 \times 10^3$ km), and Thomas obtained eigensolutions with periods of 263 sec and 338 sec for a horizontal wavelength $\lambda_x = 1500$ km. Not only do these periods agree well with those observed by Frazier, but the 263 sec component would be more important higher up which could account for the decrease in period with height (which Uchida found hard to explain). Both formulations agree that shorter horizontal wavelengths should be favored--Uchida says $\lambda_x \lesssim 3000$ km and Thomas suggests a maximum for $\lambda_x \simeq 1500$ km. Thomas (1972) has shown from computer simulation that poor seeing could cause an observer to measure $\lambda_x \sim 4200$ km for a real 1500 km wavelength, but this cannot explain the larger wavelength (20000 km) determined by Fossat and Ricort from statistical arguments using large apertures. A more serious difficulty is the prediction of a concentration of kinetic energy density near the temperature minimum, whereas observations indicate a monotonic decrease in energy with height.

The difficulty theories have had in accounting for the presence of oscillations deep in the photosphere has led to the proposal that the convection zone might play an important role in selecting the resonant period. Jones (1969) developed a model in which the outer boundary was approximated by a free surface at the corona as in the Bahng and Schwarzschild model, but the inner boundary condition was a bounded kinetic energy radially inward which could be insured by a large density scale height in the convection zone. Excitation would be by turbulence in the convective zone. Periods less than 200 sec were calculated to have energy concentrated higher in the atmosphere, periods greater than 400 sec gave an energy concentration deep in the convection zone, and periods near 300 sec gave a concentration of energy just inside the convection zone. This model claimed to account for the vertical change in amplitude and period and to match the horizontal wavelength as well.

Leibacher and Stein (1971) proposed that the oscillations were acoustic waves trapped entirely within the convective zone. Waves would be reflected under the photosphere due to the rapid drop in temperature outward, and another reflection was postulated at a depth of 1600 km. Leibacher has since shown (1973) how waves at (ω, k_x) near the acoustic cutoff become non-propagating and are therefore reflected if temperatures rise or drop out of a limited range. The resultant trapping of waves in a resonant cavity in the convection zone would cause the whole photosphere to go up and down, thus producing the small phase lags observed between different lines.

Ulrich (1970) also proposed a model based on waves trapped in the convection zone, and further suggested that such waves might be over-

stable and therefore self-sustaining. The idea that dissipation could produce an overstability in a convectively unstable region was developed by Spiegel (1964) and Moore and Spiegel (1966). In the adiabatic case, a destabilizing force displaces an element and the restoring force (compressibility for acoustic waves) will return it to its original position, thus producing symmetrical oscillations. The action of dissipation (such as radiative damping) lags behind the destabilizing force (e.g. density fluctuations driven by unstable buoyancy) and thus reduces this force more when it is opposing the return to equilibrium than when it is driving the displacement. Ulrich calculated that the resultant overstability could drive acoustic waves trapped in the convection zone. This theory made the somewhat distinctive prediction that the trapped modes would exist as diagonal ridges in the k-ω two-dimensional power spectrum. The recent report of such ridges in power spectra of observations by Deubner (1975) and Rhodes et al. (1976) agrees very well with the prediction. Some caution might still be justified by the fact that agreement is very good after the theory was presented, but diagonal ridges were not observed in k-ω power spectra (Mein, 1965; Tanenbaum et al., 1969) produced before the theory was developed. Further attempts at confirmation using very different techniques developed by Fossat (1974; Fossat and Martin, 1974) will be awaited with interest.

The possible importance of overstability in driving the oscillations is related to the suggestion by Wolff (1972b, 1973) that the resonant oscillations might be high wave number nonradial p-modes of the sun. He calculated that certain modes would be unstable, and found periods in the 300 sec range. It was suggested that the $\lambda \sim 5000$ km horizontal wavelength

often reported was much shorter than the actual value due to incomplete removal of granulation velocities. Ando and Osaki (1975) present the results of extensive calculations showing many modes in the 300 sec range to be unstable. They suggest that the modes are excited by the κ-mechanism in the hydrogen-ionization zone (by which opacity increases with temperature making the sun a heat engine). Another possibility for excitation is the γ-effect, whereby changes in thermal capacity created by ionization during the cycle produce a lag between density and pressure fluctuations. Wolff (1972a) has even suggested that a large flare might excite observable modes not necessarily restricted to periods near five minutes, and though Fossat and Ricort (1973) report three examples of 30 m/s, P = 40 min oscillations following flares, later work (Fossat et al., 1974; Fossat and Ricort, 1975a) shows that a solar origin of such longer periods could not be confirmed because of low frequency instrumental variations.

Longer-Period Oscillations

Attention will now be turned to solar oscillations or pulsations at periods longer than five minutes. Such pulsations are different from the resonant oscillations in that theoretical development anticipated observational reports by many years. Since this is primarily an observational work, it is instructive that a review of long period oscillation observations must be much shorter than that of the five-minute oscillation, even though the former are of great current interest and the area of primary contribution for the present work.

Theory

A general discussion of the theory of stellar pulsation is far beyond the scope of this work. A very complete treatment including a discussion of both the observations and the pulsation theory of variable stars is given by Ledoux and Walraven (1958). Shorter treatments are given by Ledoux (1965) and Cox and Giuli (1968), and a review on recent developments in nonradial pulsation theory is available (Cox, 1970).

Because of the high symmetry of observed properties, most variable stars are best described by the hypothesis of purely radial pulsations. The sun does not show any obvious simple periodic variation, and discussion has included consideration of nonradial modes, with the form of the perturbation assumed to be

$$f'(r, \theta, \phi) = f'(r)\, Y_\ell^m(\theta, \phi)$$

where $Y_\ell^m(\theta, \phi)$ are spherical harmonics. Cowling (1941) found the periods of pulsation for nonradial modes for a polytrope, with this important paper giving rise to the nomenclature for these modes. Ledoux and Walraven (1958) show that Cowling's result can be derived in the general case and later applied to the particular case of polytropes. The derivation outlined below is taken from the original paper of Cowling.

The three basic equations to be solved are the equation of continuity

$$\rho_1 = - \operatorname{div} (\rho_o \underline{x}),$$

the equation of motion

$$\rho_o \sigma^2 \underline{x} = \operatorname{grad} \rho_1 + \rho_1 \operatorname{grad} \Phi_o + \rho_o \operatorname{grad} \Phi_1,$$

and the equation of state

$$(P_1 + \xi \frac{\partial P_o}{\partial r}) / P_o = \gamma (\rho_1 + \xi \frac{\partial \rho_o}{\partial r}) / \rho_o$$

where the subscripts 0 and 1 refer to the equilibrium and perturbation values, ρ is the density, P is the pressure, Φ is the gravitational potential, $2\pi/\sigma$ is the period, $\underline{x}$ is the vector displacement of a particle from equilibrium (with ξ the radial component) and γ is the ratio of specific heats.

Since the mass will be concentrated in central regions of the star, oscillations will not produce large changes in gravitational potential. Cowling therefore drops Φ_1 later showing its effect to be small by perturbation theory. He also considers each of ρ_1, P_1 and ξ to be the product of a surface harmonic of order ℓ and a function of r. For a polytrope of order n, the equilibrium density and pressure are related to the central density ρ_c and pressure P_c by the equations $\rho_o = \rho_c y^n$, $P_o = P_c y^{1+n}$ where y satisfies Emden's equation

$$\frac{d}{dx}\left(x^2 \frac{dy}{dx}\right) = -x^2 y^n$$

and x is given by $x = r/r_o$, where $r_o^2 = (1+n)\, P_c/4\pi G\rho_c^2$. Cowling uses these variables and the non-dimensional quantities X, θ ϕ, and a defined by

$$X = \xi/r_o,\ \theta = P_1/P_c,\ \phi = \rho_1/\rho_c,\ a = (1+n)\ \sigma^2/4\pi G\rho_c$$

to rewrite the equations in the form

$$\gamma y\phi = \theta + Xy^n y' \ (1+n-\gamma n),\ y' = \frac{dy}{dx}$$

$$y^n aX = \frac{\partial\theta}{\partial x} - (1+n)\ \phi y'$$

$$a\phi = \frac{-\partial}{x^2\partial x}\ (ay^n x^2 X) + \frac{\ell(\ell+1)}{x^2}\ \theta$$

Further substitution and manipulation reduces the problem to two first-order equations

$$\frac{\partial w}{\partial x} = fz \text{ and } \frac{\partial}{\partial x}(x^2 z) = wq$$

where

$$w = \theta y^{-(n+1)/\gamma}, \quad z = Xy^{(n+1)/\gamma}, \quad Q = \frac{2(n+1)}{\gamma} - n$$

$$f = y^{-Q}\left[a + \frac{1}{2}(Q-n)(n+1)\frac{y'^2}{y}\right], \text{ and } q = y^{Q}\left[\frac{\ell(\ell+1)}{a} - \frac{x^2}{\gamma y}\right]$$

These two equations are equivalent to a single second-order equation. For very small a, this equation approaches

$$\frac{2}{(Q-n)(n+1)}\frac{\partial}{\partial x}\left(\frac{x^2 y^{1+Q}}{y^2}\right)\frac{\partial w}{\partial x} \simeq \frac{\ell(\ell+1)}{a} w y^{Q}$$

which has infinitely many solutions for a indefinitely small. For very large a, this equation approaches

$$\gamma\frac{\partial}{\partial x}\left(\frac{y'^{-Q}}{x^2}\frac{\partial}{\partial x}(x^2 z)\right) = -azy^{-Q}$$

which has infinitely many solutions for a indefinitely large. Cowling found the small a (longer period) solutions to correspond to small variations in pressure and density with motion chiefly horizontal and due to gravity acting to smooth out density differences. These he called g-modes. The large a (short period) solutions are characterized by large pressure fluctuations and chiefly radial motion driven by pressure variations, and are hence called p-modes. In addition, there is an intermediate period solution such that ξ and $-\rho_1$ have the same sign at all points along any radius, which he termed the fundamental (f-) mode.

The p- and g- modes are distinguished by a subscript denumerating the number of nodes in the function giving the radial dependence of the perturbed quantities. The p-modes have shorter periods and the g-modes have longer periods with increasing radial wave number. The period of the f, p, and g modes decreases with higher order spherical harmonics.

The dependence of period of the different modes on radial wave number and the order of the spherical harmonic may be illustrated schematically by plotting the periods as shown in Figure 2, with periods and format taken from Iben and Mahaffy (1976). It may be seen that the g-modes are present only for $\ell \geq 1$ and the f-mode for $\ell \geq 2$. It is also clear that unless consideration is restricted to certain modes or spherical harmonics, on either physical or observational grounds, the interval of periods plotted quickly becomes densely covered with modal periods.

Since Cowling's paper on nonradial oscillations, the basic picture remains the same. There has been much added in details and sophistication because of developments in models of stellar structure and evolution, especially fed by improved understanding of nuclear energy generation processes. More detailed models have also been more accessible because of the development of large, high-speed computers. Recent calculations for the sun (Scuflaire et al., 1975; Iben and Mahaffy, 1976; Christensen-Dalsgaard and Gough, 1976) all give results qualitatively similar to those obtained by Cox (1976) for the n = 3 polytrope. Models with different assumptions about the sun's evolution do yield different periods which could be used to distinguish between the models if measured with sufficient accuracy. Table 1 shows the periods computed for different assumptions. Christensen-Dalsgaard and Gough assume an initial heavy element abundance Z = 0.02 and a mixing length $\ell/H_p = 1.10$. Iben and Mahaffy try three different values of Z (0.01, 0.02, and 0.03) and vary the mixing-length and hydrogen abundance (X) to match the sun's present luminosity and radius. Scuflaire et al. test the effect of a fast mixing of the inner 83% of the total solar mass, with periods computed at intervals

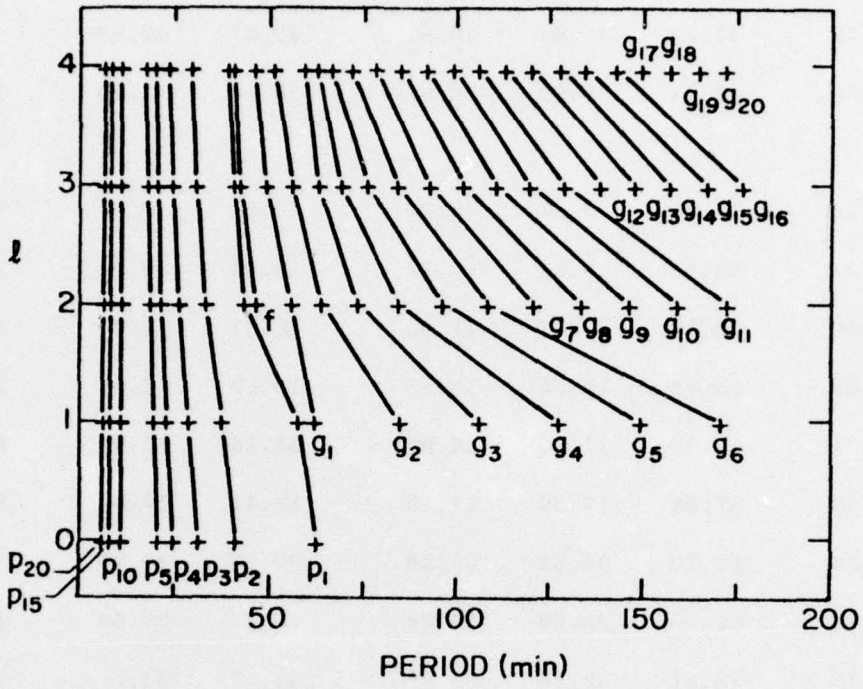

Figure 2. Periods for non-radial pulsations of different modes and different spherical harmonics, from Model 2 of Iben and Mahaffy (1976).

Table 1

Periods Calculated for Various Solar Models

Mode	Cox (1976)	Iben & Mahaffy (1976)			Scuflaire (1975)		CD&G (1976)
(ℓ=0)	n=3 polytrope	Model 1	Model 2	Model 3	S	M4	
p_1	54.88	56.22	62.29	66.14	62.05	63.61	62.7
p_2	40.52	41.32	40.94	40.81	40.67	42.84	43.8
p_3	31.29	31.31	30.93	30.67	30.93	31.96	32.6
(ℓ=2)							
p_{10}	10.91	10.21	9.97	9.84	10.01	10.03	10.4
p_9	11.93	11.18	10.87	10.72	10.91	10.94	11.4
p_8	13.08	12.33	11.97	11.82	12.01	12.06	12.6
p_7	14.51	13.74	13.35	13.18	13.38	13.46	14.1
p_6	16.31	15.54	15.10	14.90	15.14	15.23	16.0
p_5	18.60	17.88	17.39	17.19	17.42	17.55	17.9
p_4	21.66	21.10	20.52	20.28	20.56	20.75	21.5
p_3	25.93	25.60	25.09	24.74	25.13	25.48	26.7
p_2	32.30	32.61	32.19	32.02	32.27	33.01	34.3
p_1	42.74	43.75	42.50	39.18	42.91	46.76	42.2
f	58.39	49.19	45.90	43.97	47.19	63.45	46.0
g_1	75.31	56.00	55.05	50.40	56.05		55.1
g_2	99.27	65.21	63.03	58.72			61.5
g_3	123.7	77.16	72.58	67.90			70.9
g_4	148.2	90.85	83.49	77.03			81.8
g_5	172.6	104.7	95.38	86.53			93.0
g_6	196.9	118.6	107.7	96.75			105.0
g_7	221.3	132.6	120.2	107.6			117.0
g_8	245.6	146.7	132.9	118.9			130.0
g_9	270.1	160.9	145.9	130.6			142.0
g_{10}	294.2	174.9	158.9	142.6			154.0

of time following the presumed mixing. Comparisons show that distinguishing between different models on the basis of observations will be hazardous unless periods are well defined and there is some means of recognizing which pulsational mode is being observed.

Cowling originally applied the theory of nonradial pulsations to the problem of tidal distortion of binary stars, and it has since been applied to such diverse phenomena as nova outbursts (Rose, 1968) and oscillations in many electron atoms (Monaghan, 1973 and 1974). Attention has turned in recent years to the sun in response to observational developments in the area of solar neutrinos and of five-minute oscillations. The relation of these phenomena to nonradial oscillations will next be considered, followed by a discussion of possible direct observations of longer period oscillations.

As a probe of the solar interior, Davis and colleagues have attempted to detect neutrinos produced by nuclear reactions in the center of the sun, since neutrinos should pass directly out of the sun instead of being scattered beyond recognition before emerging, as is the case with photons. Measurements have thus far (Bahcall and Davis, 1976) yielded upper limits far below those predicted by models, and theorists have responded with a variety of models to explain this discrepancy. Dilke and Gough (1972) suggested that nuclear evolution of the solar core could result in instability to low order g-modes, which would cause chemical mixing in the core and yield a much lower neutrino luminosity. The suggestion that the sun might be or might have been unstable to low order g-modes has been largely confirmed by more complete calculations by Christensen-Dalsgaard, Dilke and Gough (1974), as well as by Shibahashi et al. (1975) and by

Boury et al. (1975). These calculations have used the quasi-adiabatic approximation, which Christensen-Dalsgaard et al. point out may not adequately include damping effects of the outer layers of the sun. Ulrich (1973) argues that even if the possible instability to g-mode oscillations is present, it would not produce enough mixing to lower the neutrino flux to the observed values. Christensen-Dalsgaard et al. agree that this might be the case.

The other observational development leading to new interest in possible nonradial pulsations of the sun is the discovery and study of five-minute oscillations. As discussed above, the suggestion that the five-minute oscillations might be high order p-modes was made by Wolff (1972b, 1973) and the instability of modes with periods in the five-minute range has been confirmed by the thorough linear, non-adiabatic calculations of Ando and Osaki (1975). There have also been suggestions that other periods might be observed. Wolff's (1972a) suggestion of possible excitation of nonradial modes by flares was mentioned above. Aleshin (1974) has also suggested that radial oscillations with a period near 50 minutes and an amplitude $\delta r/r \sim 10^{-7}$ might be excited by a flare. The overstability at a boundary where a convectively stable region overlies an unstable region (Moore and Spiegel, 1966) has been proposed as a means of exciting g-modes in the convective core by Souffrin and Spiegel (1967). Kato (1969) suggested that either this overstability or the horizontal velocity shear of differential rotation might excite non-spherical waves in the convection zone, giving rise to the observed sinusoidal growth in quiescent prominences. A possible connection between such oscillations and large-scale magnetic patterns (Bumba and Howard,

1965) was also suggested by Kato and independently by Wolff (1974a and b) with relation to the magnetic sector structure (see Wilcox and Howard, 1968; Wilcox, 1968).

Observations

Direct observations of solar oscillations at periods longer than five minutes have been elusive, largely because of the difficulties in obtaining sufficient instrumental stability to enable clear detection of a small, slowly changing signal. Deubner (1971) reported a long period mode from magnetograph observations using the low-lying line CIλ5052. He found predominantly horizontal motions of about 100 m/s and a repetitive (though not strictly periodic) tendency involving periods of about 40 min. Further work (Deubner, 1972a) in the line CIλ5380 gave similar results and also indicated a velocity-intensity correlation as high as for the five-minute oscillation and a spatial anticorrelation in the amplitudes of the five-minute oscillation and the longer period feature. A later paper (Deubner, 1974), including observations in the same line, reported no important periods at 20 minutes or longer. Fossat and Ricort (1973) observed similar oscillations (period $\sim$ 40 min, amplitude $\sim$ 30 m/s) from observations using optical resonance techniques and the Na-D_1 line. This oscillation was seen in three of ten cases, and in all three, later investigation showed them to have followed flares of some importance (1N twice, 2B once) in support of the flare-excitation suggestion of Wolff and Aleshin. Later work (Fossat et al., 1974; Fossat and Ricort, 1974 and 1975a) did not confirm these longer period oscillations and indeed suggested that they could not be distinguished from low-frequency noise of presumably atmospheric origin. A ten-minute mode was reported in the

later papers with lifetime < 15 hours, large horizontal scale, and intermittent temporal behavior. There has been no further published confirmation of this ten-minute mode by other observers, and in a later paper (Grec and Fossat, 1976) using an improved sodium device, the ten-minute oscillation was not observed, which makes it likely that the effect was of instrumental origin.

Longer period oscillations at radio wavelengths (9870, 9670 MHz) have been reported by Kobrin and Korshunov (1972, see also Kobrin et al., 1973). Sensitivity was enhanced by using two telescopes, in one case separated by 1500 km, to rule out an atmospheric origin. An active region source was rejected since the oscillations persist after the region disappears behind the limb. Other possible explanations include supergranulation oscillations or global pulsations. Kalinjak and Vassilyeva (1971) compared a particular feature to the full disk at meter and decameter wavelengths, and found a north-south anisotropy which they interpreted as being due to a gravity wave causing a temporary surface deformation. Kaufmann (1972) also reported oscillations at a period of about 41 min from 7 GHz radio observations. He favors the explanation that the observed periodic signal is produced by an oscillating quiescent prominence (see Kleczek and Kuperus, 1969) which generates oscillations at microwave wavelengths by dissipating its mechanical energy in the surrounding coronal plasma. The recurrent mention of 30-50 minute periods suggests that these oscillations may have a common, presumably solar origin. However, difficulties in confirming oscillations reported at optical wavelengths and the availability of alternate explanations for the periodic features observed in radio observations leave considerable room for doubt.

Current interest in longer period pulsations is especially due to observations from two groups using sensitive new techniques and obtaining different but not necessarily incompatible results. Severny, Kotov, and Tsap (1976a), of the Crimean Astrophysical Observatory have made an ingenious and straightforward modification of the Babcock magnetograph to enable very sensitive velocity measurements. The magnetograph is designed to give a sensitive measurement of the difference in wavelength of the right and left circularly polarized components of an absorption line, since these components are shifted in opposite directions (Zeeman splitting) if a line-of-sight magnetic field is present in the line forming region for a magnetically sensitive line. To measure relative solar velocities using the magnetograph, a non-magnetic line is used, and a circular polarizer is positioned so as to polarize light coming only from the center of the disk. Since light of this polarization is transmitted from any part of the disk while light of the opposite polarization may come only from the limb, the magnetograph now measures the difference in wavelength between the limb and the full disk. Because global pulsations will produce different line-of-sight velocities at center and limb, through Doppler shifts they would also produce an oscillation in the wavelength difference signal.

Observations in this mode showed small variations of the signal from the daily pattern with a period near 2 hr 40 min. Simultaneous observations made using the solar line FeIλ5123.7 and the telluric line H_2O λ5901.5 showed that the fluctuations were present in the solar line and not in the telluric line. This fact and the independence of the phase of the oscillations from local time or from the time each observation

was started led the authors to conclude that this signal was of solar origin. A superposed epoch analysis was performed using periods between 2 hr 30 min and 2 hr 50 min in steps of 0.5 min, and the best signal (largest extremum to error ratio) was obtained for a period of 2 hr 40 min $\pm$ 0.5 min with the amplitude being $\pm$ 2 m/s. Data taken in October 1974 and March 1975 showed the same period and a phase consistent with a period of exactly 2 hr 40 min, indicating phase stability over 1900 periods.

This long period was a surprising and unexpected result. The phase stability indicated would rule out a stochastic process such as super-super granulation, and the period is too long for the oscillations to be limited to the envelope of the sun. If the pulsations measured are purely radial, the long period measured would indicate a much more homogeneous sun than predicted by standard models. The result would be a reduction in nuclear reaction rates which would account for the low neutrino flux but would also leave no known mechanism for the production of the observed photon luminosity. An alternate explanation is that the observed period might be a higher order g-mode, for example a quadrupole g_{11} oscillation which has a period near 2 hr 40 min in current models. Worden and Simon (1976) have suggested that the signal is due to super-granules rotating with the sun, though this would not produce a sharply defined period and it would seem that the period would be closer to

$$27 \frac{\text{day}}{\text{rot}} \Big/ \left(2\pi \times 696{,}000 \frac{\text{km}}{\text{rot}} \Big/ 30{,}000 \frac{\text{km}}{\text{super G}}\right) \simeq 4.6 \frac{\text{hr}}{\text{super G}}$$

Whatever the explanation might be, the Crimean observers continue to report the 2 hr 40 min oscillations in 1975 and 1976 observations Severny et al. (1976b). They have also seen oscillations in the sun's mean magnetic field with the same period and in the comparative intensity

of center and limb. These oscillations could all be evidence of a common instrumental problem rather than a solar origin, though it is hard to explain reported 2 hr 40 min oscillations in the intensity of Uranus in this manner because very different instrumental techniques would necessarily be involved. Also impressive is the independent report of oscillations of similar amplitude and period (2.70 ± 0.24 m/s, 2.65 ± 0.04 hr) by a group from the University of Birmingham (Brookes, Isaak, and van der Raay, 1976). They use a resonant optical scattering device using potassium or sodium vapor Zeeman split in the laboratory by a magnet to scatter light on the wings of sodium or potassium lines (as described in the section on five-minute oscillation observations). Only two of twelve observations yielded usable data, and both showed oscillations near a 2 hr 40 min period after fitting out the velocity signal due to the earth's rotation. Power spectra also give peaks at periods of 58 min and 40 min which are close to those expected for low order radial or non-radial modes.

A second series of reports of solar oscillations has come from Henry Hill and collaborators working at the Santa Catalina Laboratory for Experimental Relativity through Astrometry (SCLERA) in Arizona. They have used distinctive techniques and analysis and have obtained results bearing much closer similarity to those predicted by standard theories than the 2 hr 40 min period discussed above. Their instrument is designed to make very precise determination of the sun's diameter, in particular so polar and equatorial diameters can be compared to look for the oblateness reported by Dicke and Goldenberg (1967). The telescope produces an image of the sun below which are placed slits adjacent and parallel to

the opposite limbs. The image is driven back and forth sinusoidally by the positioning mirror, and the slits are positioned at that point on the limb where the finite Fourier transform

$$F(G;\ q,\ a) = \int_{-1/2}^{1/2} G(q + a \sin \pi s) \cos 2\pi s \, ds$$

vanishes. Here G is the intensity, q is the radial position, and a the scan amplitude. The transform is computed by a minicomputer and the slits are positioned to achieve null, with the slit separation measured by a laser interferometer. Details on the telescope are given in Oleson et al. (1974), the oblateness measurement in Hill and Stebbins (1975), and the use of the finite Fourier transform definition (FFTD) of the limb in Hill et al. (1975). An oblateness of 18.4 $\pm$ 12.5 arc msec was reported, consistent with a uniformly rotating sun and in contrast with Dicke's value of 43.4 $\pm$ 3.3 arc msec which would require a rapidly rotating core and which would imply disagreement between the observed precession of the perihelion of Mercury and the prediction of Einstein's General Theory of Relativity.

The oblateness measurement requires alternating measurements of the sun's polar and equatorial diameters. Early indications of periodic variations in the signal led the observers to make repeated consecutive measurements of the equatorial diameter in November 1973 and of the polar diameter in the spring of 1975. Power spectra were computed for each set of observations and many peaks were noticed in the 10-50 minute range suggesting their identification with low order p-modes of the sun (Hill et al., 1976a). Observations have been extended and power spectra computed (Brown et al., 1976) and peaks identified. A comparison of the different periods measured (see Table 2) with each other and with the theoretical

Table 2

Periods Observed by Hill *et al.*

Sept. 1973	Spring 1975	Fall 1975
		68.3
52	47.9	45.5
33	30.3	28.7
23.8		24.8
	21.0	21.0
16.7	17.1	18.8
		15.6
	14.6	14.7
13.3		13.0
11.9	11.8	11.4
10.4	10.5	10.8
		9.84
9.2	8.8	9.26
		8.53
	7.9	7.90
7.6		7.54
7.0	7.2	7.18
		6.74
		6.28
		6.07

values in Table 1 shows there to be fair, though not perfect agreement, with this comparison complicated by different frequency resolution in the different power spectra computed.

These results have been welcomed by theorists who have made comparisons between the reported periods and solar models of different initial abundances (Iben and Mahaffy, 1976) or at different times from a hypothetical mixing of the interior (Scuflaire et al., 1975). Attempts at confirmation by other observers have been unsuccessful. Brookes et al. (1976) concluded that the velocities they measured at periods of $\sim$ 1 hour were an order of magnitude lower than those required by the Hill result, and Grec and Fossat (1976) reported an upper limit 30 times smaller than they calculated would be present if the SCLERA group were measuring an actual mass motion. Hill et al. (1976a) suggested that their signal was due rather to changes in the limb darkening function, and have calculated (Hill et al., 1976b and 1977a) greatly enhanced sensitivity for the FFTD, especially if there is present a substantial portion of the mode which has an exponential growth of energy with height in the solar atmosphere, as might be the result of reflections in the chromosphere or corona. Grec and Fossat (1976) have also argued that the peaks in the power spectra are not statistically significant, and Brown et al. (1976) have answered with different reasons for claiming a high statistical significance, most impressive of which is the coincidence of many peaks in power spectra computed from independent samples of the data. Musman and Nye (1976a) submitted an abstract reporting a period of 45 $\pm$ 4 minutes in measurements of intensity and velocity using the non-magnetic line FeIλ5576, but by the time the paper was presented, a negative conclusion

had been reached, as further discussed in a later paper (Musman and Nye, 1976b). Livingston et al. (1977) made direct measurements of temperature by comparing the central depth of the line CIλ5380 with the continuum and found no significant temperature variations with a 3 σ upper limit of 0.4°K estimated for periods between 5 minutes and 60 minutes. Hill et al. (1977b) have challenged the calculations used to relate intensity fluctuations to temperature fluctuations, and Livingston et al. have recognized that a comparison is difficult since they use a line formed near $\tau = 1.0$ whereas Hill's technique defines the limb near $\tau = 0.02$ where the amplitude of temperature fluctuations might be much greater. The oscillations remain unconfirmed and of great potential value as probes of the structure of the sun's interior.

As a summary of past efforts and an introduction to the present work, the following are questions that might be answered by an observational study of large-scale solar velocities:

1. Can five-minute oscillations be observed using present techniques? If so, what are the amplitude and period and how do these values (and any others measurable) agree with other observations and with different proposed theories? Regular observations of five-minute oscillations over several solar rotations would also enable the investigation of large-scale organization of five-minute oscillations in relation to magnetic sector structure or coronal holes. The possibility of some such connection might be expected in view of theories mentioned above (Wolff, 1974a and b; Kato, 1969) which identify nonradial oscillations as the source of large-scale magnetic structures. Some connection might also be expected because of observed differences in amplitude or period of

five-minute oscillations produced by small-scale, active region magnetic fields as discussed above. Five-minute oscillations are also of current interest in theories of coronal heating (see Leibacher and Stein, 1974) and since there are definite large-scale changes in coronal temperature such as indicated by coronal holes (Munro and Withbroe, 1972; Altschuler et al., 1974), it would be interesting to know if there are similar variations in the amplitude or period of five-minute oscillations.

2. Are the periods identified by Hill and co-workers present or below the threshold of techniques described herein? Can the spherical harmonics or radial wave numbers be identified, and what are the lifetimes of the modes present?

3. Are the 2 hr 40 min oscillations truly of solar origin? If so, what is their amplitude, period, and angular dependence? Is their lifetime measurable, and what mode do they represent? Are there other related modes present, or is there any observational clue as to why this one is selected?

Chapter II

THE INSTRUMENT

The observations used in the present study were made at the Stanford Solar Observatory. This is a new instrument which was dedicated on April 26, 1974 with regular observations of the sun's mean magnetic field beginning in May of 1975. The telescope is patterned after the 150 foot solar tower telescope at Mt. Wilson, with modifications generally directed toward the goal of observing large-scale magnetic and velocity fields with very high sensitivity. This chapter contains a detailed description of the basic instrument. No other such description has been published at this time, though a somewhat briefer description is in preparation (Scherrer, 1977). More detail will be devoted to an explanation of the modification which Valeri A. Kotov of the Crimean Astrophysical Observatory devised for using the Babcock-type magnetograph to measure relative solar velocities. Included will be a description of calculations and experiments performed to provide a proper calibration and interpretation of the observations. As the different components of the telescope are described in detail below, their location and relation to the whole may be better understood by reference to Figure 3, which is due primarily to Philip H. Scherrer.

The Stanford Solar Observatory is located in the foothills south of the academic center of the university on university property. It is at an elevation of 370 $\pm$ 5 ft (113 m), latitude N37° 24' 35" $\pm$ 2" and longitude 122° 10' 2' $\pm$ 2". This location is excellent for the large-scale, daily observations undertaken because there is a great deal of

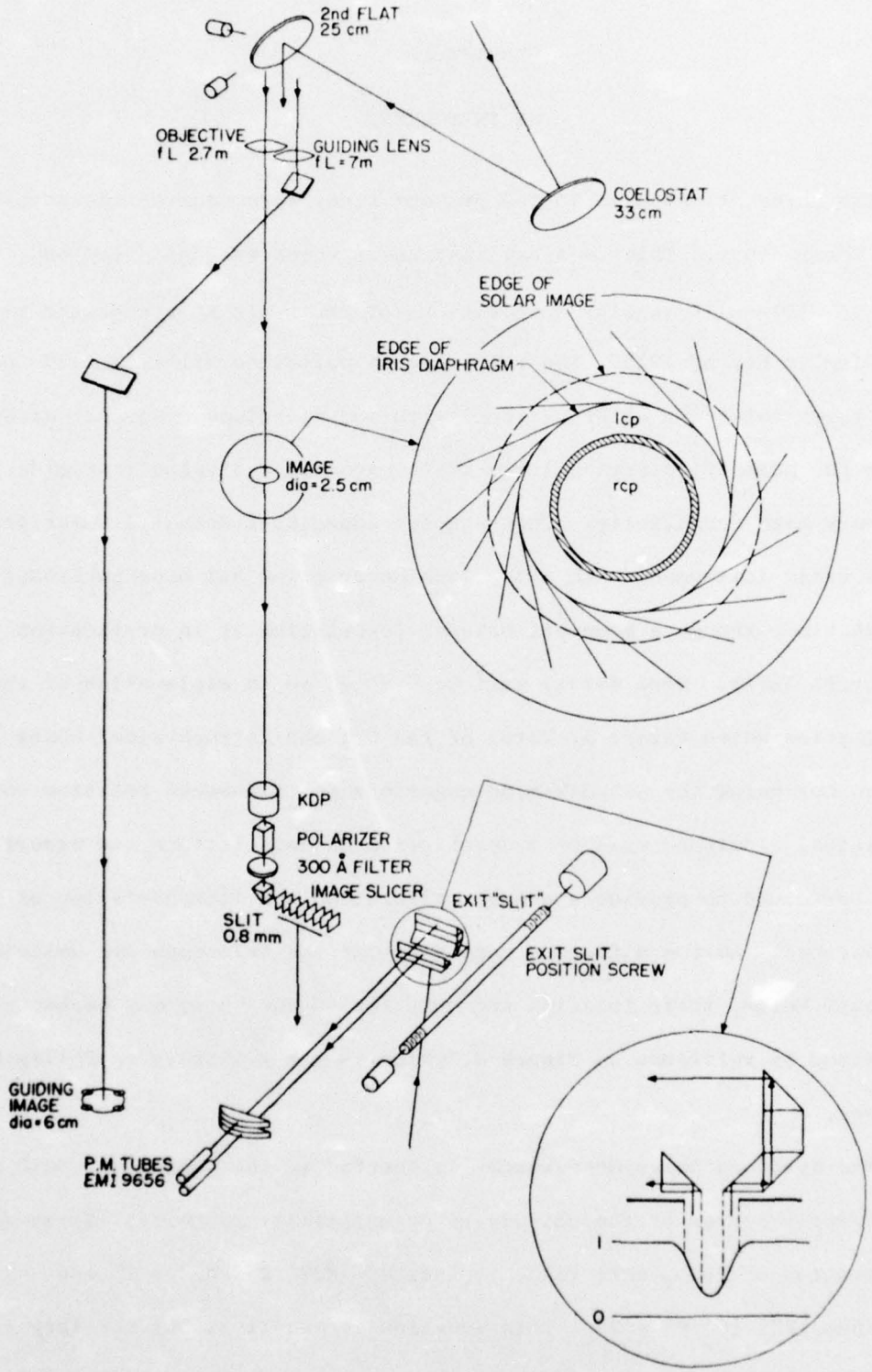

Figure 3. Optical diagram of the Stanford Solar Observatory

clear weather, especially during the summer months (May through September). It also has the advantage of being only five minutes away from the campus. The advantage of close proximity to campus in a large metropolitan area also carries with it the disadvantage of man-made atmospheric pollution. Resultant loss of transparency can be especially harmful for the present observations if there are sharp local gradients resulting in a variable weighting for different portions of the solar disk. This problem is reduced, especially in afternoons, by prevailing northwesterly winds off of the Pacific Ocean which help keep the air clear. The hilltop location also visibly improves transparency on days with relatively low wind and high pollution.

Sunlight is collected by a two-mirror coelostat system, which produces a nonrotating image of the sun. The 33 cm coelostat mirror rotates about an axis directed at the celestial north pole with a 48-hour clock drive, and reflects the light to the 27 cm second flat mirror which reflects it vertically downward. When the sun's declination is less than + 9° (September to April), the shadow of the second flat falls on the coelostat at noon, so the coelostat mirror is displaced 50 cm east of the second flat in the morning and 50 cm west in the afternoon, which produces a rotation of the solar image. Rotation of the image can have a large effect on the velocity signal measured when the observing aperture is not perfectly centered because of the sun's large rotational velocity of nearly 2 km/sec. This would make the heliostat system, which uses one mirror but produces a rotating solar image, much less suitable for the observation described herein. An advantage of the heliostat is that the angle of incidence of sunlight does not change during the day, whereas

for the coelostat system, the angles change producing changes in polarization. This polarization is not important for the present observation since the light is passed through a linear polarizer before analysis.

Two objective lenses are positioned 120 cm directly below the second flat mirror. Light passing through the guiding lens (a single element, anti-reflection coated lens with focal length f = 7.1 m, diameter d = 5.7 cm, and clear aperture 5.4 cm) is reflected off a two-mirror periscope to form a 6.6 cm image of the sun at a position 50 cm east and 660 cm below the lens. Two matched pairs of diodes are positioned on the EW and NS edges of this image, and connected by a servo system to EW and NS motors on the second flat mirror. Since the clock drive on the coelostat mirror is not adequate to track the sun perfectly during the day, this servo system is designed so that if the sun drifts to the north causing the north diode to measure more light than the south diode, this intensity difference is used as a signal to drive the NS motor on the second flat, tilting the mirror to null the signal and correct the drift. Experience indicates that the guiding system has very good sensitivity and stability in keeping the guiding image centered. It also has the dangerous disadvantage of using a different beam for guiding than is used for observing. Evidence will be presented below indicating that the stability of position of the image used for observations is not as good. Attempts to correct this problem by using the same image both for guiding and for observing will also be mentioned.

The second lens used is the observing lens (an AR coated singlet with f = 2.7 m, d = 6.3 cm and clear aperture 5.8 cm) which forms

an image of 2.52 cm (almost exactly 1 inch) diameter at a distance of 3.8 m from the spectrograph entrance slit. This image is used instead of allowing sunlight to fall on the entrance slit since it is of smaller angular extent than the sun itself (2.52cm/3.8m = 1/150, 2 x $R_\odot/r_e$ = 2 x 6.96 x 10^{10} cm /1.496 x 10^{13} cm = 1/107) which permits the use of smaller optical components at other points in the system. This image is used in the Kotov technique to separate light from different portions of the disk for the measurement of relative velocities. Another observing lens has also been in use which has the same dimensions and 6.5 m focal length and which produces a 6.1 cm image of the sun at the spectrograph entrance slit. This lens has been used to make daily scans of the sun's magnetic field with a three arc-minute aperture. Part of the procedure for the scanning observation involves moving the xy-table on which the guiding diodes are mounted until the observing image is centered at the entrance aperture, with position controlled by stepping motors in steps of 0.001 in (25.4 μ) on a 6.6 cm image corresponding to $\sim$ 1" per encoder count. Table 3 shows a record of center positions for observations during June 1976, showing an instability in positioning of the observing image of $\sim$ 10" from day to day. Possible sources and effects of such drifts on the measured relative velocity will be discussed below.

The coelostat and second flat mirrors, the two objective lenses and the periscope are supported by the main telescope structure, which consists of three triangular concrete walls of about 40 tons each tilted up to form a pyramid shape. The optical elements are housed in a 12-foot aluminum dome, with shutters opening to provide a three-foot wide observing

Table 3

Position of Guiding Image in June, 1976

Date	NS Position	EW Position
June 1	1535	1480
June 2	1535	1470
June 3	1540	1480
June 4	1535	1480
June 5	1535	1470
June 6	1535	1480
June 7	1535	1480
June 8	1530	1480
June 12	1535	1480
June 13	1535	1480
June 14	1530	1480
June 15	1525	1460
June 16	1530	1470
June 17	1530	1470
June 18	1530	1480
June 19	1530	1480
June 20	1530	1480
June 21	1530	1500
June 22	1530	1485
June 24	1525	1475
June 25	1520	1475
June 26	1520	1475
June 27	1530	1475
June 28	1515	1475
June 29	1530	1480
June 30	1520	1485

Average NS Position = 1529.81, Variance$^{1/2}$ = 5.798

Average EW Position = 1477.88, Variance$^{1/2}$ = 6.958

window. The proper dome position as a function of time of day is calculated from the Ephemeris parameters for each day of the year, and the resulting curve is fit to the expression $f(t) = A_3 t^3 + A_2 \theta(t) + A_1 t + A_0$ where $\theta(t)$ is a step function at noon, and this fit is used by the telescope driver system to keep the dome positioned properly.

Light from the observing lens passes through the analyzer, consisting of KDP (KH_2PO_4) and linear polarizer, through a 270 Å FWHM bandpass interference filter centered at 5200 Å, and an image slicer. The KDP is modulated with a 110 Hz square wave at $\pm$ 3880 V, which is the quarter-wave potential for λ = 5250 Å. This makes the crystal alternately a positive and negative quarter-wave plate retarder for light at this wavelength. Since for right (left) circularly polarized light, the x-component of the polarization vector leads (lags) the y-component by 90° or 1/4 period, if the quarter wave plate is oriented to produce a 90° phase retardation for the x-component, the x and y components are then exactly in (out of) phase, resulting in light linearly polarized with polarization vector 45° to the right (left) of the y-axis. The effect on right and left circularly polarized components is reversed for a negative $\lambda/4$ retardation (see Figure 4). If a linear polarizer is included oriented 45° to the right of the y-axis, the analyzer will pass only right (left) circularly polarized light when a positive (negative) voltage is applied.

The phase retardation ϕ for KDP is a function of wavelength, $\phi = 2\pi/\lambda \times V \times \alpha$ where α is a constant depending on crystal parameters. It follows that an applied potential which produces a phase retardation of 0.5π at 5250 Å will produce a phase retardation $\phi = 0.5\pi \times 5250/5124 = 0.512\pi$ at a wavelength of 5124 Å. This introduces a very small transmission of the undesired circular polarization by a factor of 3.55×10^{-4}.

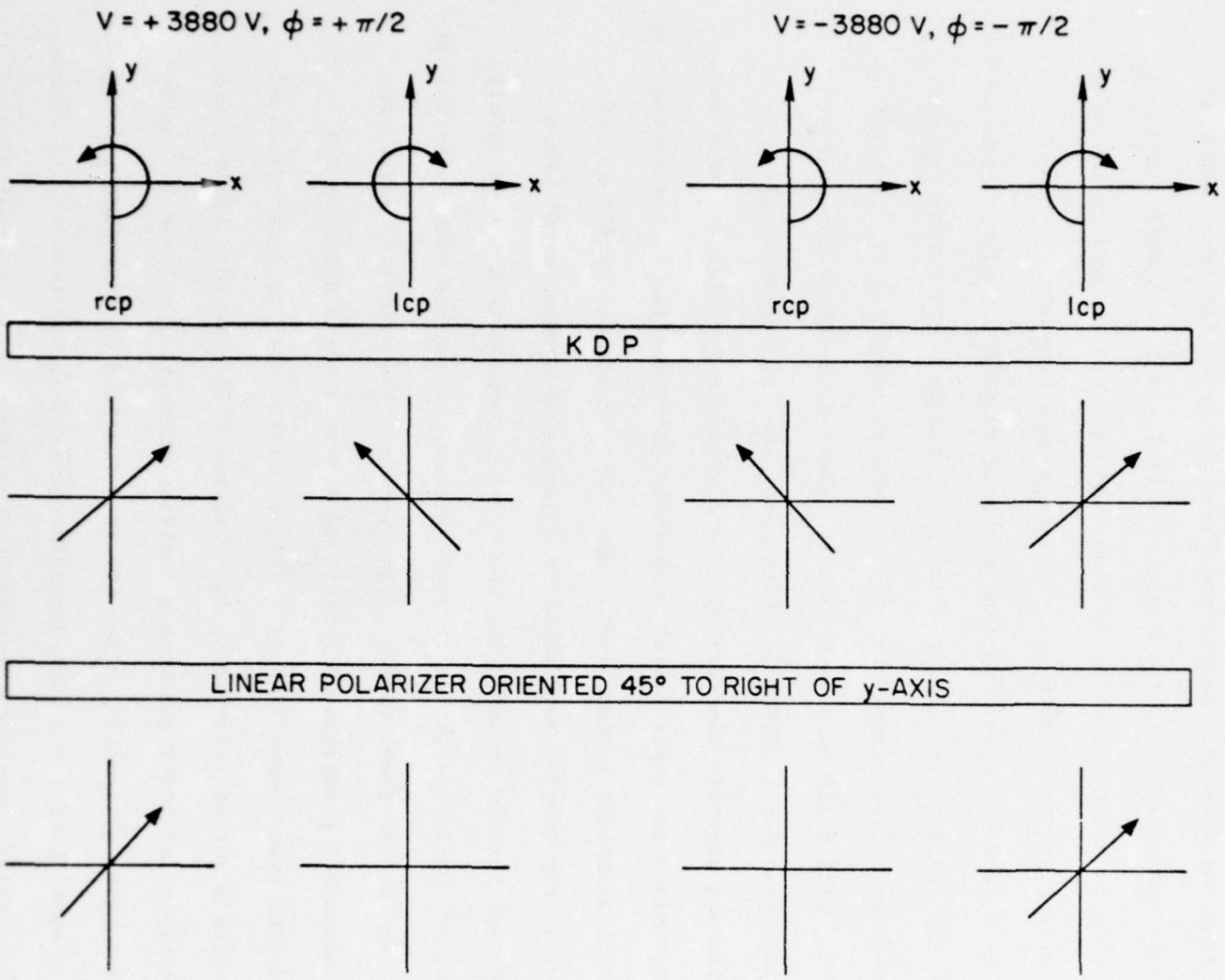

Figure 4. Diagram showing how a KDP with a linear polarizer oriented 45^{o} to the right of the slow axis can be used to pass only right circularly polarized light for a potential applied in one direction, and left circularly polarized light for the opposite potential.

The interference filter is included to remove overlapping orders in the spectrograph. For multiple sources or grating rulings separated by distance d, wavelength λ will have an nth order maximum at $n\lambda = d \sin \theta$, so a grating angle giving 5124 Å light in fifth order will also produce 6405 Å in fourth order and 4270 Å in sixth order.

The image slicer converts a square beam of light (a required shape for the analyzing optics) into a long, thin beam required for the spectrograph. The instrument consists of an internally reflecting prism which deflects the incident beam horizontally, and a series of mirrors, each sticking successively farther into the beam to "slice off" a piece of this beam and reflect it downward through the entrance slit into the spectrograph. The illustration (Figure 5) shows only 4 slices--the actual image slicer used consists of 10 slices, matching the 9mm x 9 mm entrance aperture to the 0.8 mm x 10 cm spectrograph entrance slit, with some light lost. The mirrors are in theory aligned so that each directs light to the center of the Littrow lens at the bottom of the spectrograph pit. However, experimentally it was found by taking each slice, one at a time, and masking off the others, that the end slices are not perfectly aligned. A copy of the sketch made showing the positions of the images associated with each slice is shown in Figure 6.

The spectrograph is a vertical Littrow spectrograph with a 22.8 m focal length. It is contained in a 75-foot deep pit lined with a 1/2 in steel liner, 6 feet (1.8 m) in diameter. The Littrow lens is six times as large (6 in or 15.36 cm clear aperture) as the mean field observing image and six times as far (22.8 m) from the entrance slit so that a pinhole image of the mean field image will just fit in the Littrow

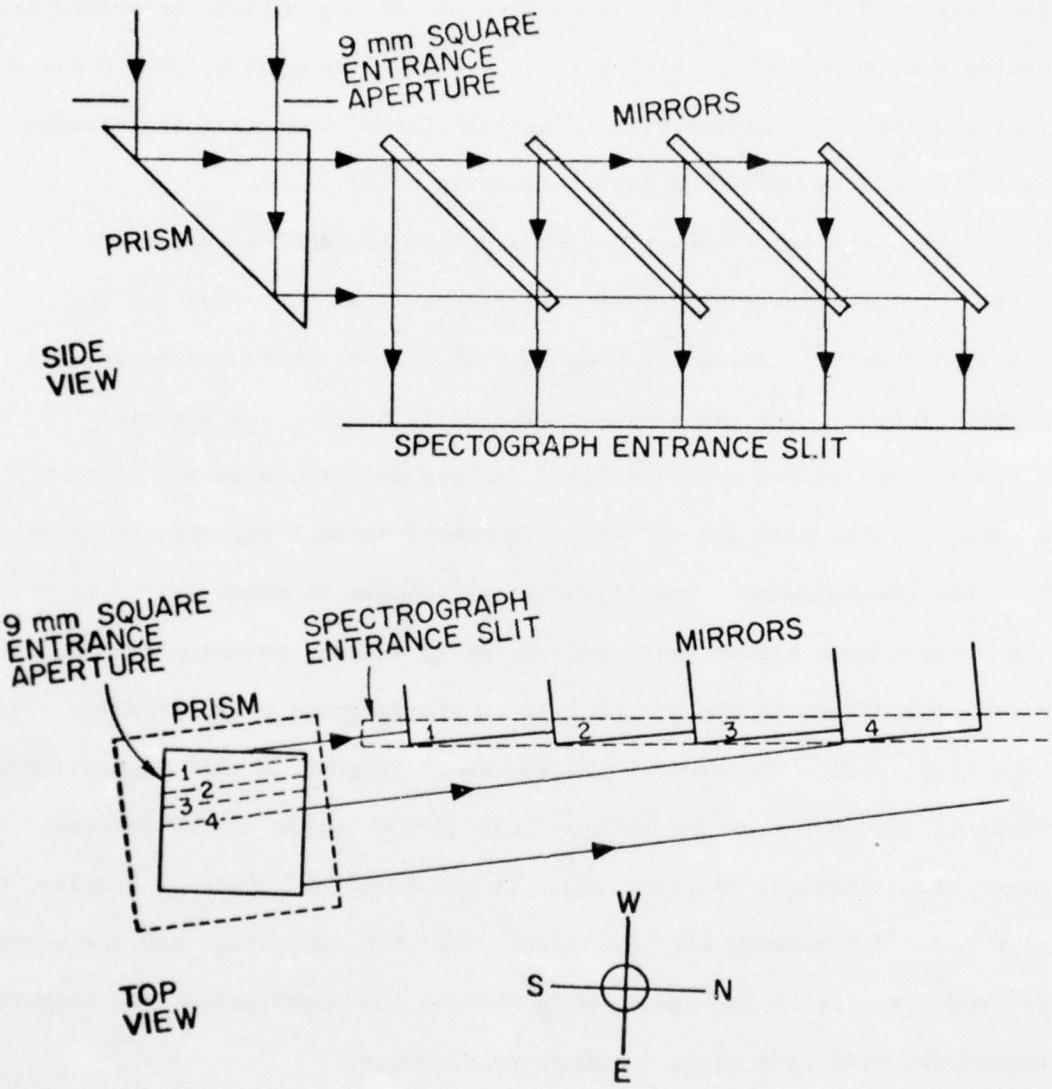

Figure 5. Diagram showing side view (top) and top view (bottom) of an image slicer. Only four of the ten slices are illustrated.

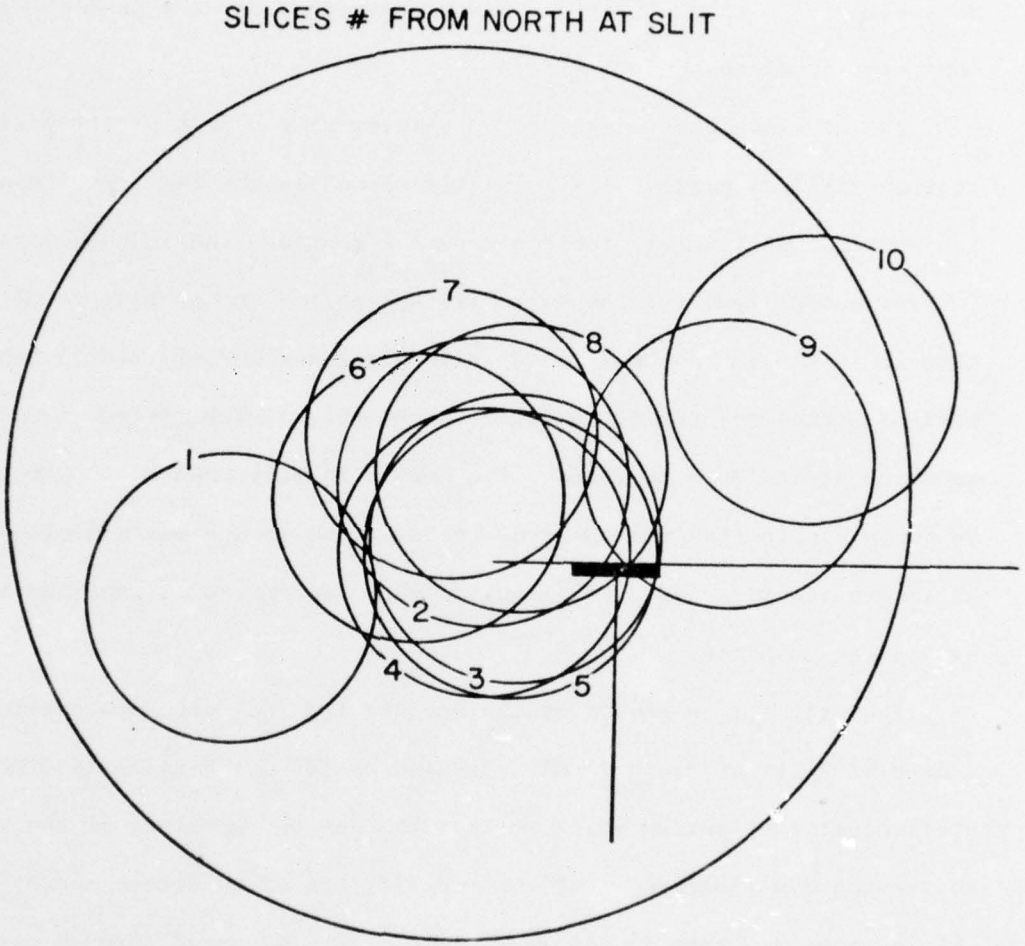

Figure 6. Diagram made from an experiment mapping the orientation of the different slices of the image slicer. The large circle represents the boundary of the Littrow lens, the smaller circles are the image produced by the central 1/4 of the solar image for each of the ten slices of the image slicer. The lines are the shadows of masks used to catch reflected light. North is to the right.

lens. Unfortunately, the entrance slit is not a pinhole, as point out in private communication by A. B. Severny. The result is that the image at the Littrow lens is not sharp and some vignetting results. Measurements of this effect and its consequences for the present measurement will be discussed below.

The Littrow lens (an AR coated triplet of f = 22.8 m diffraction limited within a plane 86 cm in diameter) collimates the light from the entrance slit before incidence on the grating, and in turn focuses the reflected light for the exit slit assembly. The grating is of ruled area 12 in x 6 in (30 cm x 15 cm) with 633 lines per mm, blazed for maximum efficiency for fifth order in the green. The Littrow lens can be moved up and down to focus. The method finally used by Thomas L. Duvall to focus was to find the spectrograph position giving maximum slope for an absorption line, with other optics and electronics aligned and balanced as well as possible.

The exit slit assembly of the Babcock-type magnetograph consists of a pair of slits of width 75 mA separated by 18 mA. Physically, these slits consist of prisms which reflect the desired portions of the spectrum to the photomultipliers, with the width of the slits determined by adjustable screens as shown in Figure 7. The light is passed through elongated segments of spherical lenses (to match the slit shape) which produce an image of the grating on the photocathodes of a matched pair of photomultipliers type EMI 9656 RM with spectral response S-11. The exit slit assembly can be driven manually along the spectrum, or it can be set to follow an absorption line (or an emission line) by a servo mechanism. The position of the exit slit assembly is read by a 12-bit encoder to an accuracy of 0.6 μ per encoder count.

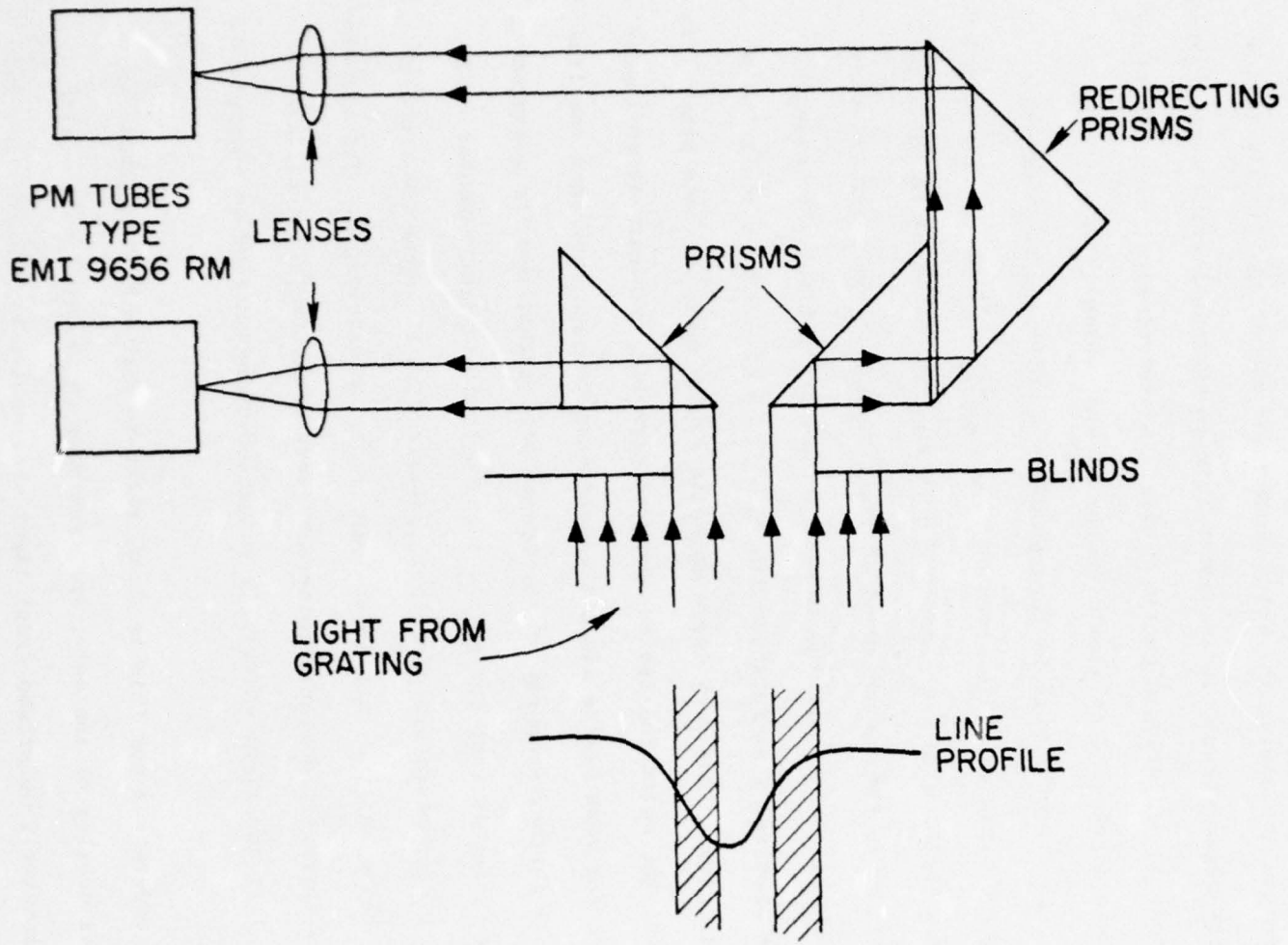

Figure 7. Diagram of exit slits used in the Stanford Solar Observatory. Light is collected from the wings of an absorption line and sent to each of two matched phototubes for measurement.

Before explaining the Kotov method for measuring velocity fields with the magnetograph, it is appropriate to explain how the magnetograph functions in measuring magnetic fields. A line-of-sight magnetic field removes a degeneracy in atomic energy levels, which is referred to as the Zeeman effect. This in turn produces a splitting in Fraunhofer absorption lines which is given by $\Delta\lambda = (\mu_o/hc)\, g\lambda^2 B$ where μ_o is the Bohr magneton (9.273×10^{21} erg/gauss), h is Planck's constant (6.626×10^{-27} erg-sec), c is the vacuum speed of light, and g is the Langé g-factor which depends on the quantum numbers of the transition. For example, for the spectral line FeIλ5250.216, g = 3 and $\Delta\lambda = 3.86 \times 10^{-5} B$ for B given in gauss. For very large magnetic fields such as those present in sunspots, the splitting can be observed directly, but this is no longer possible for weak fields since the splitting is much less than the line width. A further property of the Zeeman effect that permits measurement of weak fields is that for $\Delta m = \pm 1$ and a line of sight magnetic field, the two σ components are circularly polarized in the opposite sense as well as being shifted in opposite directions in wavelength. The magnetograph is therefore designed to measure very sensitively the difference between left and right circularly polarized components of an absorption line.

To understand how this is done, refer to Figure 8 which shows an idealized drawing of the solar spectrum near an absorption line with right circularly polarized (rcp) light represented by a solid line and left circularly polarized (lcp) light by a dashed line. The exit slit assembly is positioned so that one phototube measures the intensity on the red wing of the line and the other on the blue wing. To avoid

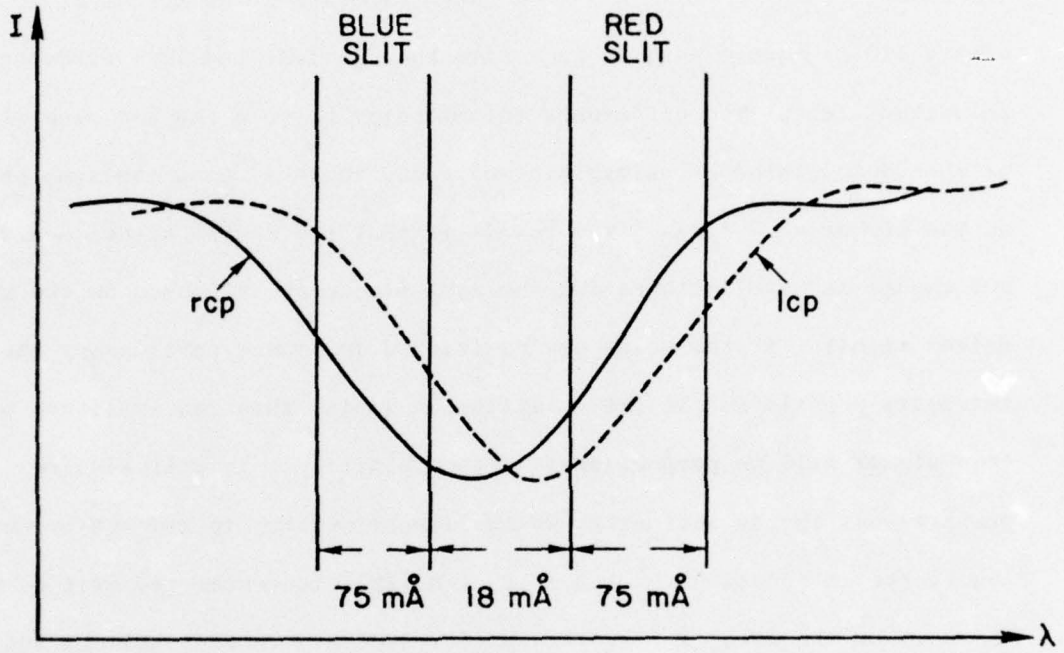

Figure 8. Diagram showing a typical line profile for an absorption line. The solid line represents right circularly polarized light, the dashed line represents left circularly polarized light. Exit slits are not drawn to scale--actual dimensions are given. Comparison may be made with the measured line profile of Figure 12.

confusion, the rcp and lcp light may be distinguished by + and -, and the intensity measured at red and blue slits by R and B respectively. R^+ then becomes the red wing intensity of rcp light, etc. A signal Zeeman $\equiv (B^+ - R^+) - (B^- - R^-)$ is defined by driving the KDP crystal with a 110 Hz square wave to pass alternately right and left circularly polarized light. The difference in intensity between red and blue slits is then demodulated by multiplying by a square wave using the same phase as the KDP driver signal. The result is that the Zeeman signal measures any change in wavelength having the same frequency and phase as the KDP driver signal. If the slits are positioned in linear portions of the intensity profile and if the splitting is small, then the amplitude of this signal will be proportional to the splitting. It will also be proportional to the intensity, which proportionality is removed by dividing by the intensity $\equiv (R^+ + R^- + B^+ + B^-)/2$. To center the exit slit assembly on the line, the average difference in intensity between the two wings, called the DC difference signal $\equiv (R^+ + R^-)-(B^+ + B^-)$, is used by the servo system which drives the slit to null this signal and center the slit assembly on the line. The servo system is designed with a response time that is slow compared to the modulation frequency so that the servo will not respond to shifts in wavelength produced by the KDP modulation.

Velocity Measurements Using the Servo Encoder

Since the servo keeps the exit slit centered on the line, using an encoder to record the position of the exit slit enables one to measure shifts in wavelength of the line at the same time the magnetic measurement is made. Since a line-of-sight velocity produces a Doppler shift in

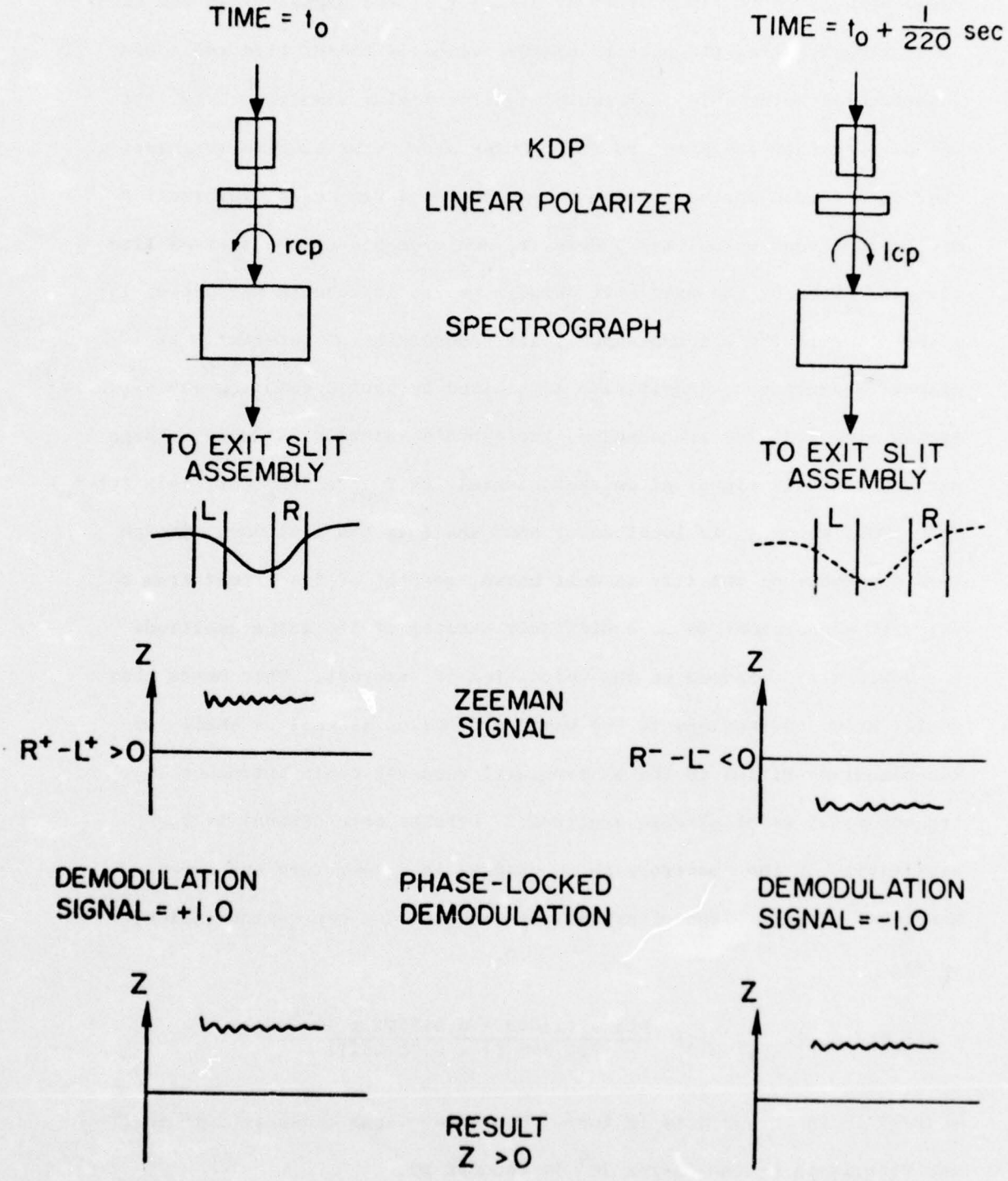

Figure 9. Diagram showing how the magnetograph obtains the Zeeman signal.

wavelength given to first order by $\Delta\lambda/\lambda = v/c$, the magnetograph has been used extensively in the past to measure velocity fields with the added advantage of being able to measure magnetic fields simultaneously. It was planned that the Stanford Solar Observatory make such measurements over an extended period of time to search for large-scale organization of low-amplitude velocities. However, measurements of the average line position given by the exit slit encoder proved inadequate because of instabilities in the spectrograph at all frequencies of interest. At highest frequencies, sensitivity is limited by photon counting and servo response time. At low frequencies, the earth's rotation produces a large diurnal velocity signal given approximately by $V_{rot} = 2\pi R_e \cos(\ell)\sin((t-t_o)/24h)/24h$, where t_o is local solar noon and ℓ is the latitude. Though this component of velocity is well known, removal of its effect from a velocity measurement is more difficult because of its large amplitude ($\pm$ 367.9 m/s) compared to the velocities of interest. This means that small, known corrections to the basic expression as well as small, unknown nonlinearities in the instrumental response could introduce low frequency drifts of sizable amplitude. Perhaps more serious is the sensitivity of the spectrograph to changes in temperature and pressure. The index of refraction of dry air is given by the expression (Allen, 1973):

$$n(p,T)-1 = (n_{15,760}-1)\ \frac{P[1 + (1.049 - 0.0157T) \times 10^{-6} p]}{720.883\ (1 + 0.003661T)}$$

where T is in °C and p is in torr. For water vapor pressure f in torr, the refraction factor $(n-1) \times 10^6$ is reduced by:

$$\frac{0.064 - 0.000680/\lambda^2}{1 + 0.003661T}\ f$$

Since the grating spectrograph measures wavelength which depends on the index of refraction, changes in temperature, pressure, or relative humidity cause changes in wavelength which are hard to distinguish from those which are caused by velocity fluctuations. A wavelength shift corresponding to 10 m/s for the FeIλ5124 spectral line can be produced by a change of 0.09 torr in pressure or 0.03°C in temperature or 3% in relative humidity for ambient conditions of 760 torr, 20°C, and 10% relative humidity. Such variations have been previously recognized as being responsible for low frequency components in a velocity signal. For example, Tanenbaum (1971) recorded a 1.4 mA/hr (= 57.2 m/s/hr) trend in velocity measurements which could largely be accounted for by a pressure change of -0.63 torr/hr. Accurate pressure measurements are not yet available for the Stanford Solar Observatory, so such effects could not be removed.

Another low frequency drift in wavelength is produced by imperfections in the computer algorithm used to rotate the grating for observation of different spectral lines. After such motion is performed, a slow drift in the recorded exit slit position is apparent, suggestive of a slow relaxation of some small stress introduced by the change in grating angle. A procedure for moving the grating which removes most of these drifts has been developed by Thomas L. Duvall, though not until after the observations described herein had been made.

Even with these previously known limitations at high and low frequencies, it was hoped that at intermediate periods, especially in the neighborhood of the well-known five-minute oscillation, sufficient spectrograph stability might be obtained to permit a long-term study of amplitude variations in these oscillations observed over the full disk. Attempts to study such

oscillations directly were unsuccessful due, ironically, to the same kind of physical mechanism responsible for vertical motions in the outer layers of the sun. Observations and theories currently indicate that the outer layers of the sun are convectively unstable because of a super-adiabatic temperature gradient. The Stanford vertical Littrow spectrograph was found to be convectively unstable because of the geothermal temperature gradient. The first indications of such a problem were that measurements of rms fluctuations of the measure velocity signal, filtered to pass only periods between 1 and 15 minutes, gave an amplitude of 50-100 m/s. A convective origin was suspected, and measurements were made which indicated a temperature of 18.5°C at the bottom and 17.5°C at the top of the spectrograph pit. Consultation with a local geologist indicated that such a gradient (1.0°C/22.8 m ~ 45°C/km) could be of geological origin. Heaters were installed at the top of the spectrograph pit, but did not eliminate the instability because, as revealed by further measurements, the stable gradient was established for only the top third (~ 25 ft or 8 m) of the pit. Further confirmation of the convective origin was obtained by forcing air cooled by an air conditioning unit into the bottom of the pit, which reduced the amplitude of fluctuations. An improvement was also produced by gradual penetration of summer warmth down to a 50 ft depth giving a stable gradient over most of the vertical distance. A thorough and difficult insulation of the lower 40 ft of the pit was undertaken in an attempt to reduce the conductive transport of heat energy (which drives the convection) into the bottom of the pit. These efforts had little effect on the measured temperature gradient, but may have contributed to smaller fluctuations in the velocity signal.

Velocity Measurements Using the Kotov Subtractive Technique

The history of this investigation might well have ended (without ever being told) were it not for the development by Valeri A. Kotov of the Crimean Astrophysical Observatory of a technique for separating wavelength shifts of instrumental origin from those originating in line-of-sight velocities on the sun. The basic idea is to measure the difference in wavelength for light originating at different places on the solar disk. This is accomplished very simply by inserting optics at the position of the mean field image to produce right circularly polarized light for the center of the disk and left circularly polarized light for the limb. Since the magnetograph is designed to measure the difference in wavelength between the two oppositely polarized σ components of a magnetically sensitive absorption line, this modification gives a direct measure of the difference in wavelength between the center and the limb of the disk.

The apparatus used in the present investigation is shown in Figure 10. The light first passes through a linear polarizer, then through a quarter-wave plate. These are aligned to produce lcp light. The light next passes through a half-wave plate, mounted on optical quality glass so that it covers only the center portion of the image, which changes lcp light to rcp light. Finally, the light passes through an iris diaphragm which is adjusted so that rcp and lcp components are of equal intensities. This is done since the magnetograph is designed for rcp and lcp light of equal intensities.

Masks were made to pass only center or limb light and the KDP modulation could be turned off to measure only lcp or rcp intensity. Measurements of these intensities and of the ZI signal produced by displacing

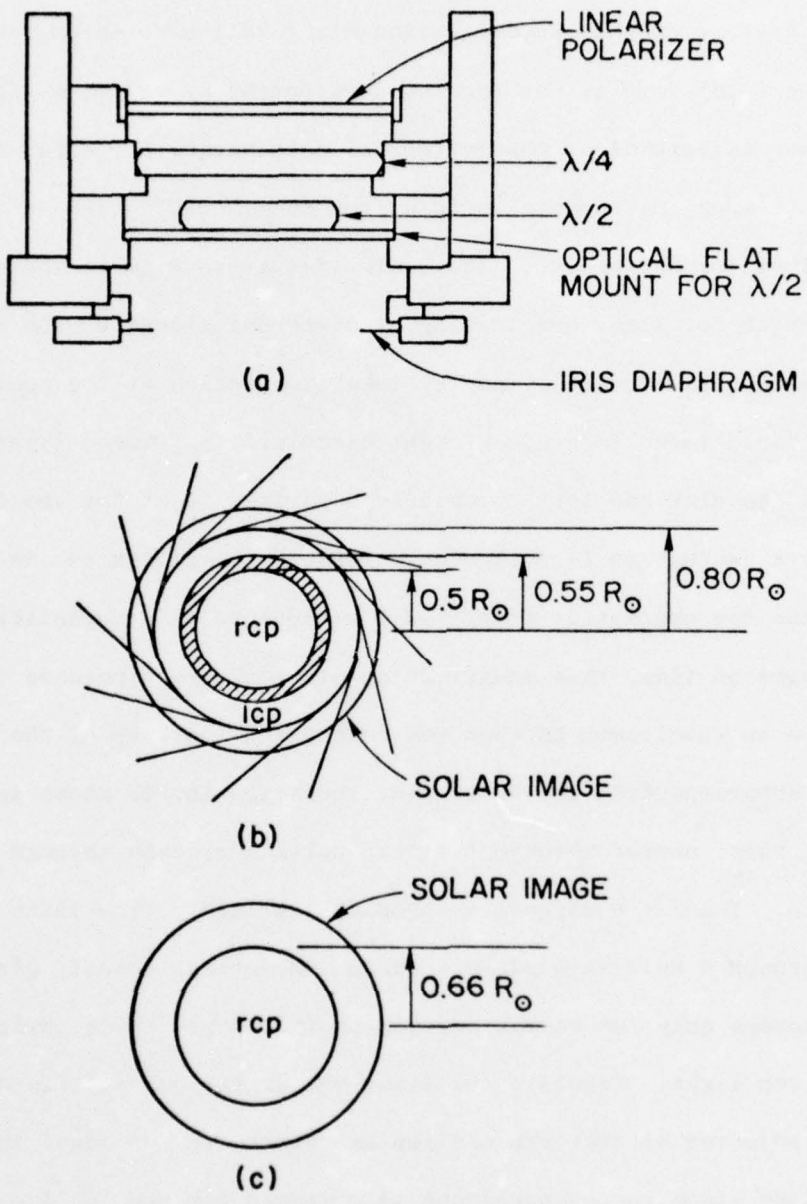

Figure 10. Diagram showing (a) side view of the Stanford polarizing aperture, (b) top view of the Stanford aperture, and (c) top view of the Crimean aperture.

the exit slits from line center while passing only center light were used to calibrate the instrument, using the following expression, derived in Appendix A:

$$\lambda_\ell - \lambda_c = \frac{ZI\ (\Delta\lambda_{calib})}{K} \frac{(I_c^+ - I_c^-)(I_c^+ + I_c^- + I_\ell^+ + I_\ell^-)^2}{2(I_c^+ + I_c^-)(I_c^+ I_\ell^- - I_c^- I_\ell^+)}$$

Here $\lambda_\ell - \lambda_c$ is the difference in wavelength between center and limb corresponding to a Zeeman/Intensity signal of ZI, $\Delta\lambda_{calib}$ is the known wavelength shift introduced in calibration and K is the resulting signal, and the intensities are the continuum intensities measured separately for the two different circular polarizations and the two different portions of the image. An example of the September 13, 1976 alignment and calibration is given in Appendix B.

The apparatus used for similar measurements at the Crimean Astrophysical Observatory is different in two important respects:

1) A right circular polarizer of radius 0.663 $R_\odot$ is placed over the center of the image of the disk, but there is no circular polarizer over the limb. This means that the apparatus and analyzer will pass light from the full disk for half of the modulation cycle, and only from the limb during the other half. The signal may still be interpreted as the difference in wavelength between center and limb light with the addition of a factor $(2 + \beta)/2$, where β is the ratio of center to limb intensity, I_c/I_ℓ. The derivation of this factor is similar to that described in Appendix A.

2) No iris diaphragm is used to mask off the extreme limb. The two apertures are shown side by side in Figure 10. The consequences of the differences will be discussed in detail below.

The great advantage of this technique is that the difference in wavelength is measured. Since the non-solar changes in wavelength described above (earth's rotation, changes in temperature or pressure, grating drifts, and convection in the spectrograph) affect center and limb light in the same way, a measure of the difference in wavelength permits the removal by subtraction of most of these effects. Since the magnetograph is designed to measure very small wavelength differences. the result is great sensitivity. This can perhaps best be shown by plotting side by side (Figure 11) the power spectra from a single observation (May 23, 1976) taken in one case from the encoder on the exit slit assembly, in the other case from the ZI signal using the Kotov technique. To quantify the increase in sensitivity, 18 one-minute observations were made while observing in the Kotov mode. The average standard error was equivalent to 3.68 m/s for the servo encoder, and 1.04 m/s for the ZI signal, which is a factor of 3.55 reduction. From magnetic measurements, an error of only $\sim$0.1 m/s would be expected from photon statistics. The remainder is probably due to turbulence, which was shown to affect the ZI signal by turning on a spectrograph fan in the middle of an observation.

There are also complications and subtleties in this relative velocity technique that should be explained. Two which proved to be of small importance are differences in center and limb profiles due to rotation and limb red shift. Robert Howard of the Mt. Wilson observatory pointed out that rotation would be expected to broaden the limb line profile more than the center line profile therefore confusing the calibration and/or interpretation of the signal. To examine this effect, line profiles were made in lcp (limb) and rcp (center light, as shown

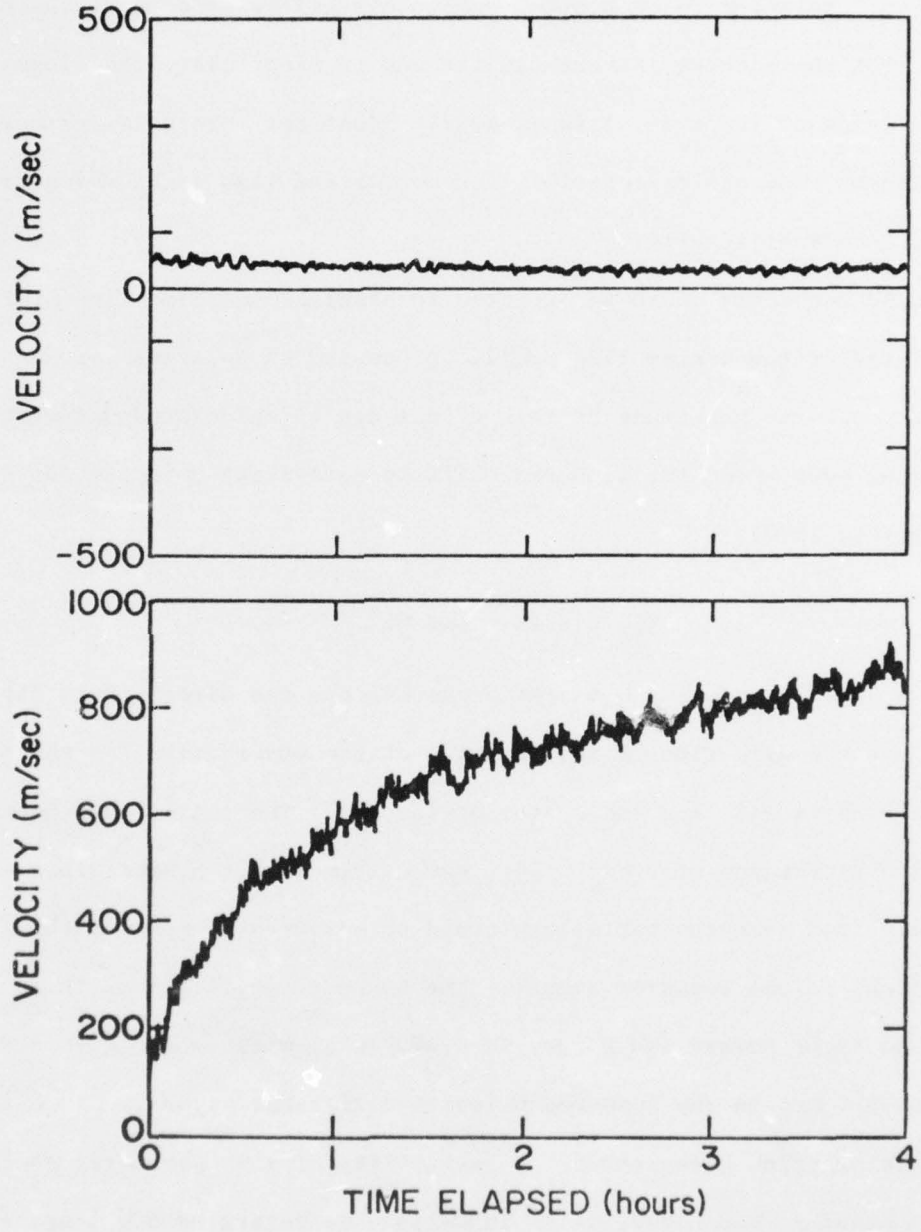

Figure 11. Plots of the velocity signal obtained using (top) the ZI signal using the velocity difference technique, and (bottom) the exit slit position recorded by the encoder. Both are taken from the May 23, 1976 observation.

in Figure 12. The two line profiles are displaced in intensity and wavelength relative to each other due to misguiding effects discussed below, but their shape is very similar and in particular, the slope at the position of the exit slits is nearly identical. This is further verified by separate calibrations for center and limb light which give almost identical results.

Limb red shift would be expected to displace the limb line profile to the red of the center line profile producing an apparent velocity difference. The magnitude of this effect can be calculated using the following expression for limb red shift in equivalent velocity (Howard and Harvey, 1970):

$$V_{ls} = e\ (1 - \cos\ \theta)^2$$

where $e = 0.339$ km/s and θ is the angle between the direction to the earth and the direction of the location of the observation (on the solar surface) as viewed from the center of the sun. The result is a measured velocity difference of $V_c - V_\ell = 24.1$ m/s. This is not a negligible quantity, and even the variations could be a source of some of the variations in the measured signal. The standard deviation of the e values in Table II of Howard and Harvey is 0.079 km/s, which would give a deviation of 5.6 m/s in the measured velocity difference signal. Since there is no information given about the variability of this parameter on time scales shorter than a day, it is impossible to determine how large a source of signal variations it may be. In any event, the amplitude of variations thus produced would be much less than those observed, (see Figure 20) which suggests an instrumental rather than solar origin.

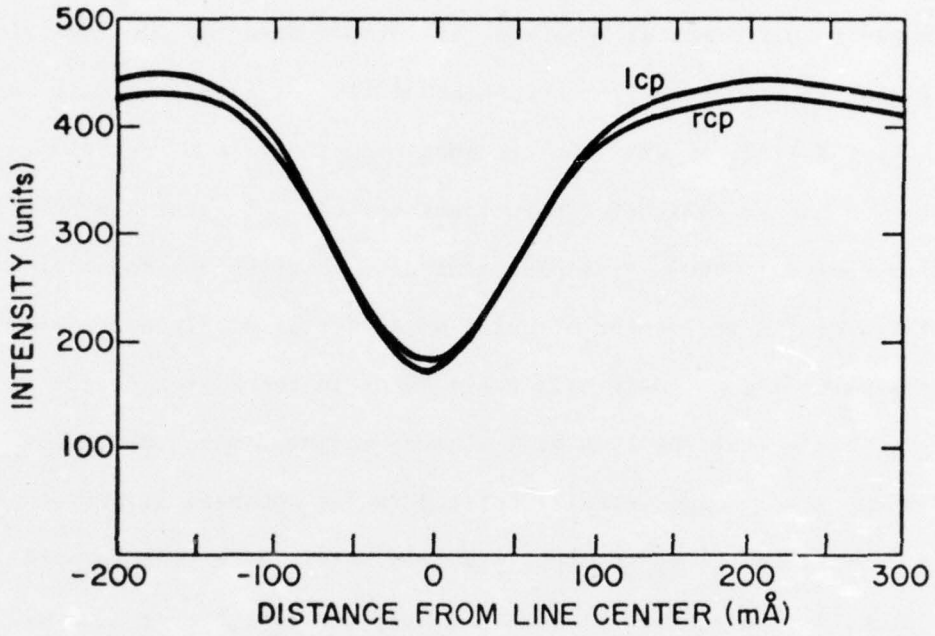

Figure 12. Line profiles for the line FeIλ5123.730 Å, measured May 17, 1976. The top line is for left, the bottom line for right circularly polarized light.

The effect of imperfect centering of the aperture which defines and separates limb and center light may be seen most clearly for an aperture not surrounded by a diaphragm, such as used in the Crimea (Figure 10). If one neglects differential rotation, it follows directly from spherical geometry that the line-of-sight component of the rotational velocity on the disk varies linearly with the distance from the axis of rotation. Since the sun has an equatorial rotational velocity of about 2 km/sec and an angular radius of 960", a displacement of 1" corresponds to a velocity of about 2 m/s. If the center circular polarizer is displaced toward the east limb by 1", not only will every point in the center gain a velocity of 2 m/s, but the limb will also be weighted more toward the west limb and its average velocity shifted in the opposite direction, though by much less. When the apparatus includes a diaphragm to mask off the limb, a displacement of the apparatus toward the east limb will result in an increase in average velocity measured for both center and limb. If the disk were a circle of uniform intensity, there would be no instrumental signal, but due to the effects of limb darkening, there is still an error for improper guiding, though of reduced amplitude.

A computer calculation was made of the signal produced for an improperly centered aperture. The center or limb velocities were assumed to be average velocities weighted for intensity:

$$\langle V \rangle = \int VI d\tau \Big/ \int I d\tau$$

The velocity expression used was that computed by Howard and Harvey (1970) from magnetograph observations, which expressed in solar disk coordinates becomes:

$$V(r,\theta) = r \sin\theta(1.93-0.244(r\cos\theta)^2-0.308(r\cos\theta)^4)+ 0.339(1-\sqrt{1-r^2})^2$$

where r is the distance from the center of the disk in units of $R_\odot$, θ is the angle from solar north, and the velocity is given in km/s. The intensity is taken from the limb darkening expression given by Allen (1973):

$$I(\theta) = 0.26 + 0.96 \cos\theta - 0.22 \cos^2\theta$$

where θ is the angle between the line of sight vector and the sun's radius vector for the point being observed. The effect of improper positioning was simulated by displacing the aperture relative to the disk, and the result is shown for the Crimean and Stanford apertures in Figure 13.

It was also possible to simulate this effect experimentally in three different ways:

1) The guiding box was displaced and the aperture kept fixed,

2) the aperture was displaced with guiding box fixed, and

3) the aperture was displaced, with guiding diodes positioned at the edges of the aperture so the image would remain in the same position with respect to the aperture. The results are plotted, along with the calculated error signal, in Figure 14.

The first two experiments resulted in an aperture improperly centered on the image and produced errors of a magnitude close to the calculated value. The third aperture also produced an error of similar magnitude even though image and aperture remained in the same relative positions. The reason for this can be seen with the aid of Figure 15. Since the spectrograph entrance slit produces a near pinhole image of the sun at the Littrow lens, if the mean field image is displaced and the slit and Littrow lens are fixed, this pinhole image will be displaced off of the Littrow

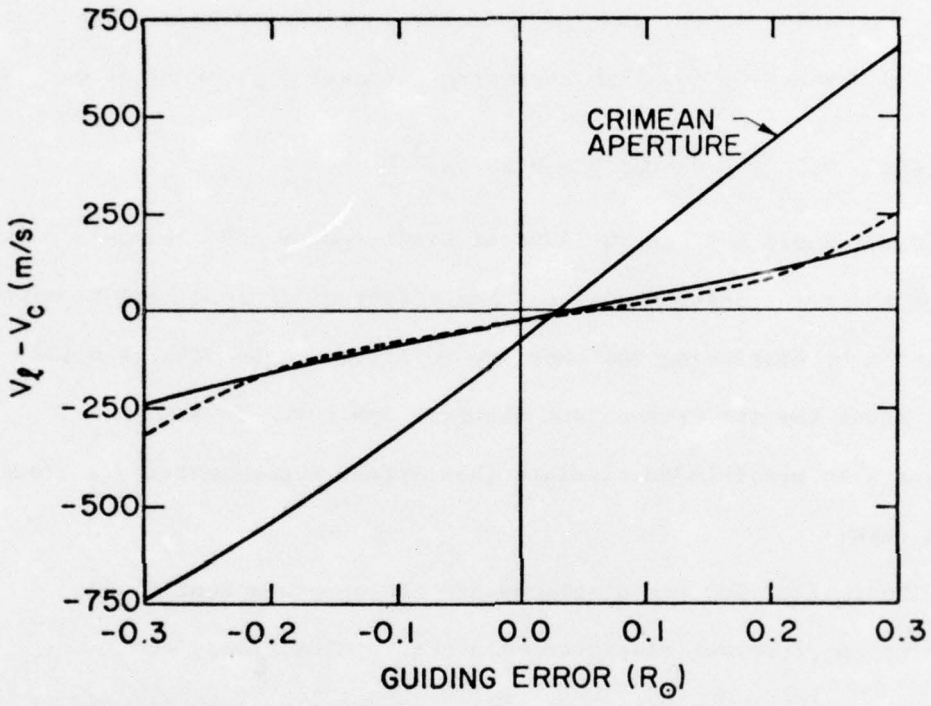

Figure 13. Plot of calculated values of signal produced by guiding errors for the Crimean and Stanford apertures. The dashed line is the curve calculated for a displacement of the Stanford image relative to the grating, the unlabelled solid line for a displacement of the Stanford image relative to the polarizing optics.

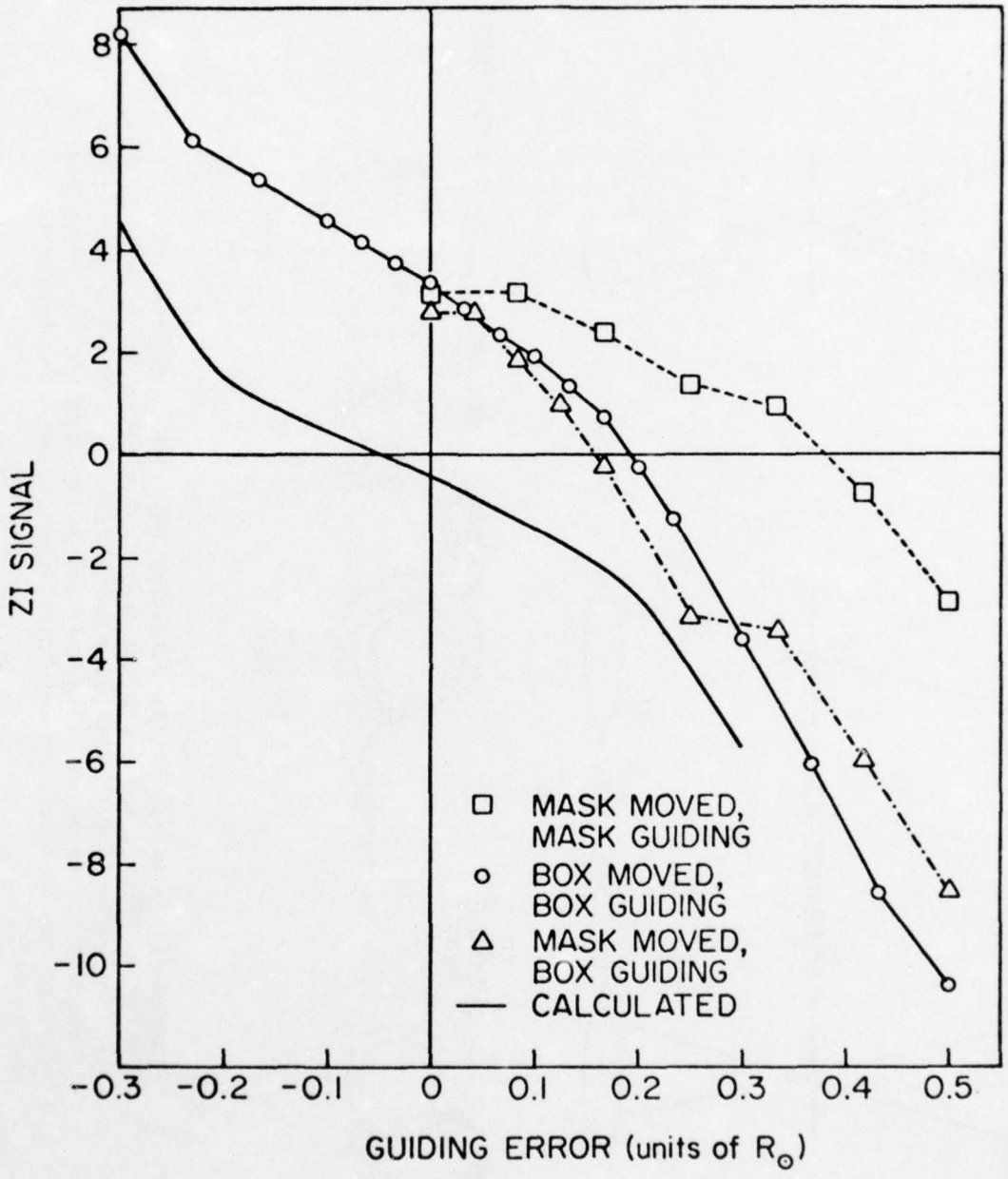

Figure 14. Plot of signal measured for solar image displaced relative to polarizing optics and/or Littrow lens. The mask is the polarizing aperture, the box is the box containing the diodes ordinarily used to position the guiding image, unless mask guiding is specified. The lower solid line shows the calculated signal for comparison--the offset is the actual offset produced by the instrument.

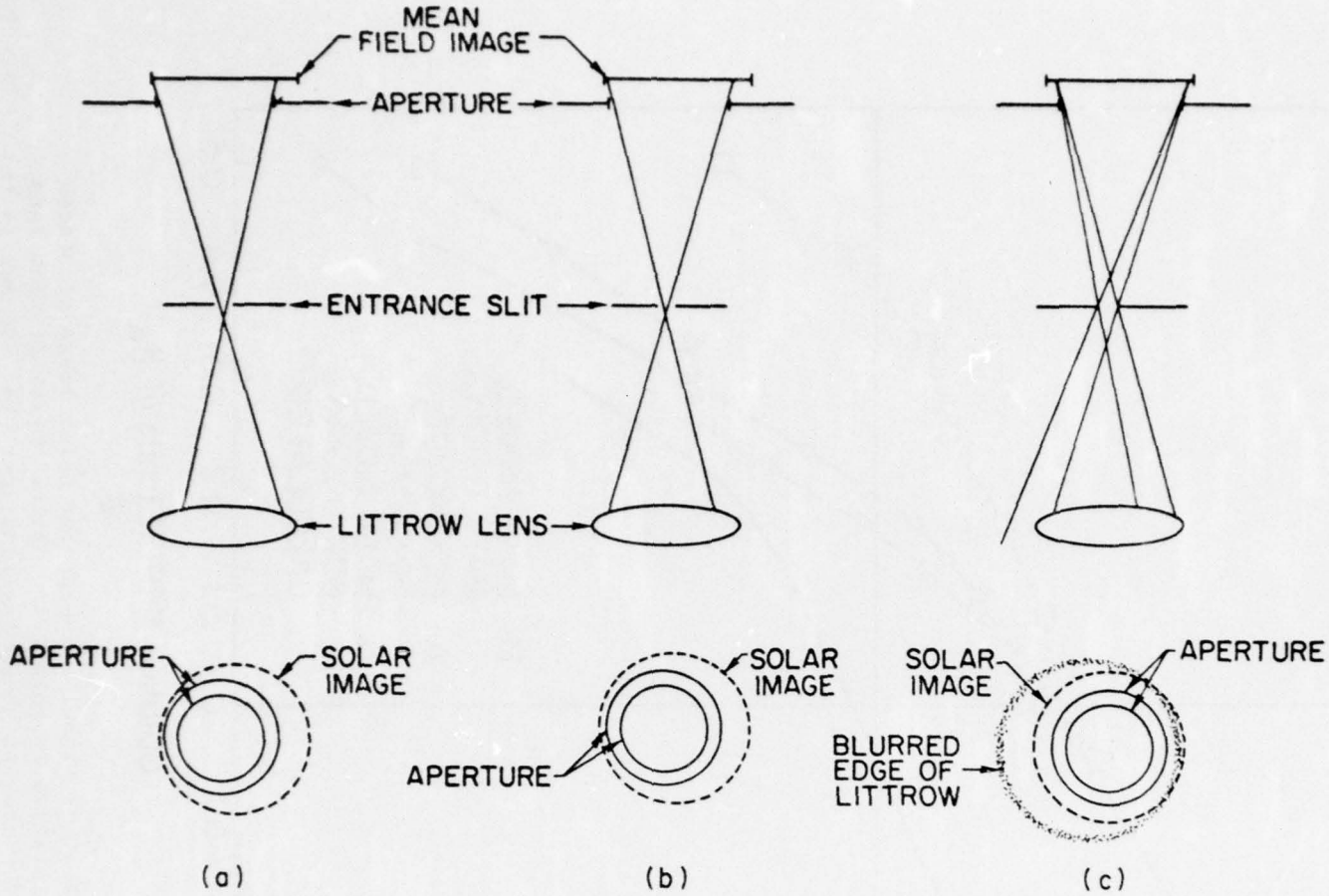

Figure 15. Diagram of the effect of the different experiments plotted in Figure 14. Figure (a) shows the result of displacing the polarizing aperture while keeping the solar image fixed, (b) shows the result of displacing the image with the aperture fixed, and (c) shows the result if image and aperture are both displaced (together) relative to the spectrograph.

lens, and light from the limb will be lost. If the pinhole image formed were perfect, no light would be lost unless the displacement was as great as the portion of the image masked off ($\sim 0.2\ R_\odot$). However, for a finite entrance slit and an imperfect image slicer, the pinhole image is out of focus so that any displacement causes a loss of light which changes the weighting for different parts of the disk and produces a velocity signal due to the sun's rotation. The error signal for such displacements was also simulated on the computer, assuming an isotropic smearing of a point source at the image to approximate the effects of a 9 mm long entrance aperture, Fraunhofer diffraction from the 0.8 mm wide slit, and the imperfectly oriented elements in the image slicer. The calculated values are also plotted in Figure 15. The same error results if the image slicer is not aligned properly, causing light to be deflected off of the Littrow lens. A large, abrupt change in the baseline of the velocity signal near the end of June 1976 was caused by such a misalignment, apparently caused by a workman bumping the spectrograph head while most of the observers were at the 148th AAS meeting. Though this misalignment was unfortunately not discovered until August, calculations indicate only small changes in sensitivity to either the five-minute oscillation or to low order global modes. It does not seem likely that drifts in the image slicer could produce the regular diurnal variations in the observed signal.

The sensitivity to solar rotation would not be a problem if the guiding system positioned the image perfectly, and could even be of little consequence were it a constant offset. However, as mentioned above, there is good evidence that there is a variable error in the relative

positioning of image and polarizing aperture and/or of the image and aperture relative to the Littrow lens. This is believed to be the principal cause of slow drifts in the observed velocity difference signal. The best example of cause and effect is from the observation made August 26, 1975 as shown in Figure 16. The position of the image with respect to the aperture was recorded at various times during the observation, and later analysis showed good qualitative agreement between image displacement and signal. There are at least three possible sources of such variations in image position:

1) The mirrors and lenses are supported by the basic pyramidal support structure, consisting of three tilt-up triangular concrete walls. These were originally painted only with a clear sealer and absorbed sunlight readily. It is postulated that the southeast wall would heat up and expand in the morning and the southwest wall in the afternoon, thus causing displacements of the top of the building to the west in the morning and to the east in the afternoon. Since the mount for the polarizing aperture is a beam suspended from the mirror support structure and attached at the floor, displacements of aperture and image relative to each other might be small. However, since the image would still be displaced relative to the fixed entrance slit and Littrow lens, an artificial velocity could still be produced as demonstrated by the third experiment above. The error which would be expected over the course of a day agrees in sign with observed diurnal shifts in signal. The support structure was painted white to reduce heating effects, and the diurnal drift was reduced but not eliminated. This might suggest that the other effects described below are important, though they would not be as likely to produce a regular daily pattern.

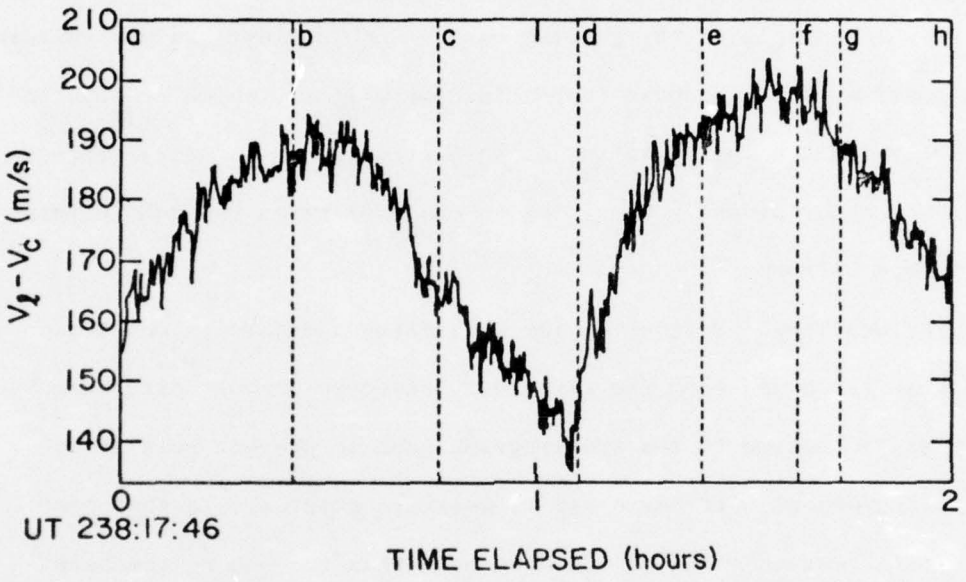

Figure 16. Observation of August 26, 1975. The image position relative to the polarizing aperture was estimated visually (in units of approximately 0.3 - 0.5 mm) as follows: (a) centered, (b) 1/2 - 1 unit SE of center, (c) centered, (d) 1/4 unit SSW of center, (e) 3/4 - 1 unit E of center, (f) 3/4 - 1 unit E of center, (g) 1/2 - 3/4 units E of center, and (h) 1/2 - 3/4 units ENE of center. The aperture used was of different dimensions and geometry than that illustrated in Figure 10.

2) Since guiding is done on a different beam of light than observing, any shifts in relative position will introduce an error. Such shifts have been noticed, as mentioned above, with an amplitude of $\sim 10''$. This is believed to be due to shifts in position of the two mirrors of the periscope which displaces the guiding beam. Such distortions may in turn be due to stresses in the beam supporting the mirrors, which are caused by thermally induced shifts in the support structure. A similar effect was produced experimentally by having an observer twist the beam holding the periscope mirrors.

3) As mentioned previously, the polarizing aperture is mounted on a steel beam suspended from the pyramidal telescope support structure and fastened at the bottom to the spectrograph head to prevent relative lateral displacement. If there are temperature gradients in the room sufficient to heat one side of the beam more than the other, the beam would bend like a bimetallic strip in a thermostat, displacing the aperture relative to the image. Early observations showed large irregular deviations in signal with 30-60 minute periodicities. Since the air-conditioning system was known to have a cycle time in this range, the temperature was recorded during observations and the temperature variations seemed well correlated with many of the 30-60 minute variations. A first order solution was possible with the coming of cooler fall weather when the air conditioner could be turned off if doors in the observing room were left open. This modification greatly reduced the signal fluctuations in the 30-60 minute period range. The air conditioner was later modified with ducting and more delicate controls to maintain a constant temperature in space and time in the observing room.

Since painting the building white and remodelling the air conditioner did not eliminate slow drifts in the signal, guiding diodes were placed at the aperture to eliminate relative motions of image and aperture. This also failed to eliminate the slow drifts. It is not clear whether the modifications were insufficient to eliminate positioning errors or whether there might be some other source of slow drifts. One possibility is that the changes in mirror polarization which are believed to be responsible for the non-zero magnetic field observed in a nonmagnetic line might find their way into the signal. Such a possibility seems unlikely because the amplitude of the drift in the velocity signal indicates a much larger wavelength shift than that corresponding to the magnetic field error. A more promising possibility is that atmospheric transparency gradients cause different weighting for different portions of the disk and create a velocity signal due to the sun's rotation (see Grec and Fossat, 1976; Grec et al., 1976). Simple arguments suggest that this effect would produce a monotonic drift during the day rather than the inverted U shape observed. Whether the slow drifts are of atmospheric origin or, as seems more likely, of instrumental origin, they are present throughout the data used in the present investigation and must be further contended with in the analysis of results.

One other important feature of the Kotov apparatus is its dependence on the geometry of any velocity fluctuations observed. The five-minute oscillations are believed to have a small spatial coherence length relative to the aperture used. We may approximate them by independent cells of period P_i = 5 min, line of sight amplitude A_i, and random phase ϕ_i:

$$V_i = A_i \sin\left(\frac{2\pi t}{P_i} + \phi_i\right)$$

The total velocity for many such cells will be a sum weighted for intensity

$$< V > = \frac{\Sigma I_i A_i \sin (2\pi t/P_i + \phi_i)}{\Sigma I_i}$$

The apparatus measures $V_c - V_\ell$:

$$<V>_c - <V>_\ell = \frac{\Sigma_{\text{center}} I_i A_i \sin(2\pi t/P_i+\phi_i)}{\Sigma_{\text{center}} I_i} - \frac{\Sigma_{\text{limb}} I_i A_i \sin(2\pi/P_i+\phi_i)}{\Sigma_{\text{limb}} I_i}$$

Subtraction of the contribution from limb cells is equivalent to shifting the phase by π. Since the phases are assumed to be random, one defines $\phi_{i'\,\text{center}} = \phi_i$, $\phi'_{i\ \text{limb}} = \phi_i + \pi$, and the average velocity difference signal is the same as would be obtained by directly measuring the velocity over the full aperture:

$$<V>_c - <V>_\ell = \frac{\Sigma_{\text{center + limb}} I_i A_i \sin(2\pi t/P_i + \phi'_i)}{\Sigma_{\text{center + limb}} I_i}$$

For velocity fields of global coherence scales, such as might result from normal mode oscillations of the sun, the effect is more complicated. For example, if the sun is expanding radially, at the same time as the center of the disk is moving toward the observer, the limb also has a smaller component of velocity toward the observer. For the Stanford aperture, for example, the velocity difference signal $V_c - V_\ell$ will be only 0.208 times the actual radial expansion velocity V_o. Calculations have been made of this sensitivity factor $(V_c - V_\ell)/V_o$ for different spherical harmonics and different apertures as shown in Table 4. It follows from a comparison of different instrumental sensitivities that for a spherical pulsation of amplitude 1.75 m/s using the Birmingham apparatus, the Stanford apparatus would measure only 1.04 m/s, and for the apparent amplitude of 2.75 m/s from the Birmingham group, the Stanford apparatus would measure only ~ 0.8 m/s.

AD-A040 653 STANFORD UNIV CALIF INST FOR PLASMA RESEARCH F/G 3/2
LARGE-SCALE PERIODIC SOLAR VELOCITIES: AN OBSERVATIONAL STUDY.(U)
MAR 77 P H DITTMER N00014-76-C-0207
UNCLASSIFIED SU-IPR-686 NL

2 OF 3
AD
A040653

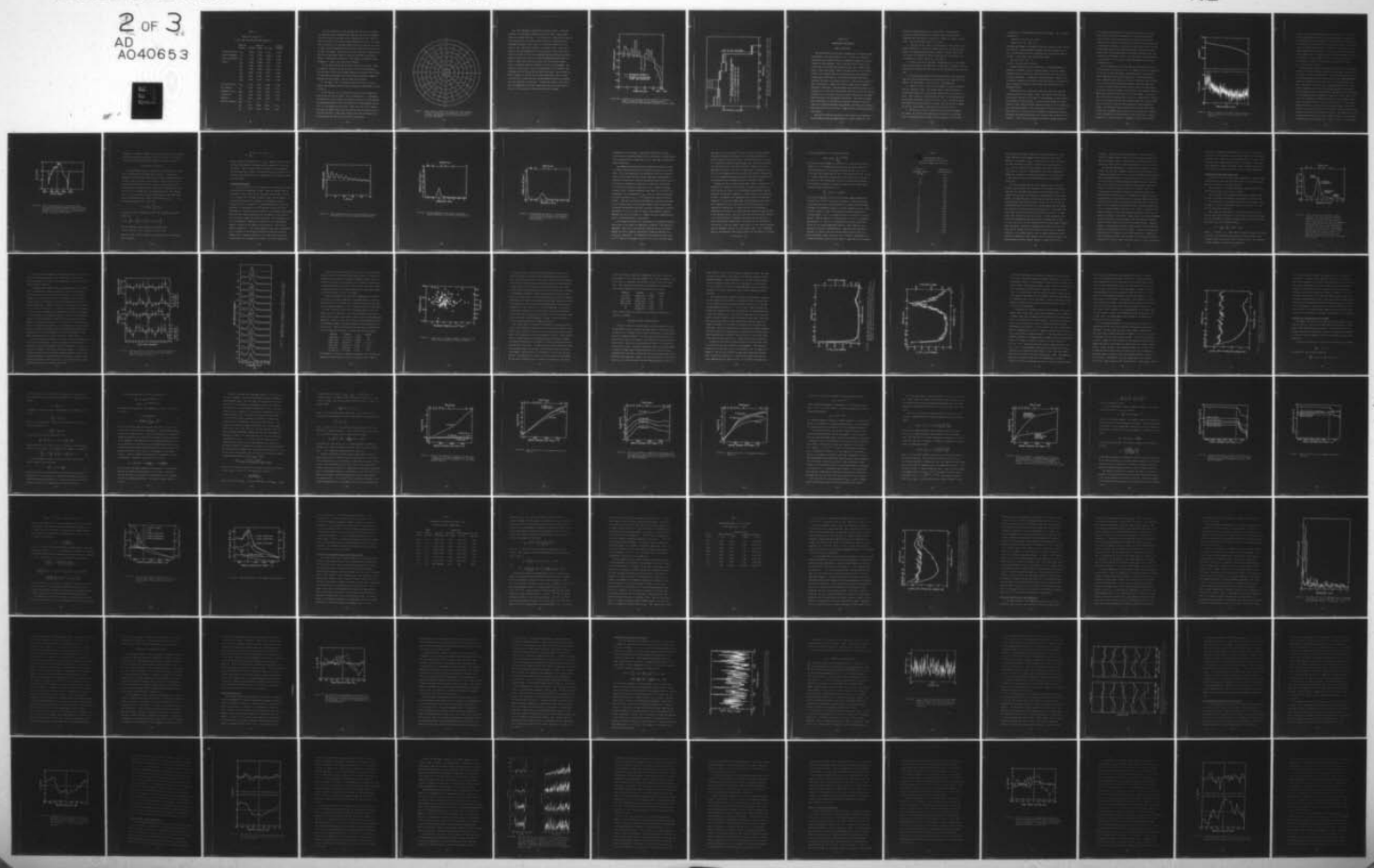

Table 4

Sensitivity Factors for

Different Apertures and Spherical Harmonics

	Spherical Harmonic	Aperture			Stanford / Crimea
		Stanford	Crimea	full disk	
radial motion with	Y_{00}	0.208	0.349	0.716	0.596
angular dependence	Y_{10}	0.165	0.240	0.282	0.688
given by spherical	Y_{11}	0.168	0.238	0.279	0.706
harmonic	Y_{20}	0.204	0.298	0.077	0.685
	Y_{21}	0.227	0.256	0.141	0.887
	Y_{22}	0.218	0.253	0.139	0.862
	Y_{11n}	0.243	0.303	0.357	0.802
	Y_{20n}	0.266	0.340	0.106	0.782
	Y_{22n}	0.387	0.378	0.210	1.024
horizontal motion	Y_{11n}	0.245	0.374	0.323	0.655
with angular	Y_{11}	0.218	0.292	0.282	0.747
dependence given	Y_{22n}	0.210	0.310	0.496	0.677
by negative	Y_{22}	0.141	0.208	0.329	0.678
gradient of	Y_{20n}	0.334	0.250	0.388	1.336
spherical harmonic	Y_{10n}	0.0	0.0	0.0	
	Y_{10}	0.170	0.239	0.224	0.711
	Y_{20}	0.261	0.194	0.308	1.345

A further difficulty in this interpretation is that A. B. Severny has suggested (private communication, 1976) that the optical arrangement described herein could produce extreme vignetting with only a small fan beam in the center of the disk actually producing the signal. To examine such a possibility, two different methods were used to measure the amount of light actually registered by the instrument from different portions of the mean field image. One method was to place apertures of radial extent $R_\odot/8$ and varying angular extent at different positions on the disk to produce a complete map of intensity. The average of two maps is shown in Figure 17. From it one learns the following:

1) The masks used are not perfectly centered on the image. Since the image was centered visually at the top of the polarizing aperture, this indicates a tilt in the cylinder holding the polarizers which results in a horizontal displacement as the light passes vertically through the different optical elements. This has since been corrected.

2) The edge of the $\lambda/2$ separating center from limb is a finite, largely nontransmitting bevelled edge extending from approximately 0.50 $R_\odot$ to 0.55 $R_\odot$.

3) The intensity is less going toward north and south limbs than going toward east and west limbs. This is probably due to a combination of imperfections in the image slicer which are largely in the NS direction and vignetting produced by the finite extent of the spectrograph entrance slit, as first pointed out by Severny. Since each slice of the image is 9 mm long, the image formed at the Littrow lens will be smeared by 6.3 cm in the NS direction, so some light from the north and south poles falls off the Littrow lens and is not reflected by the grating.

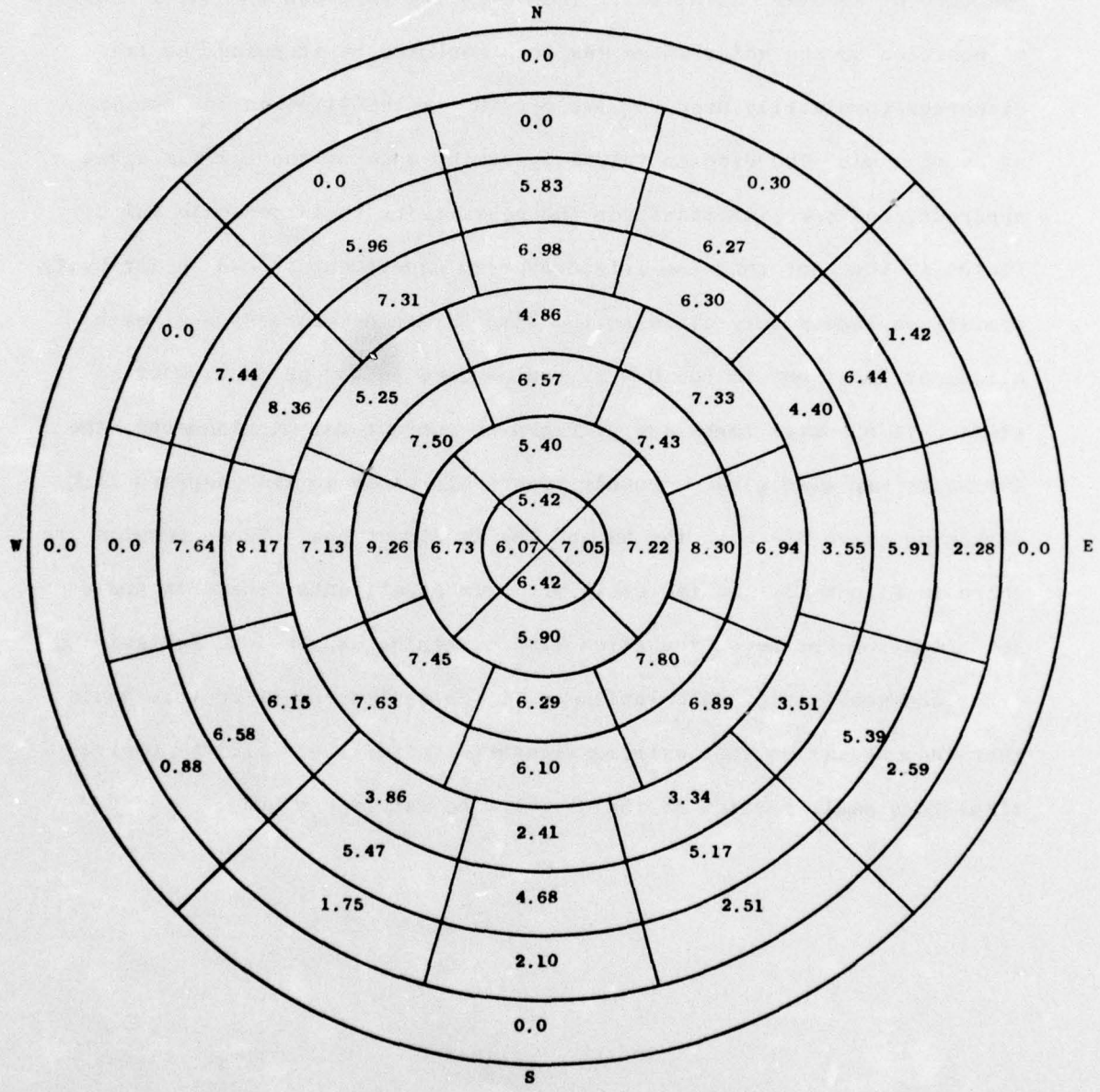

Figure 17. Map of intensity transmitted through the optical system as a function of position on the solar image. The units are arbitrary, and the numbers are average values from two different measurements.

Two other experiments substantiated the above results. The NS/EW asymmetry was confirmed by rotating on the solar image a wedge shaped aperture of angular extent 45°. The intensity as a purely radial function of position on the solar image was then measured by stepping the iris diaphragm (ordinarily used to mask off the extreme limb) in and out in steps of 1 mm. The drop in intensity at the edge of the $\lambda/2$ was again apparent, and more important for the sensitivity to large-scale velocity fields is the fact that the iris diaphragm experiment showed an intensity profile vs radius very close to the limb darkening expression given by Allen, at least out to the 0.8 $R_{\odot}$ radius used in the present observations. If opposite limbs are averaged to correct for misalignment, the intensity map also gives a result reasonably close to the standard limb darkening curve for both the NS and the EW directions. These results are shown in Figure 18. On the basis of these experiments, there is ample justification for using the Allen limb darkening expressions for guiding error and sensitivity calculations. It would also appear on this basis that the suggestion that extreme vignetting effectively limits observations to a small portion of the disk can be safely excluded.

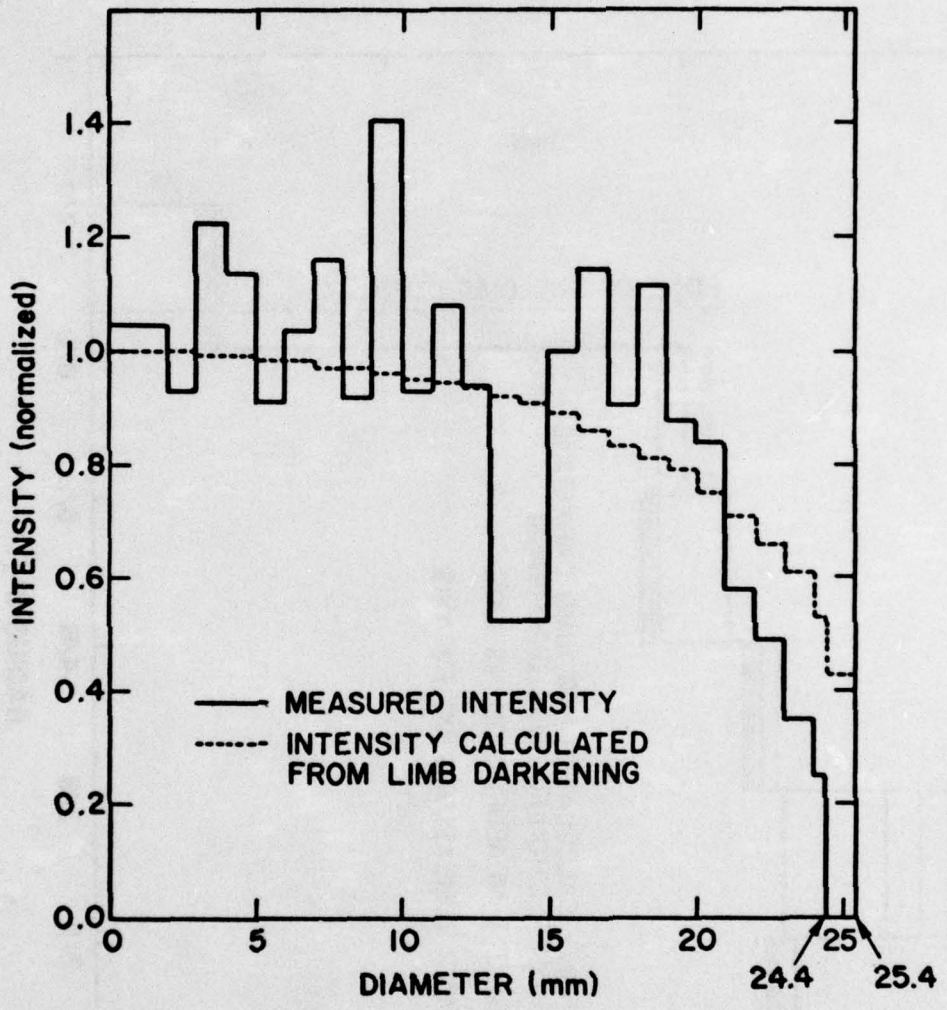

Figure 18a. Intensity as a function of radial position on the solar image, as measured using the iris diaphragm and as calculated from the limb darkening expression of Allen (1973).

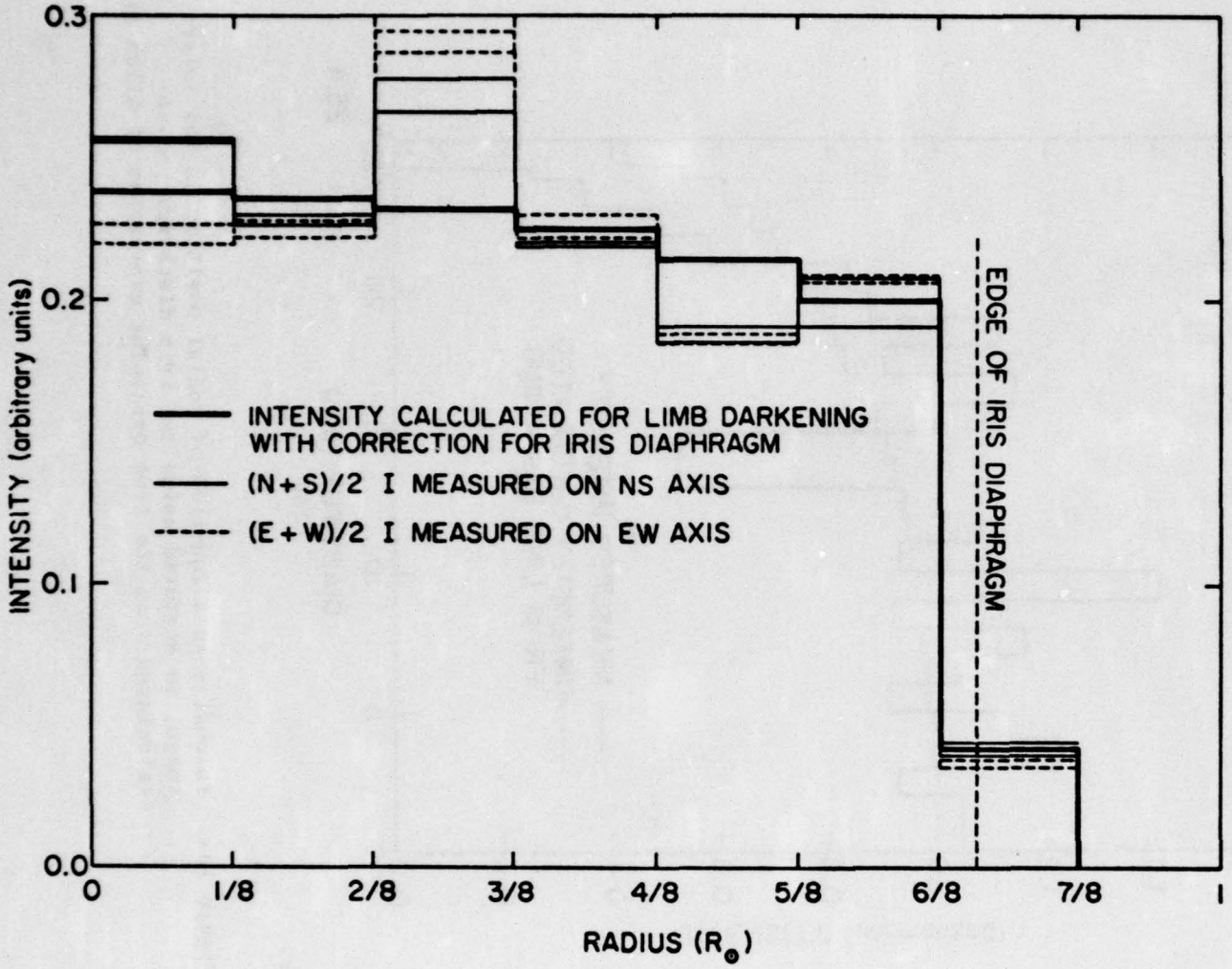

Figure 18b. Intensity as a function of radial position on the solar image, taken from the map shown in Figure 17. The value calculated from the limb darkening expression of Allen (1973) is again included for comparison.

Chapter III

OBSERVATIONS AND ANALYSIS

General Procedures

The three major questions under investigation in the present study (as detailed at the end of Chapter I) are: 1) Does the five-minute oscillation show variations related to large-scale magnetic structures observed in the photosphere, corona, and solar wind? 2) What can be learned about the oscillations reported by Hill and co-workers (Hill et al., 1976a; Brown et al., 1976) at periods between 5 and 70 minutes? 3) What can be learned about the 2 hr 40 min oscillation reported by Severny et al. (1976a and b)? In order to investigate these three questions, the plan of the present study was to obtain several months of daily observations of length 2 hr 40 min or longer with no changes in procedure or instrument. Long individual observations were needed to investigate the 2 hr 40 min oscillation and would also give better frequency resolution at 5 to 70 minute periods and better definition of the amplitude and period of the five-minute oscillations. The search for large-scale organization of five-minute oscillations required several solar rotations of daily observations using identical procedures and instrument, which would also aid in the study of longer periods by improving signal-to-noise ratios.

The goal of identical procedure was well achieved by having most of the instrumental setup performed directly by computer (PDP11/10) with

software developed specifically for this purpose. Functions which could not be performed directly by computer (such as initial mirror alignment) were performed by an operator in response to computer instructions. The basic procedure used is as follows:

1. Telescope set up. (This is not performed if done previously for another observation.) Covers are removed from optics and grating, dome is opened, and computer dome positioning is begun. Coelostat and second flat mirrors are aligned, the 48-hour clock drive on the coelostat and the guiding servo on the second flat are turned on.

2. Find the line in the spectrum. The grating is set at the proper angle using an encoder. The spectrum is scanned until two lines of desired separation are found and the exit slits are then positioned on the λ5123.730 line.

3. The polarizing aperture is moved into position at the mean field image (the line finding routine is done previously since light levels are higher). The KDP voltage is turned on with 110 Hz modulation.

4. Balance and zero. The exit slit assembly is moved to λ5122.502 where the spectrum is flat. The operator makes a manual adjustment so intensity measured in the two phototubes, hence in the two exit slits, is equal. Then a shutter is closed cutting off light to the phototubes and the intensity and Zeeman zero levels are set to zero. The difference in dark signal in the two phototubes is zeroed. Then the shutter is opened and the exit slit assembly is positioned on the λ5123.730 line.

5. The exit slit servo is turned on and the observation begins. Two signals are measured continuously and an integration is performed every 0.1 second giving the average for the previous 0.1 second, which

is converted to a digital number by 14-bit A/D encoders. The two signals measured are:

$$\text{Intensity} \equiv (R^+ + R^- + B^+ + B^-)/2$$

$$\text{Zeeman} \equiv (B^+ - R^+) - (B^- - R^-)$$

Two additional signals are obtained at the end of each 0.1 second interval--the signal ZI ≡ Zeeman/Intensity by digital division performed in software, and the signal Doppler by reading the exit slit position from the encoder. A fifth signal, the DC difference signal,

$$DC\Delta \equiv (B^+ - R^+) + (B^- - R^-)$$

is used to drive the exit slit servo.

Digital integration of 150 consecutive 0.1 second measurements is performed in software, and the 15-second averages of the four signals mentioned above are recorded on tape along with the start time of each 15-second integration. In addition to these quantities, a long list of instrumental parameters is recorded at the start and end of each observation, including such things as the observer and the position of the guiding mechanism.

Observations used in the present study were made at the Stanford Solar Observatory in the summer of 1976. The period of time with best observational coverage was from April 13 through August 6, which interval is included in all data analysis. On two occasions during this period (April 29 - May 6 and June 25-30) calibration showed a loss of sensitivity due to improper alignment of the linear polarizer and the quarter-wave plate which loss of sensitivity was confirmed by reduced power measured throughout the frequency spectrum--these intervals were excluded from the analysis. A wider interval extending from March 11 through September 21

was included in investigations of periods shorter than an hour, but generally was not used in the search for 2 hr 40 min oscillations since the data are more intermittent and a broader interval would require greater frequency resolution in searching for an oscillation of constant period and phase. In addition to these observations, velocity measurements using the same apparatus were made from November 1975 to February 1976 and polarizing optics of different dimensions were used between July and November of 1975. The velocity was also measured from a smaller portion of the disk in October and November of 1976 using the Doppler servo.

For each observation, plots were made of the intensity and of the velocity signal as functions of time. An example is plotted in Figure 19, for the May 23, 1976 observation. The observation is four hours in length consisting of 960 15-sec integrations. There were sometimes large, sharp deviations present in intensity and velocity due to clouds or to errors in the dome positioning program. When such excursions occurred, the questionable integrations were replaced by dummy values so that they were not included in later analysis but timing was preserved. Three other features may be pointed out in this example. One is that the velocity has an average value of $\sim +55$ m/s, compared with a value of -24.1 m/s calculated from the limb darkening expression of Allen (1973) and the rotation and limb red shift parameters of Howard and Harvey (1970). The difference between measured and calculated baseline was probably due to improper positioning of the solar image which resulted in uneven weighting of different parts of the disk, giving a velocity signal due to the sun's rotation. Attempts to correct this baseline

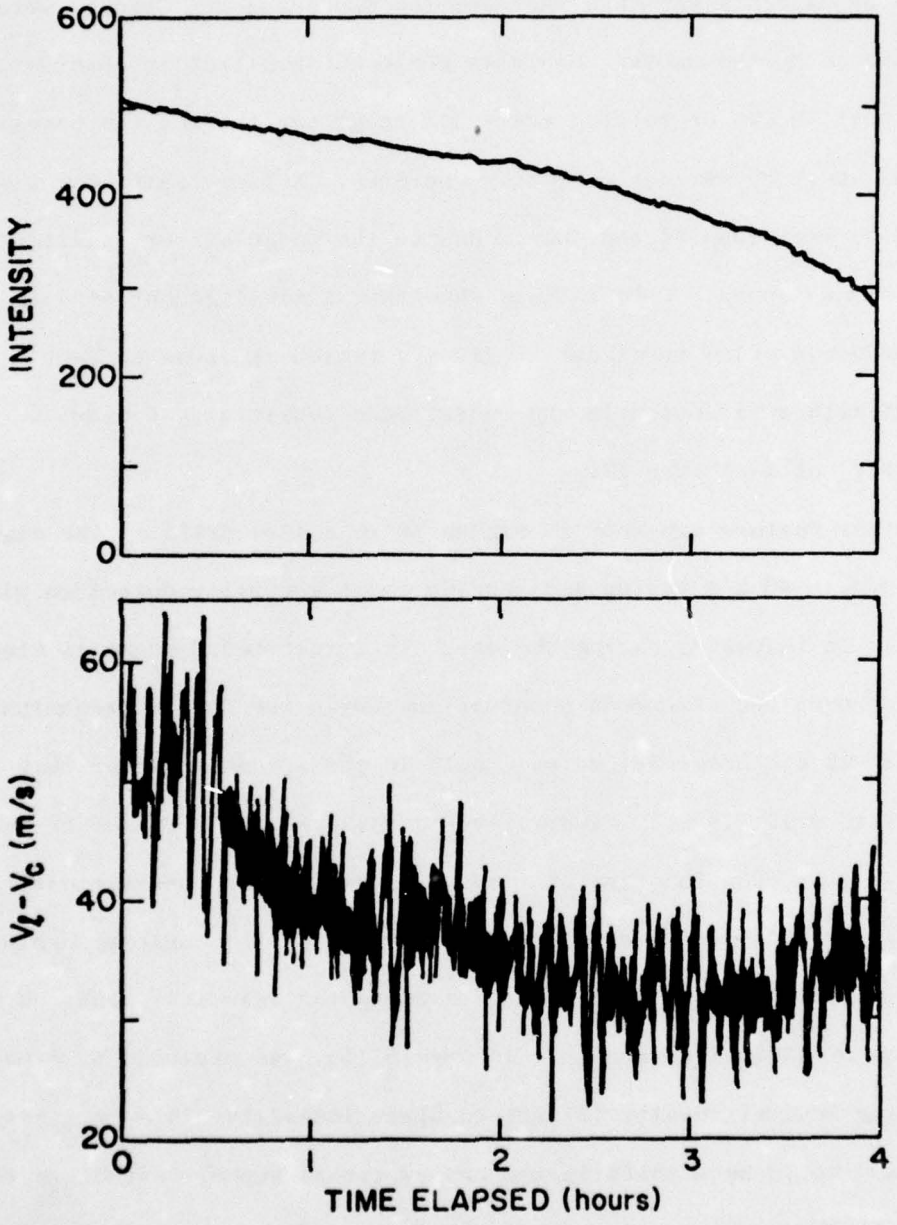

Figure 19. Plots of intensity (top) and ZI signal calibrated in relative velocity (bottom) for the May 23, 1976 observation.

offset by more careful adjustment were not successful, but the result of these adjustments was that the baseline was changed. Changes were also produced by the midday change in coelostat position in observations before April 30, which rotated the sun's image and shifted the baseline since the aperture was not perfectly centered. A large shift was also produced between June 24 and July 1 due to the image slicer misalignment mentioned above. Calculations show that a misalignment of 0.30 $R_\odot$ would produce a velocity signal of 210 m/s (which is close to that observed) with a reduction in the radial mode sensitivity factor, $(V_c - V_\ell)/V_o$ of less than 1%.

Another feature apparent in Figure 19 is a slow drift in the signal from 65 m/s to 40 m/s having a direction which generally coincided with the change in intensity during the day. This inverted U shape is clear in both morning and afternoon observations (with the former predominant before May 22 and observations made only in the afternoon after that date). This drift is seen clearly in Figure 20 which is a plot of the velocity signal as a function of time of day with each observational mean subtracted to remove baseline shifts. This drift could be explained by a non-linearity in the electronics causing the velocity signal to be a function of intensity, though this possibility was excluded by experiments using neutral density filters to alter intensity. A more likely explanation would be a shift in the observational support structure to the west in the morning and to the east in the afternoon caused by thermal expansion of the walls of the support structure. This explanation, which was discussed in detail above, would correctly account for the inverted U shape of the observed diurnal drift. The drift was of large amplitude

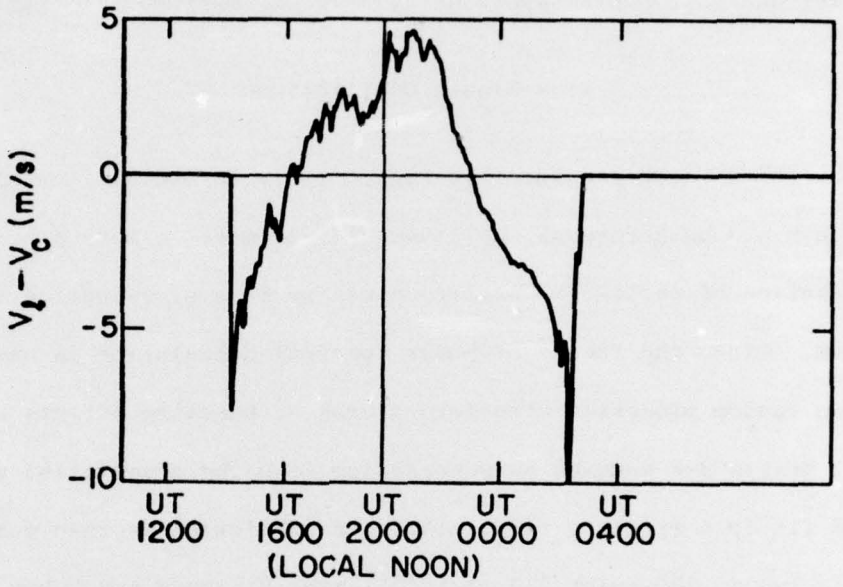

Figure 20. Plot of the daily drift in the Stanford signal. The observational mean has been subtracted from each observation to remove the effect of base line shifts, and data have been averaged as a function of time of day. Local noon is at UT 2000.

compared to the expected signals and left the dilemma of either removing the drift (along with some possible signal) by fitting, or of leaving the drift and introducing spurious signals of instrumental origin.

Five-Minute Oscillations

The third feature evident in Figure 19 is an oscillation of period near 5 min and peak-to-peak amplitude of 5-10 m/s. A more precise determination of period and amplitude may be made by computing the power spectrum. Since the theory of power spectral calculation is based on Gaussian random processes with zero averages, baseline offsets and diurnal drifts are removed by subtracting from the observation a least-squares fit to a straight line. The autocorrelation is then computed out to a lag of 200 point (50 min) following Blackman and Tukey (1958). For a record consisting of n equally spaced values $x_1, x_2, x_3, \ldots x_n$, the autocorrelation at lag ℓ is given by

$$C_\ell = \frac{1}{(n-\ell)} \sum_{i=1}^{n-\ell} x_i x_{i+\ell} \quad .$$

The power spectrum is then given by the cosine transform of the auto-correlation

$$P(f) = \left[C_o + 2 \sum_{\ell=1}^{m-1} C_\ell \cos \frac{\ell f \pi}{m} + C_m \cos (f\pi) \right] \quad .$$

This was smoothed by convoluting with a hanning window

$$P'(f) = 0.25\ P(f - \Delta f) + 0.5\ P(f) + 0.25\ P(f + \Delta f),$$

where $\Delta f = 2/m\Delta t$, which is equivalent to weighting the autocorrelation with a function

$$D_\ell = \begin{cases} 0.5\ (1 + \cos \pi\ell/m), & \ell > m \\ 0.0 & , \ \ell = m \end{cases}$$

giving a modified autocorrelation $C' = D_\ell C_\ell$. Figure 21 shows the autocorrelation and Figure 22 the power spectrum computed for the May 23 observation. The five-minute resonant oscillation is again apparent, with the recurrence of peaks in the autocorrelation and the position of the peak in the power spectrum both indicating a period slightly longer than five minutes.

Average Characteristics

A total of 475 hr 41.5 min of observation was reduced for the period between April 13 and September 21, 1976. Since the aperture used was of diameter 0.8 $R_\odot$ = 768", the area observed was about 1.85 x 10^6 arc sec^2, or about 1.85 x 10^4 times as great as with a $(10")^2$ aperture. If five-minute oscillations are assumed to be independent at points separated by 10", the present set of observations would in a sense be equivalent to observing with a $(10")^2$ aperture for about 10^3 years. Unfortunately, the lack of spatial resolution in the present observations means that only limited information can be gained as to the nature of the five-minute resonant oscillation in general. This information can be well displayed by computing the average of all the power spectra measured, weighted by the length of the observation. The result is plotted in Figure 23. A very smooth peak may be seen near five-minutes, with no evidence of the multiple periodicities described by Frazier (1968a and b). Frequency resolution is not good with the lag in the autocorrelation only extended to 50 minutes, and further smoothing is

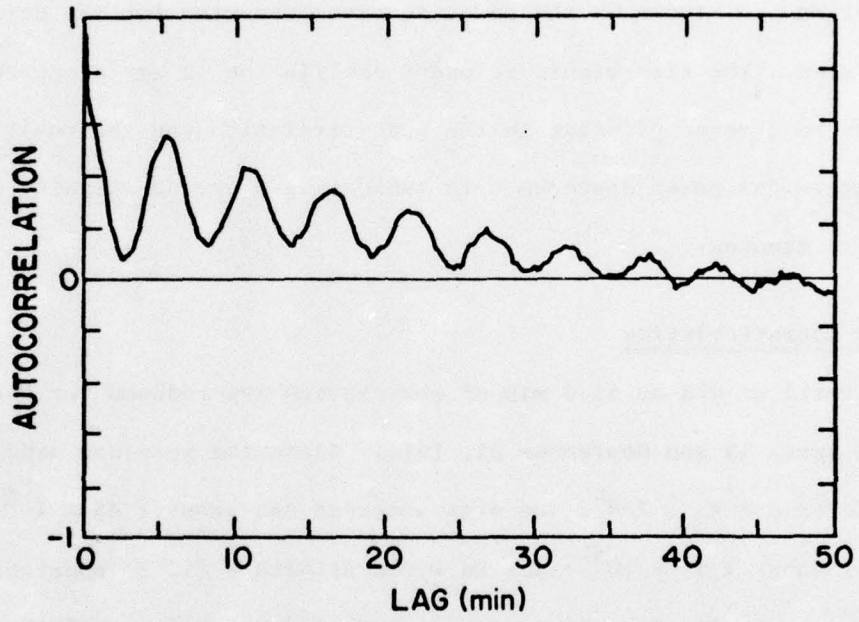

Figure 21. The autocorrelation of the velocity difference signal, calculated for the May 23 observation (Figure 19b).

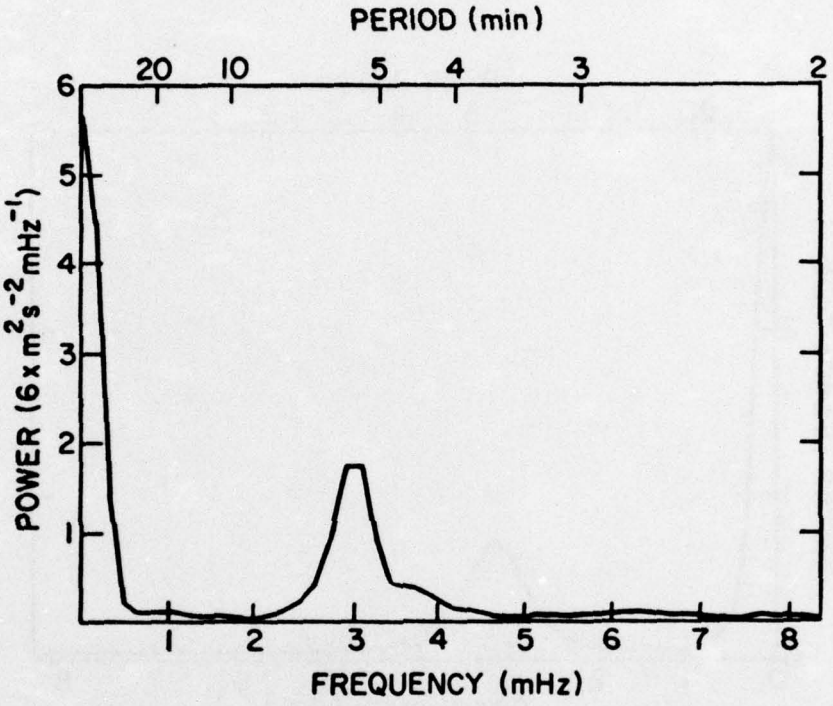

Figure 22. The power spectrum of the velocity difference signal calculated for the May 23, 1976 observation.

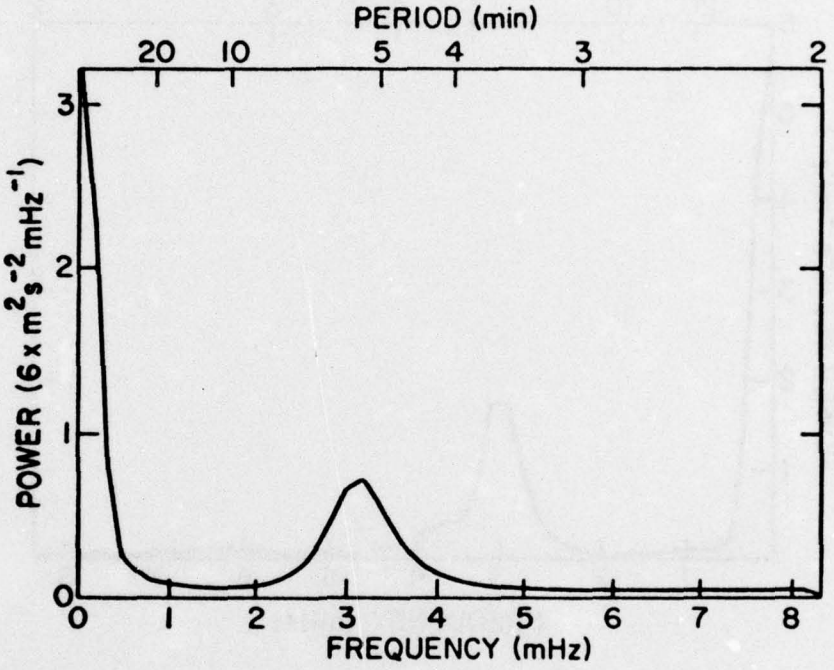

Figure 23. Average power spectrum for the Stanford data. In performing the averaging, each individual power spectrum is weighted for the length of the observation.

introduced by use of hanning. Power spectra computed with greater resolution and no smoothing (Figure 28) are less smooth, but fluctuations are not separated from a smooth curve by more than might be expected for random fluctuations.

Two parameters characterizing the average power spectrum as shown are somewhat different than might be expected from small scale observations. One is the amplitude of the oscillation, which was measured by taking the area under the curve between frequencies corresponding to periods of 10 min and 3-1/3 min and then subtracting the portion due to noise power as estimated by taking the area under the curve between 3-1/3 min and 2 min where the spectrum is flat as might be expected for white noise. The power measured in this manner is 4.03 $(m/s)^2$ corresponding to an rms amplitude of V_{rms} = 2.01 m/s. This result agrees well with the value of V_{rms} = 2.4 m/s published by Fossat and Ricort (1975a). Since they used the line NaIλ5896 (D_1) for which oscillations are 1.5 times as large as for FeIλ5124 (Deubner, 1971), and have used an aperture including the full disk, they might be expected to record an amplitude 1.5 x 0.8 = 1.2 times as large as that presently reported. Agreement may not be as close as it appears since their published value did not include correction for noise power.

A discrepancy with small scale determinations of amplitude and scale size arises if one accepts the amplitude $\propto$ $(\text{diameter})^{-1}$ rule derived by Tanenbaum. This relation was derived by representing the oscillating regions or cells by harmonic oscillators of identical amplitude and period and random phase. The amplitude of the ensemble average varies as $N^{-1/2}$ where N is the number of cells, so for a slit one would expect

amplitude to vary as $(\text{length})^{-1/2}$ and for a round or square aperture, the amplitude should vary inversely with the linear dimension for apertures greater than the cell size. Tanenbaum simulated a long slit by averaging one-dimensional magnetograph scans, and found his results to be consistent with a cell size of 3000 km. However, for an rms amplitude of 100 m/s at 3000 km, this would imply an amplitude of about 0.25 m/s for an aperture of 0.8 $R_\odot$ as used in the present investigation. The 2.0 m/s amplitude presently measured is more nearly consistent with the 20000 km cell size estimated by Fossat and Ricort (1975a).

Because the sun is a sphere rather than a disk, a calculation of the amplitude to be expected for an aperture as large as presently used should include the effects of limb darkening, foreshortening, and the decreasing line-of-sight component of radial velocity as one approaches the limb. In addition, the assumptions used to derive the amplitude $\propto (\text{diameter})^{-1}$ rule will no longer apply since oscillations will not be of equal amplitude and since the existence of well-defined cells is not supported by observations. A relation similar to that derived by Tanenbaum may be derived with somewhat greater generality using the work of Cha and White (1973). They have shown from velocity records made with a 10" aperture that the five-minute oscillation has the behavior of a narrow-band Gaussian random process. The signal may be represented in the form $V(t) = A(t) \exp [i(2\pi\bar{f}t + \phi(t)]$ where $\bar{f}$ is the average frequency, $A(t)$ the amplitude, and $\phi(t)$ the instantaneous phase. For a narrowband process, the probability distribution function for the phase is a constant

$$W_1 \text{ (for } \phi(t)) = \frac{1}{2\pi} \quad ,$$

and for the amplitude it is a Rayleigh function

$$W_1(\text{for } A(t)) = \frac{A}{V_{rms}^2} e^{-A^2/2V_{rms}^2} \quad .$$

The velocity signal weighted for intensity for a given aperture may be thought of as a two-dimensional random walk in the complex plane with length proportional to the intensity times the velocity. The vector sum of many such random walks will have a distribution equivalent to that of a single random walk of length given by the square root of the sum of the squares of the contributions from all of the individual apertures. For N identical oscillators of identical intensity, the velocity times intensity signal will therefore go as

$$\left[\sum_{i=1}^{N} (VI)^2\right]^{1/2} = VI(N)^{1/2},$$

and since the intensity will be NI, the velocity signal measured will be $VI(N)^{1/2}/NI = VN^{-1/2}$, as derived by Tanenbaum. Using this approach, calculations were made of the amplitude to be expected with the present instrument for independent elements of various dimensions, and the result is shown in Table 5. Since the calculation is greatly simplified for circular geometry, the linear dimension used is the radius of a circular aperture, with the length of a square aperture of equal area obtained by multiplying by $\sqrt{\pi}$. The 2.0 m/s amplitude reported above would be consistent with an average independent region of radius 14500 km, corresponding to a square of length 25700 km. Since noticeable decreases in coherence are observed over much smaller horizontal differences (e.g. Lynch and Chapman, 1975), it follows that an "average" independent size of 25700 km requires there to be some power at larger physical wavelengths.

Table 5

Calculated Amplitudes for
Independent Regions of Various Sizes
Each with an Amplitude of 100 m/s

Radius of Independent Region (10^3 km)	Amplitude with Stanford Aperture (m/s)
1.5	0.21
2.0	0.28
2.5	0.35
3	0.42
4	0.56
5	0.70
6	0.85
8	1.13
10	1.40
12	1.69
14	1.91
14.5	1.99
15	2.09
16	2.19
18	2.60
20	2.75
30	4.16
40	5.54
50	7.52
60	7.91
80	9.63
100	15.28

This conclusion is further supported by direct measurements of five-minute amplitude from the Doppler servo encoder and using a $(3')^2$ aperture. An amplitude of V_{rms} = 10.56 m/s was measured, which using the same calculations as above, is consistent with an amplitude of V_{rms} = 1.02 m/s using the 0.8 $R_\odot$ aperture. This result indicates that even regions as large as 3' (130000 km) are not totally independent. Though this conclusion is weak since obtained in a very indirect way, it does support a global excitation mechanism for the five-minute oscillation.

The other parameter measured with a different result from that expected was the period. The frequency of the resonant peak was determined from the individual power spectra in three different ways. The simplest was to measure the frequency of the high point in the resonant region. The other two ways involved taking the weighted average of the power spectrum in the resonant region. In one case, this was done by measuring the noise level in the 5.0 - 8.33 mHz region and then finding the centroid of the resonant power above this level. In the other case it was done by taking the centroid of the power in the 1.67 - 5.0 mHz region with correction for the noise power. As might be expected, the latter two determinations agreed very closely, giving values of 312.1 $\pm$ 1.3 sec and 312.8 $\pm$ 1.0 sec respectively from 110 power spectra between April and August. Inclusion of September data, making a total of 135 power spectra, changed the latter result to 312.9 $\pm$ 0.9 sec. When the frequency of the resonant peak was used, the period obtained was 320.2 $\pm$ 2.2 sec, indicating a slight asymmetry in the resonant peak due to the high frequency tail which becomes dominant at higher levels in the

atmosphere. Every period determination gives a result longer than Leighton's original report of 296.1 $\pm$ 1.3 sec from the CaIλ6103 line (Noyes and Leighton, 1963). The difference in measured period is not large--only about 5%--but is much larger than the statistical errors.

One possible explanation for the difference in period is that different lines were used. Attempts to settle this question directly by comparing measurements made in the same line (NaIλ5896) were inconclusive. Noyes and Leighton measured a period of 285.8 $\pm$ 1.5 sec, and only four observations were available using present methods, giving a period of 294 $\pm$ 11 sec, which is only 3% longer than the previous value but is within an error bar of being 1% shorter or 7% longer. The use of different lines is unlikely to explain the longer period since the CaIλ6103 line is formed low in the photosphere (see Figure 1 of Noyes and Leighton) as is the FeIλ5124 line. In addition, Howard (1962) also measured a period of 296 sec using the FeIλ5250 line which is formed at least as low as FeIλ5124, which would mean that its period should be at least as long were identical apertures used. Howard's measurement also makes it unlikely that the longer period found herein is due to use of different techniques to define the average period, since Howard determines the period from the secondary maximum in the autocorrelation function, which is closely related to the peak in the power spectrum. Secondary maxima in autocorrelations computed using the present data consistently indicated a period longer than five minutes. An increase in period for large aperture size remains the most likely explanation. Attempts to detect a shorter period by using apertures of $(3')^2$ and $(30'')^2$ were not successful, so if such a shift in period is present, it must occur between

5" and 30". The physical significance of this 5%, 10 σ difference is not clear, but it does agree in sign with the direction of the diagonal lines in the k-ω diagram of the Ulrich (1970) model. It would further seem that such a change between 5" and 30" is evidence of the large-scale character of these oscillations, since a change in period would not be likely if regions separated by 30" were totally independent.

The Search for Large-Scale Organization

In order to search for large-scale organization of the five-minute oscillation, each observation was characterized by the following parameters, calculated from the power spectrum:

The peak power - the maximum amplitude of power measured in the interval of periods from 3-1/3 min to 10 min.

The noise power - the integrated power over the frequency range 5.0 mHz to 8.33 mHz, corresponding to periods of 3-1/3 min to 2 min.

The signal power - the integrated power over the frequency range 1.67 mHz to 5.0 mHz corresponding to periods of 10 min to 3-1/3 min, with the noise power subtracted.

The average resonant frequency - the average frequency of the resonant peak in the 1.67 mHz to 5.0 mHz interval. Correction was made for the noise power by taking the average power above the noise rather than above zero, in the following manner:

$$< f > = \frac{1}{f_2 - f_1} \int_{f_1}^{f_2} f(P(f) - P_n)\, df$$

where f_1 = 1.67 mHz, f_2 = 5.0 mHz, P(f) is the power measured at frequency f, and P_n is the noise power per frequency interval measured in the frequency range 5.0 mHz to 8.33 mHz as described above. The calculation of these parameters is illustrated in Figure 24.

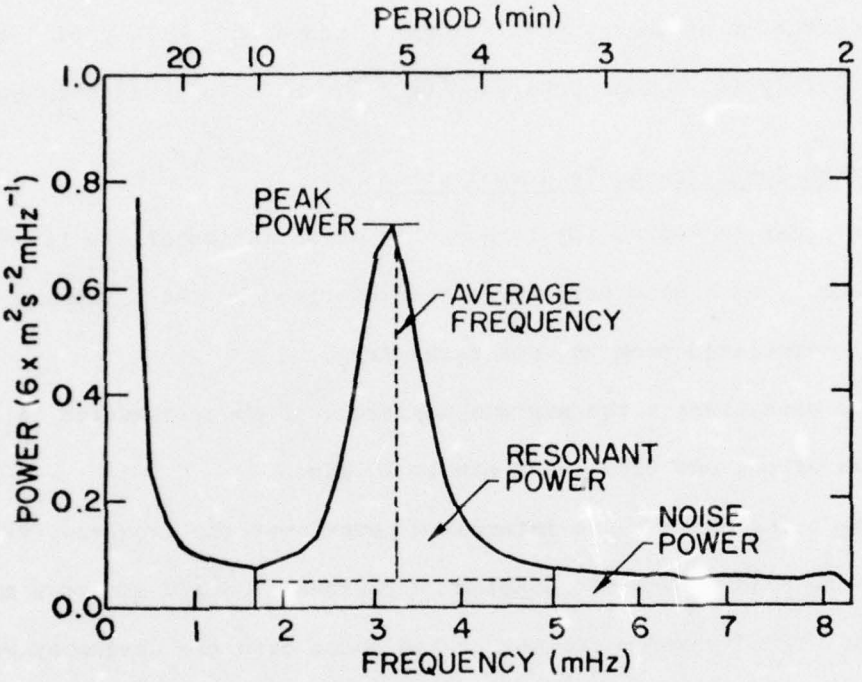

Figure 24. Figure showing how signal power, average frequency, noise power, and peak power are measured from a power spectrum. The noise power is the area under the curve between 5.0 mHz and 8.33 mHz. The signal (or resonant) power is the area under the curve and above the dashed line (which is the noise power) between 1.67 mHz and 5.0 mHz. The average frequency is the centroid of this same area, and the peak power is the high point of the curve between 1.67 mHz and 5.0 mHz. The power spectrum used is the average power spectrum of Figure 23, plotted with a different vertical scale.

These values were computed for each day's observation. If more than one observation was made during a day, the average of the two power spectra weighted for the length of the observation was used to calculate the parameters for that day.

A superposed epoch analysis was then performed about sector boundaries as determined by changes in polarity of the sun's mean magnetic field as measured at the Stanford Solar Observatory. The boundary was assumed to be located between two days of opposite polarity, and the average value of the parameter of interest was computed for all days immediately preceding a boundary, for all days two days before a boundary, and so on until an interval of $\pm$ 7 days about the boundary was included. In performing the averaging, each parameter was weighted for the length of the observation. The superposed epoch of each of the four parameters computed is shown in Figure 25, along with the grand average for each parameter and the computed error bar. In each case, it can be seen that there is no conspicuous organization of the parameter about sector boundaries. In addition, the number of daily averaged values falling within one error bar of the grand average is in every case comparable to the 68.3% value expected for a normally distributed random variable.

There were four other attempts to look for a large-scale organization of five-minute oscillations. One was to superpose the power spectra themselves instead of some parameter about the boundaries to see if any variation is apparent. The result is plotted in Figure 26. Though small variations can be seen in the averages taken at different intervals from the sector boundary, no obvious organization is present, and 453 of the 714 points or 63.4% are within one error bar of the grand average, again consistent with normal statistical fluctuations.

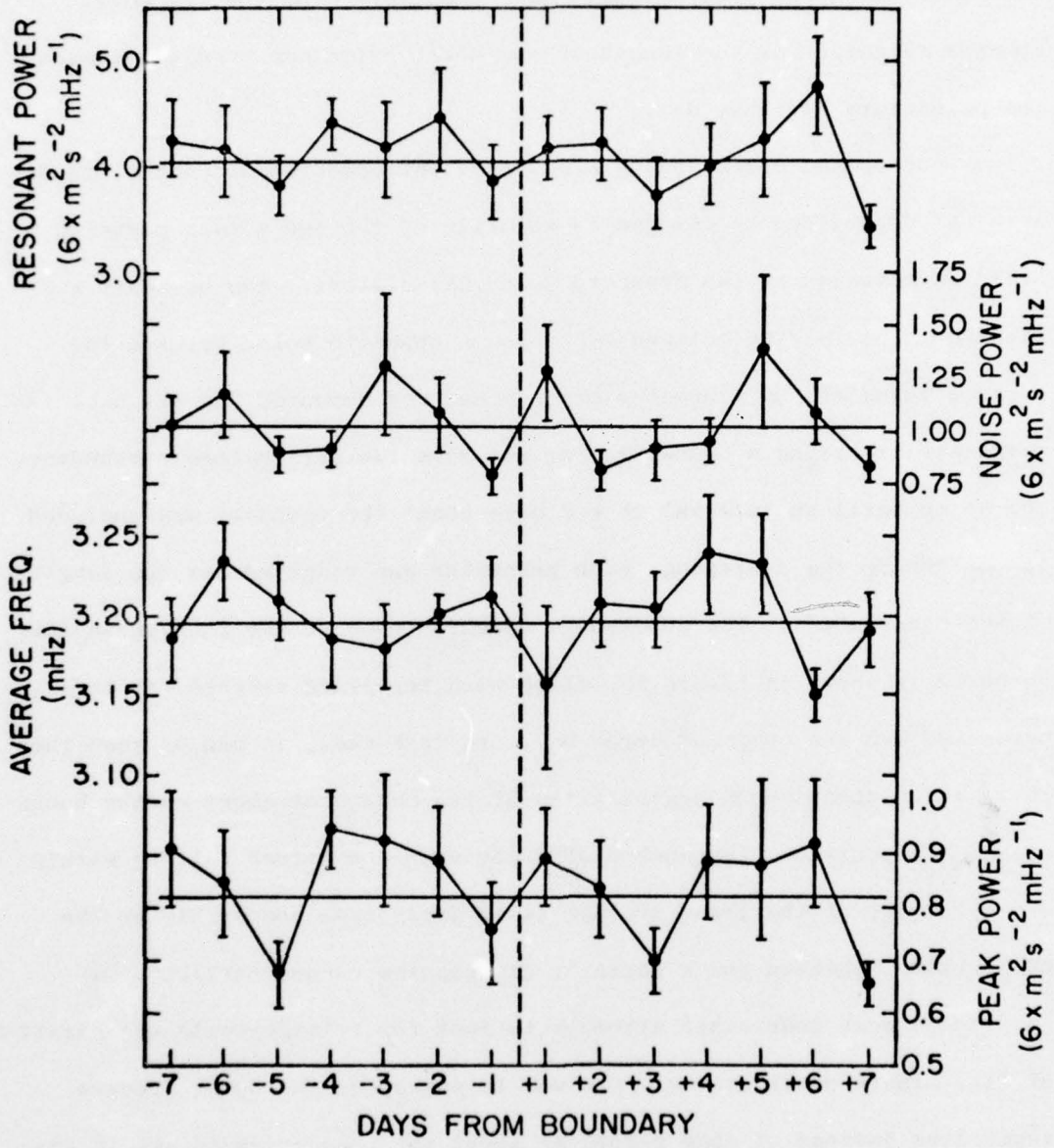

Figure 25. Superposed epoch of five-minute oscillation parameters about polarity reversals of the mean solar magnetic field as measured at Stanford.

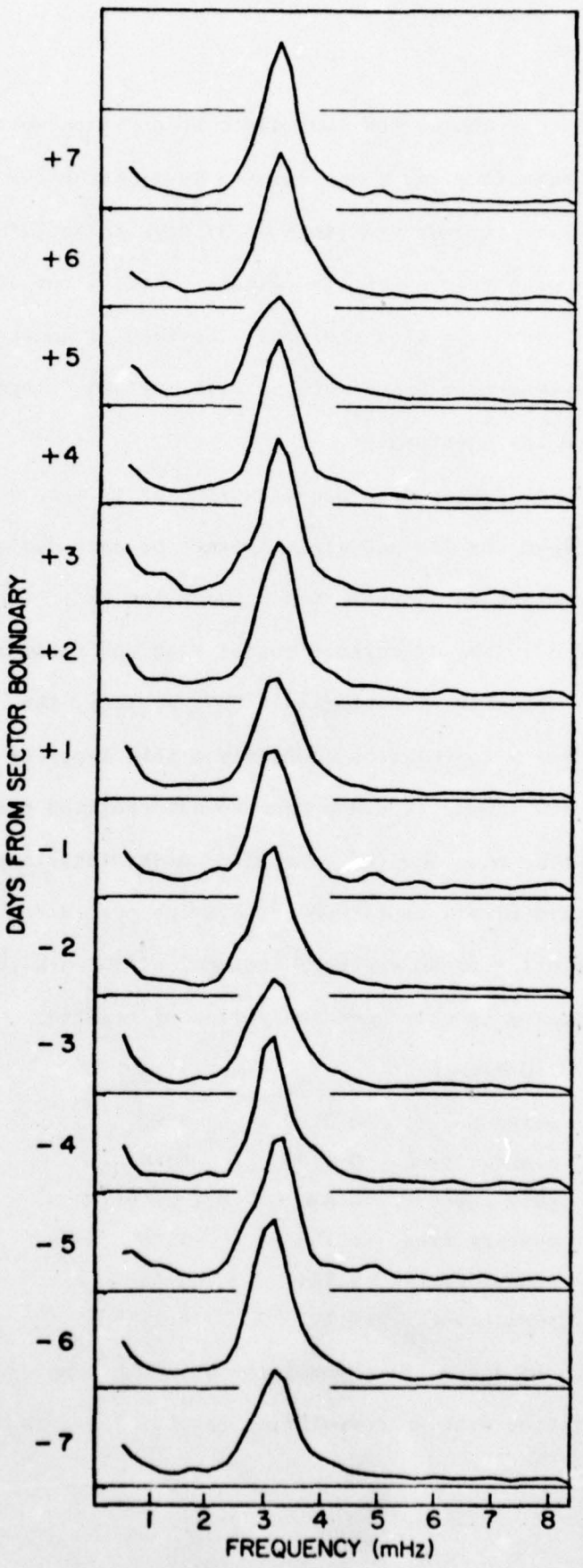

Figure 26. Superposed epoch of power spectra of Stanford velocity difference data about polarity reversals of the mean solar magnetic field.

Next, the four parameters chosen for each day's observation were used to calculate autocorrelations and power spectra in a search for periodicities near 27 days or integer fractions of 27 days to see if there was any large-scale organization of five-minute oscillations of sufficient persistence to co-rotate with the sun. The results showed a conspicuous lack of any long-term organization, with periods integer fractions of 27 days in no way outstanding.

Another investigation of large-scale organization was to make a scatter plot of average frequency $\langle f \rangle$ and signal power for each day's observation to see if there was any correlation between the two. The result is shown in Figure 27. The calculated correlation coefficient is $r = 0.0139$. Using the expressions of Bevington (1969, p. 124), the probability is $P = 0.88$ that a correlation coefficient this large or larger would be found if the sample is drawn from an uncorrelated parent population. Both the scatter plot and the calculated probability show no relationship between five-minute amplitude and average period for this data set. Similar scatter plots and correlation coefficients for all four parameters (six pairs in all) gave the following results:

Abscissa	Ordinate	r	P (ρ=0)
signal power	noise power	0.0186	0.84
signal power	average freq	0.0139	0.88
signal power	peak power	0.835	3.7×10^{-9}
noise power	average freq	-0.104	0.26
noise power	peak power	0.124	0.18
average freq	peak power	-0.103	0.27

The probability calculated is again the probability that the sample was taken from a parent population with no correlation (ρ=0). There is

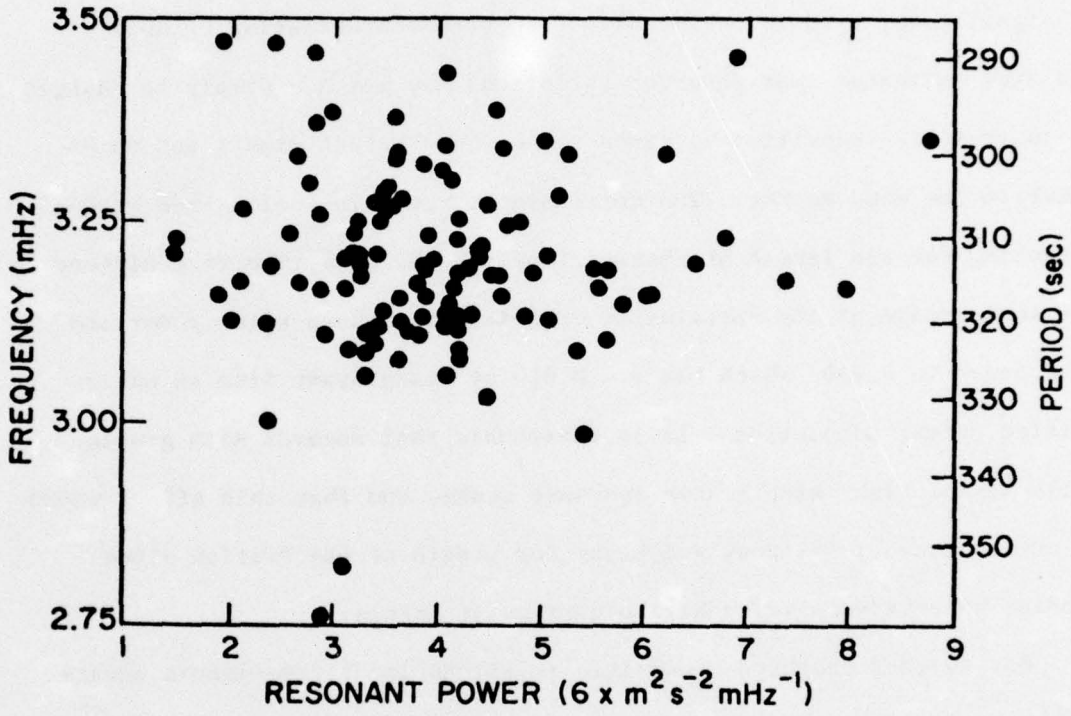

Figure 27. Scatter plot of average frequency (ordinate) versus signal power (abscissa) for the Stanford data.

no evidence for any correlation between the parameters with the conspicuous exception of the correlation between signal power and peak power, which is to be expected. The lack of correlation between signal power and noise power provides encouraging evidence that the definition of signal power used is essentially free from contamination by noise, and also indicates that observed variations are not due simply to changes in instrumental sensitivity, since these would affect signal and noise power in the same manner. The correlations were also calculated without weighting for the length of observation, and the only important difference was an increase of the correlation coefficient between noise power and peak power to 0.236, which has $P = 0.010$ of being drawn from an uncorrelated parent population. It is reasonable that records with greater noise levels might have higher resonant peaks, and that this effect would be more noticeable without weighting for length of observation since shorter observations would have higher noise levels.

One further check on a possible relationship of five-minute oscillations with large-scale structures in the corona and solar wind was made. Sheeley et al. (1976) have shown a very close correlation between coronal holes, solar wind velocity, and the geomagnetic C9 index. Because measurements of coronal holes and solar wind speed were not readily available, the amplitude and period of five-minute oscillations measured herein were compared with the C9 index. In addition, since Scherrer (1976) has found good agreement between the C9 index and the absolute value of the mean solar magnetic field as measured at Stanford, it was also used for comparison. The method used was again to plot one quantity as the ordinate and the other as abscissa and to calculate the correlation coefficient.

Since the C9 index is measured at UT1200 and five-minute oscillation measurements are near local noon (UT2000), the former was lagged in time by five days to approximate the expected 4-1/2 day solar wind transit time. The correlation coefficients and probabilities of being drawn from a parent population with no correlation are as follows:

Abscissa	Ordinate	r	P (ρ=0)
mean field	signal power	-0.0456	0.63
mean field	average freq	0.131	0.16
|mean field|	signal power	0.124	0.20
|mean field|	average freq	0.110	0.24
C9	signal power	-0.129	0.16
C9	average freq	-0.0412	0.66

There is again clearly no evidence for any correlation between the quantities considered.

Periods from Five to Seventy Minutes

In order to search for periodicities in the data between five and seventy minutes, spectral analysis was again employed. Each observation was again fit to a straight line and the fit subtracted to remove diurnal drifts and changes in baseline. To insure that the filtering effect of subtraction of this fit was minimal, only observations of duration $\geq$ 180 min were used. There were 92 observations used with a total observing time of 420 hr 13 min. To achieve the greater spectral resolution needed to search for longer period oscillations would have required extensive computing time if the cosine transform of the autocorrelation were used to obtain the power spectrum. Instead, the Fourier transform of the data was found by use of the fast Fourier transform (FFT) algorithm of Cooley and

Tukey (1965) as adapted from the program of Singleton (1969). The power spectrum is then given by the modulus of the Fourier transform, with no smoothing employed. Since implementation of the FFT is greatly simplified for a number of points equal to an even power of 2, each observation was centered in an array of length 2048 points (512 min), with the remainder of the array filled with zeroes, before computing the power spectrum.

The 92 power spectra computed were then averaged together, weighted for the length of the observation. The standard error of the mean power was also computed for the frequency interval of interest (0 - 4.167 mHz corresponding to periods of $P = \infty$ to $P = 4$ min). Figure 28 shows the average power spectrum--the two lines plotted are the average power plus or minus the standard error. Two features evident are the low frequency power with peak at 256 min and the five-minute resonant peak. The latter peak is much less smooth than the previous power spectrum (Figure 19) though fluctuations are not larger than expected from statistical considerations. The low frequency peak is sharpened by the higher frequency resolution, and can be accounted for by diurnal drifts of 24 hour period with frequencies below $1/256$ min^{-1} filtered out due to the finite observation times and the subtraction of a linear fit from each observation.

Between the five-minute resonance and the low frequency peak, there is no feature in the power spectrum of any prominence. This frequency interval may be seen more clearly if the vertical scale is changed as in Figure 29. The two lines plotted are again the average power spectrum plus or minus the standard error. There are fluctuations but none are large compared with the computed errors. It can then be concluded that

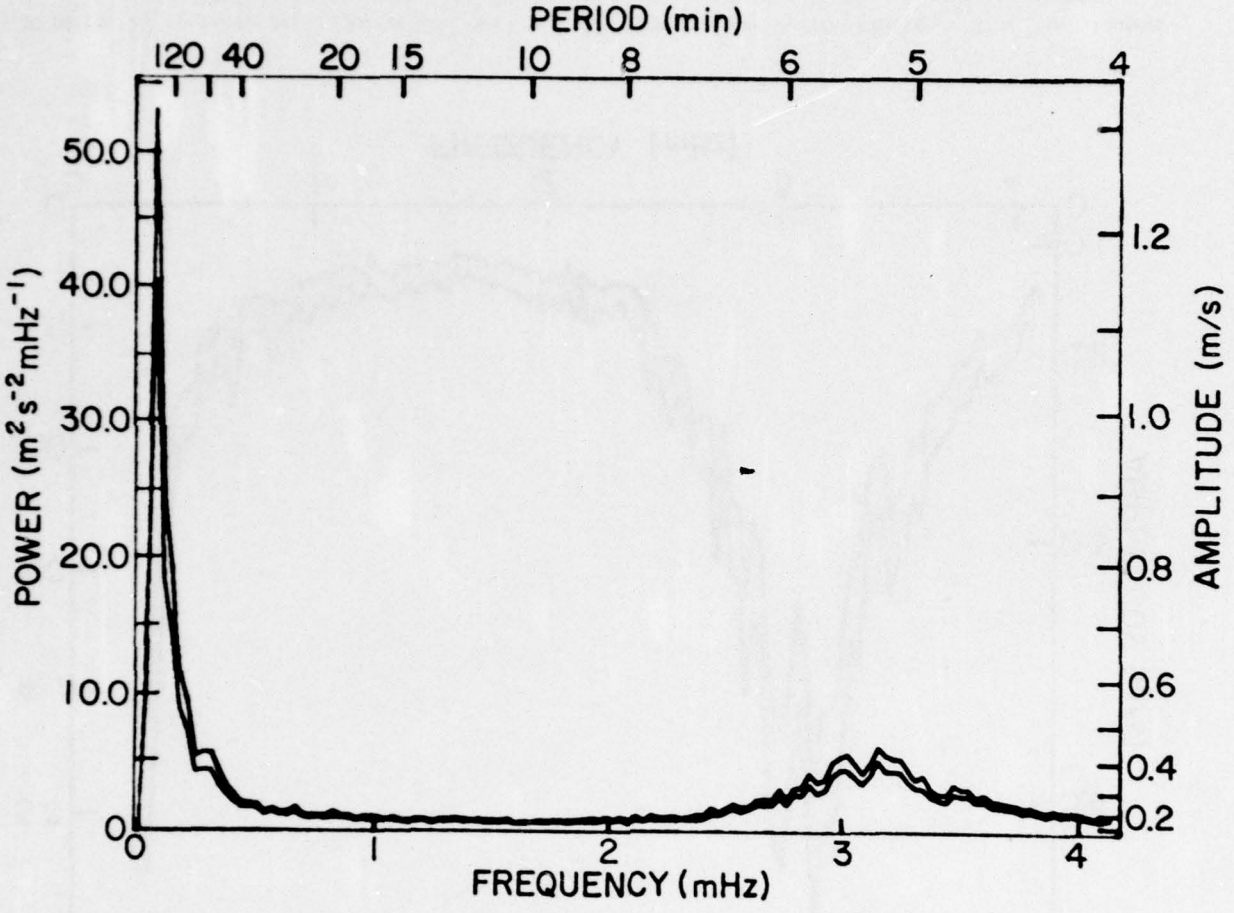

Figure 28. Average power spectrum of the Stanford observations. The power spectra have been computed using the fast Fourier transform algorithm, and observations shorter than three hours have been excluded. In averaging, power spectra are weighted for the length of the observation.

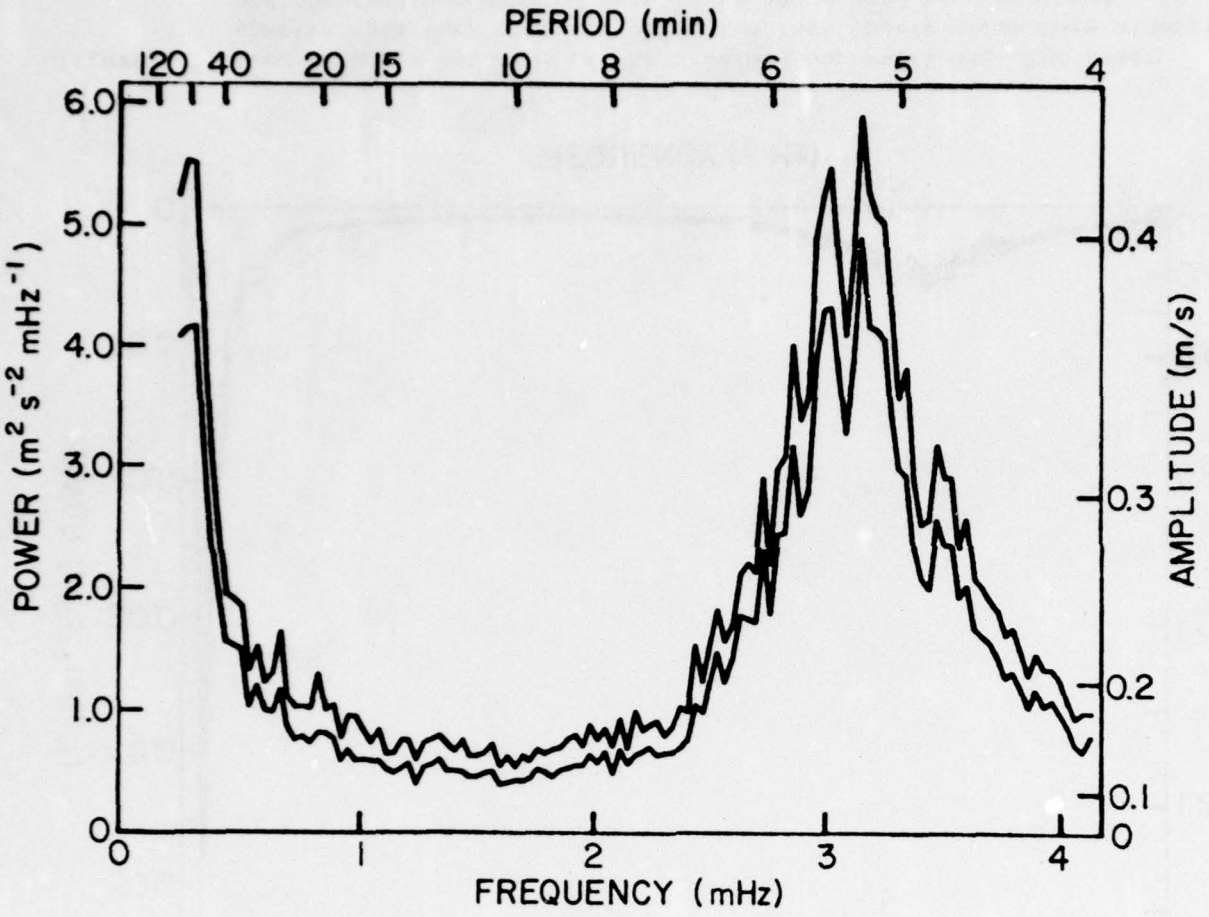

Figure 29. Same as Figure 28, with a different vertical scale. The two lines plotted are the average power plus or minus the standard error.

the present investigation has detected no pulsations in this interval. Such a null result might perhaps be unworthy of mention were it not for the positive results of other observers, especially those of Fossat and Ricort (1975a) and Hill et al. (1976a). Early attention was directed to the 10-min period reported by Fossat and Ricort, but with no signal seen. A few observations were even conducted using the Na-D_1 line (to investigate the possibility that the feature could be located higher in the atmosphere) but with the same result. A more recent paper from Grec and Fossat (1976) has not confirmed the existence of this feature, and its reality is questionable.

A comparison with the Hill report of several periods in the five to seventy minute period range is much more challenging. Such a comparison is simpler since both the SCLERA positive report and the present negative report are expressed by use of power spectra. Correction for different units used (arc msec and m/s) and for different quantities measured (displacement and velocity) can easily be made, but there is much greater room for disagreement or error in a comparison because of the very different observational techniques employed. If the fluctuations in the solar diameter measured by the SCLERA group are assumed to be due to actual mass motions, the change in diameter is related to a radial velocity by $\Delta d = 2\Delta r = Pv/\pi$. Using this expression and the conversion factor 1 arc msec = 725.3 m, the amplitudes of power plotted in Figure 29 have been converted to (arc msec)^2/bin and plotted on a copy of the most recent power spectrum of the Arizona group (Brown et al., 1976). The amplitudes measured in the present study have been multiplied by a factor of $1/0.208 = 4.81$ since calculations discussed in a previous chapter indicate

that the velocity difference signal measured with present techniques would be only 0.208 times the actual velocity for a radial pulsation. This scaling factor has also been used in the five-minute period range since the area scanned by Hill et al. (2 x 100" x 161".4 since there are two 100" slits and a 6".8 scan at the limb samples a segment of the sun corresponding to 161".4 at disk center) is about the same as for a $(3')^2$ aperture, and measurements described above show the amplitude of five-minute power to be 5.25 times as great with a $(3')^2$ aperture as with the 0.8 $R_\odot$ aperture used herein. The results of this comparison are plotted in Figure 30, with the logarithm of the power plotted because of the great range covered. Clearly, if the interpretation of the SCLERA signal as a mass motion is correct, the amplitudes measured in the present study are much smaller and would suggest that the peaks in the SCLERA power spectrum are not of solar origin.

As was discussed in Chapter I, this is not the first attempt at a confirmation of the oscillations reported by Hill et al. using spectral techniques. Brookes, Isaak, and van der Raay (1976), using potassium and sodium cells, measured amplitudes at periods < 1 hr "at least an order of magnitude" less than those reported by Hill. Grec and Fossat (1976) also used a sodium cell and concluded that the amplitudes reported by the SCLERA group were 30 times larger than upper limits they found at similar periods. Hill's response to this apparent conflict has been that "since the FFTD was used to define the solar edge in these data, the observed amplitudes depend on changes in the limb darkening function as well as actual motions. Consequently, the actual displacement of the surface may be only a small fraction of the observed effect." (Hill et al., 1976a.)

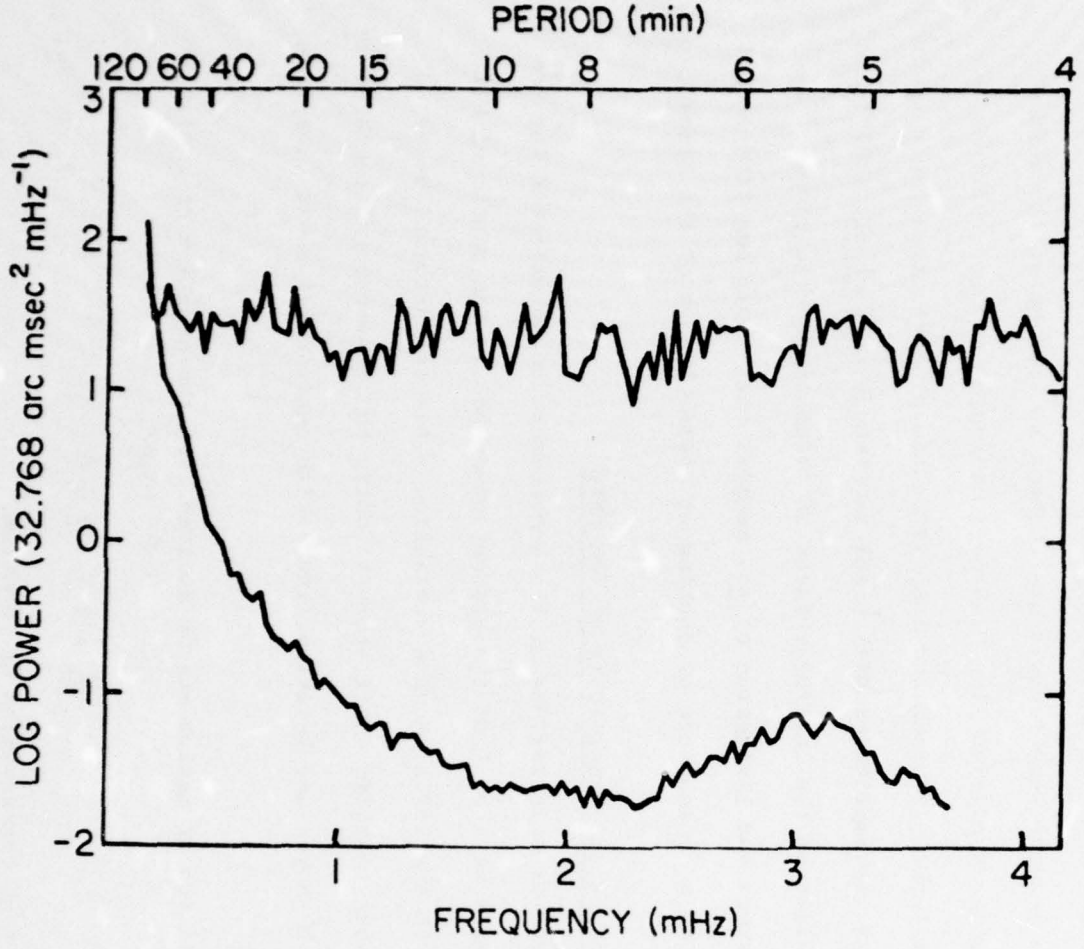

Figure 30. The upper line is the logarithm of the SCLERA power spectrum (Brown et al., 1976). The lower line is the logarithm of the limb shift produced by mass motions computed from the power spectrum plotted in Figure 29.

In a later paper, Hill, Caudell, and Rosenwald (1977a) have presented calculations to show how a small amplitude oscillation could produce much larger temperature fluctuations, thus changing the sun's limb darkening function and giving a much larger change in the apparent diameter measured by the FFTD than would be produced by actual mass motions. Attempts to measure such temperature changes by looking at the core of the temperature sensitive line CIλ5380 (Livingston et al., 1977) or the continuum intensity (Musman and Nye, 1976a and b) have given upper limits smaller than the amplitudes Hill predicts, though Hill et al. (1977a and b) have challenged the interpretations of intensity fluctuations of the other observers and Livingston et al. suggest that their negative result may simply be a consequence of looking at deeper levels of the atmosphere.

Calculations of the Sensitivity of the FFTD

Independent calculations of the enhancement to be expected for the FFTD were made as a part of the present study before the papers of Hill et al. (1976b and 1977a) became available. This calculation was based on expressions relating oscillatory velocity and temperature fluctuations as derived by Noyes and Leighton (1963) with substantial assistance from Lamb (1945).

An equation of motion may be derived from the equation of continuity,

$$\frac{D\rho}{Dt} + \rho \, \underline{\nabla} \cdot \underline{v} = 0 \, ,$$

the equation of conservation of momentum,

$$\rho \frac{D\underline{v}}{Dt} = - \underline{\nabla} P + \rho \underline{g} + \frac{1}{4\pi} (\nabla \times \underline{B}) \times \underline{B} \, ,$$

and an equation of state. For vertical propagation in a planar atmosphere (dependent only on the vertical component), the continuity equation becomes

$$\rho(1 + \frac{\partial \xi}{\partial z}) = \rho_o \quad .$$

If magnetic fields are assumed to be unimportant, the momentum equation becomes

$$\rho_o \frac{\partial^2 \xi}{\partial t^2} = - \frac{\partial P}{\partial z} - g\rho_o \quad ,$$

where ξ is the displacement. From the static relation $\partial P_o / \partial z = -g\rho_o$, this may be expressed as

$$\rho_o \frac{\partial^2 \xi}{\partial t^2} = - \frac{\partial}{\partial z} (P - P_o) \quad .$$

If one assumes an ideal gas equation of state,

$$\frac{\Delta P}{P} = \frac{\Delta \rho}{\rho} + \frac{\Delta T}{T} \quad \text{or} \quad P - P_o = P_o \left(\frac{\Delta \rho}{\rho_o} + \frac{\Delta T}{T_o} \right) .$$

Defining $\theta \equiv \Delta T / T_o$, $c_o^2 \equiv \gamma P_o / \rho_o$, and $H \equiv c_o^2 / \gamma g$ (c_o is the sound speed and H is the scale height, the equations may be combined and simplified

$$\gamma \frac{\partial^2 \xi}{\partial t^2} - c_o^2 \frac{\partial^2 \xi}{\partial z^2} + \frac{c_o^2}{H} \frac{\partial \xi}{\partial z} + c_o^2 \left(\frac{\partial \theta}{\partial z} - \frac{\theta}{H} \right) = 0 \quad . \qquad (1)$$

Noyes and Leighton introduce a second equation to describe the thermal response of the atmosphere:

$$\frac{\partial \theta}{\partial t} = - \beta\theta - (\gamma - 1) \frac{\partial^2 \xi}{\partial z \partial t} \qquad (2)$$

The first term on the right-hand side is the radiative cooling which is proportional to the amplitude of the temperature perturbation, with the radiative relaxation time given by $1/\beta$. The second term is the adiabatic heating due to the rate of compression $\partial(-\partial \xi / \partial z)\partial t$ by the wave.

It is next assumed that ξ and θ may be expressed as

$$\xi(z,t) = 2H\ A\ e^{(p+1)z/2H}\ e^{-i\omega t}$$

$$\theta(z,t) = B\ e^{(p+1)z/2H}\ e^{-i\omega t}$$

Substitution into equations 1 and 2 permits one to relate A to B and to solve for p:

$$B = (\gamma-1)\ \frac{i\omega}{\beta-i\omega}\ (p+1)\ A$$

$$P = \pm i\left(\frac{\beta-i\omega}{\beta-i\gamma\omega}\ \frac{\gamma\omega^2}{(c_o/2H)^2} - 1\right)^{1/2} \qquad (3)$$

Since the expression under the radical has the form $k + i\kappa$ with k and κ both positive, the + sign for p corresponds to a wave propagating upward though heavily damped, and the - sign for p corresponds to a damped wave propagating downward, which means that wave energy increases with height in the atmosphere. Hill argues that the downward propagating solution may be present due to reflections in the chromosphere and corona so the calculations described herein were performed with either choice of sign, though reasons will later be given for a predominance of the upward solution. Equation 3 permits the definition of a parameter α relating the amplitude of temperature oscillation to the velocity

$$\theta = \alpha\ \frac{v}{c_o} \text{ where } \alpha = \left|\frac{B}{-i\omega 2HA/c_o}\right| = (\gamma-1)\frac{c_o}{2H}\left|\frac{p+1}{\beta-i\omega}\right| \quad .$$

Since the above development assumes the same exponent for the displacement and the temperature perturbation but later gives an expression relating the two that will change with the properties of the atmosphere, it cannot be a good approximation if very large or sudden changes are involved.

In order to calculate the temperature change for an oscillation in the sun's atmosphere, the Harvard-Smithsonian Reference Atmosphere, or HSRA (Gingerich et al., 1971) was used. An oscillation was put in at the bottom of the atmosphere with amplitude such that if multiplied successively by the local exponential growth rate, $v(z_2) = v(z_1)\exp[(p(z_1)+1)(z_2 - z_1)/2H(z_1)]$, it would reach an amplitude of 1.0 m/s at an optical depth of 0.2. This level was chosen since Athay (1976, p. 170) gives the height of formation of FeIλ5124 as 0-200 km and optical depth 0.2 corresponds to the center of this interval. The periods used were those of peaks in the power spectra of Hill et al. (1976a) (47.9, 30.3, 24.8, 21.0, 17.1, and 14.6 min) plus a 68.3 min period obtained from personal communication and later published in Brown et al. (1976). A 5.0 min period was also used, with an assumed amplitude of 1.0 m/s at $\tau = 0.2$. The values for optical depth (τ), temperature (T), pressure (P), electron pressure (P_e), opacity (κ), fractional ionization of hydrogen (α), density (ρ) and vertical distance (r) were taken from the HSRA. The sound velocity was given by $c^2 = \gamma P/\rho$, and the ratio of the specific heats was taken from Cox and Giuli (1968) using the simplifications of Thomas et al. (1971)

$$\gamma = \frac{2+\xi}{2}\,\frac{5+\xi[5/2 + \chi/k_BT]^2}{3+\xi[(3/2 + \chi/k_BT)(5/2 + \chi/k_BT) - \chi/k_BT]}$$

where χ is the ionization potential of hydrogen and k_B is the Boltzmann constant ($\chi/k_B = 1.578 \times 10^5$). The quantity ξ is given by

$$\xi = \frac{2\alpha\nu r(1-\alpha)}{r(1+r) + \alpha\nu(1-\alpha)}$$

where ν is the ratio $n_H/n_{He} = 0.9$ in the HSRA and $r = n_e/(n_{atoms} + n_{ions})$.

The number density of nuclei, $n_{atoms} + n_{ions} = \rho/1.2877\ m_H$ for the abundances given in the HSRA, and the electron number density was taken to be $n_e = P_e/k_B T$. The inverse radiative relaxation time was taken from Spiegel (1957)

$$\beta = \frac{16\ \sigma\kappa T^3}{C_p}\ (1 - \tau_e\ \cot^{-1}\ \tau_e)$$

where σ is the Stefan-Boltzmann constant and τ_e the effective optical thickness of the perturbation, given by Ulrich (1970) to be approximately

$$\frac{1}{\tau_e^2} \simeq \frac{1}{\tau^2} + \frac{1}{\tau_p^2}$$

where $\tau_p = \Lambda\rho K/2\pi$ and Λ is the horizontal wavelength given by $\Lambda = 2\pi R_\odot/\sqrt{\ell(\ell+1)}$ for a spherical harmonic of order ℓ (ℓ=2 was used). The specific heat at constant pressure was also taken from Cox and Giuli

$$C_p = \frac{3c^2}{2T}\ (1 + \frac{\xi}{2})\left[1 + \frac{2\xi}{3(2+\xi)}\ (3/2 + \chi/k_B T)^2\right] \quad .$$

This expression, like the one for γ, is taken assuming the radiation pressure to be a small fraction of the total, which is a good assumption up to $\tau = 10^{-5}$ though decreasingly good above this level.

Using the expressions detailed above and the assumed velocities, Figures 31-34 show the calculated velocity amplitudes in m/s and temperature perturbations in °K as functions of height for both choices of sign on the exponential damping factor p and for four of the eight periods studied. Physically, the growth of longer period oscillations with height and the corresponding temperature fluctuations are less than for the five-minute period because radiative damping becomes increasingly important for longer periods. It is also clear that the change in amplitude of the downward propagating wave is much greater than it is for the upward wave.

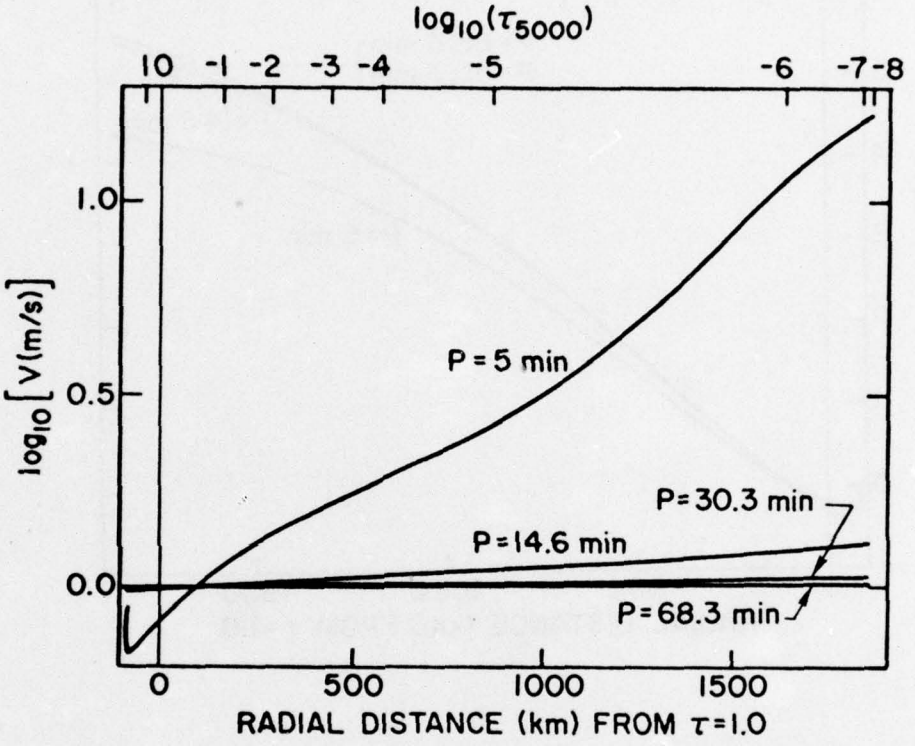

Figure 31. Plots of the logarithm of velocity as a function of position in the solar atmosphere for the upward propagating solution at periods of 5.0, 14.6, 30.3, and 68.3 minutes.

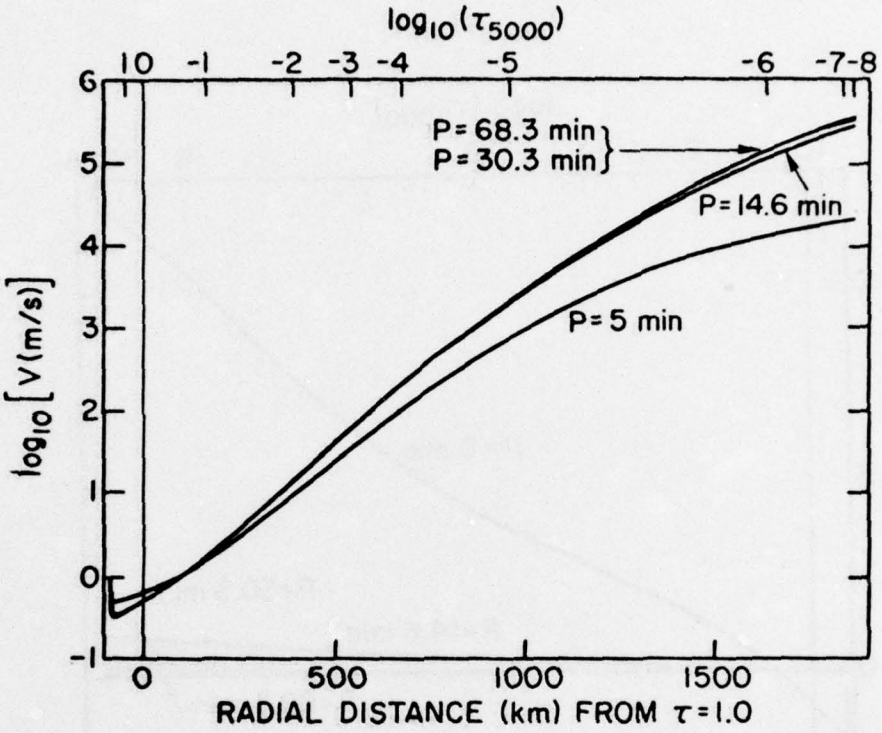

Figure 32. Same as Figure 31 for the downward propagating solution.

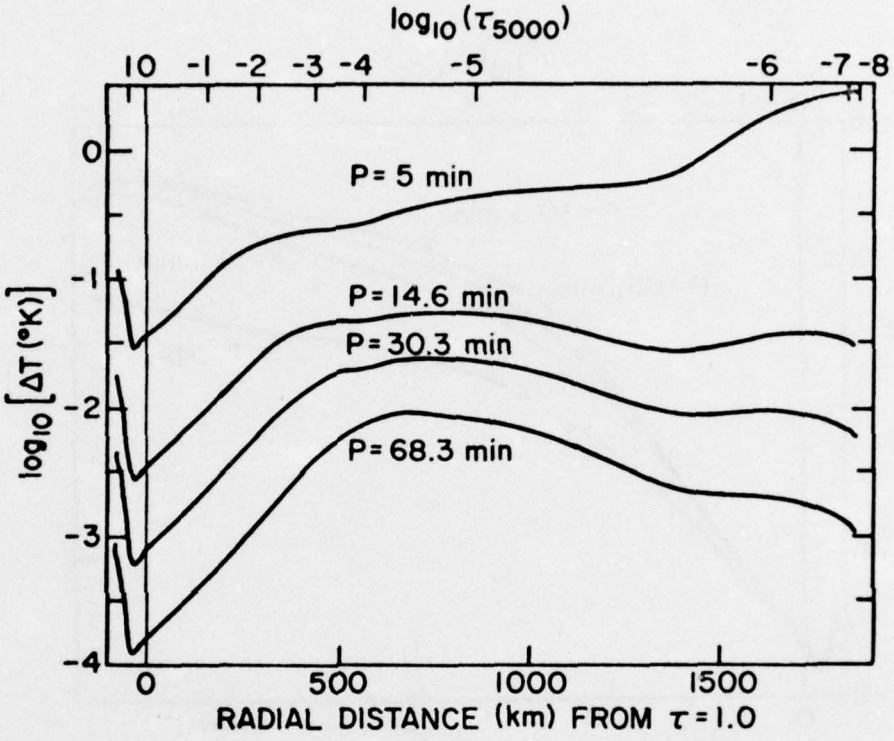

Figure 33. Plots of the change of temperature (logarithmic scale) as a function of radial position in the atmosphere for the upward propagating solution at periods of 5.0, 14.6, 30.3, and 68.3 minutes.

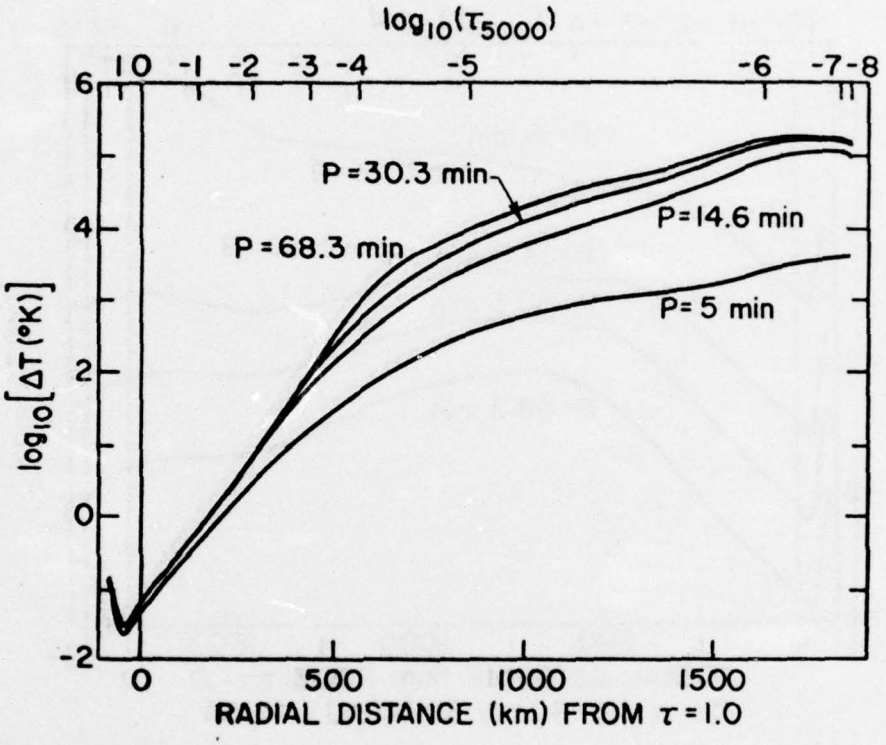

Figure 34. Same as Figure 33 for the downward propagating solution.

The reason is that for an atmosphere of decreasing upward density

$$\rho(z) = \rho(0)\ e^{-z/H}\ ,$$

if the oscillation propagates adiabatically, for its kinetic energy, K.E. = $1/2\ \rho v^2$, to remain constant, its velocity amplitude will have an exponential dependence

$$v(z) = v(0)\ e^{+z/2H}\ .$$

If radiation damping is included, it largely suppresses the exponential growth to be expected for an upward propagating wave, but nearly doubles the exponential decay to be expected for a wave propagating downward.

At five-minute periods, observational checks can be made on the calculations described above and are encouraging. It has previously been mentioned that Deubner (1971) reported the amplitude of five-minute oscillations to be 1.5 times greater in the Na-D_1 line than in FeIλ5124. Athay (1976, p. 170) gives the height of formation of the D_1 line as 400 - 600 km ($\tau = 1.4 \times 10^{-3} - 5 \times 10^{-5}$) and the present calculation gives an amplitude of 155-195 m/s in this range for an oscillation of 100 m/s at the height of formation of FeIλ5124. Measurements of five-minute temperature oscillations give widely scattered results and agreement with present calculations is mixed. Hudson and Lindsey (1974) estimate a 3°K oscillation from IR continuum measurements corresponding to 200 km above $\tau = 1$, and present theory predicts a 14°K oscillation. Noyes and Hall (1972) measured intensity fluctuations of 275°K peak-to-peak (80°K rms) in a molecular line which they believe to be formed at $\tau = 10^{-4}$, where present calculations predict $\Delta T_{rms} = 26.5$°K. Holweger and Testerman (1975) estimate a 20°K rms temperature fluctuation at

$\tau = 10^{-2}$ from oscillations in equivalent widths, and present calculations give 19.2°K. These three points are plotted in Figure 35 along with the curves predicted for upward and downward propagating waves, and though agreement is not good in the former case, it is much better than in the latter.

Intensity as a function of apparent position on the disk is next calculated, beginning with the following expression, taken from Gibson (1973):

$$I_\lambda(0,\theta) = \int_o^\infty S_\lambda(\tau_\lambda') \exp\left[-\left(\frac{\tau_\lambda'}{\cos\theta}\right)\right] \frac{d\tau_\lambda'}{\cos\theta}$$

where θ is the angle between the line of sight and the sun's radius vector and τ_λ' is the disk center optical depth of the contributing layer. When the effect of the sun's sphericity is included, as it must be near the limb, and the integral is changed to a summation over finite layers, the expression becomes:

$$I_\lambda(0,\theta) = \sum_i S_\lambda(\tau_i) \exp\left[\frac{-\tau_i \Delta s_i}{\Delta r_i}\right] \frac{\Delta\tau_i \Delta s_i}{\Delta r_i}$$

where Δr_i is the radial thickness and Δs_i the line-of-sight thickness of the layer in question. The intensity was calculated successively for rays passing tangentially through each layer in the HSRA, and then through layers inward from the innermost layer of the HSRA (82.6 km below $\tau = 1.0$) in steps of 10 km to a depth of 5692.6 km (7".8). Since the optical depth in the HSRA is given in steps of $10^{0.10}$, the change in optical depth $\Delta\tau_i$ is assumed to be $\Delta\tau_i = \tau_i (10^{0.05} - 10^{-0.05})$. The change in radius is taken as $\Delta r_i = (r_{i+1} - r_{i-1})/2$, and the line of sight thickness is then

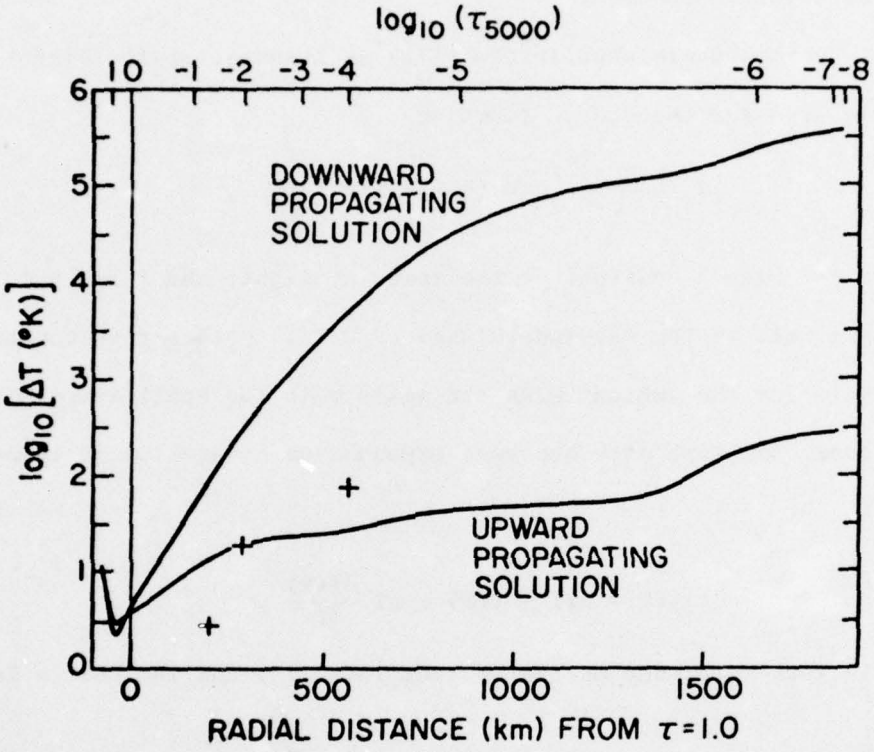

Figure 35. Plots of the change of temperature for a wave with 5.0 minute period. Upward and downward propagating solutions are plotted, along with the measured values of (left to right) Hudson and Lindsey (1974), Holweger and Testerman (1975), and Noyes and Hall (1972).

$$\Delta s_i = \left[\left(\frac{r_i+r_i+1}{2}\right)^2 - \left(\frac{r_i+r_i-1}{2}\right)^2\right]^{1/2}$$

from the Pythagorean Theorem.

Local thermodynamic equilibrium (LTE) is assumed, so the Planck function is used for the source function

$$S_\lambda = \frac{2hc^2}{\lambda^5}\left[\exp\left(hc/\lambda k_B T\right) - 1\right]^{-1} ,$$

where h is the Planck constant, c the speed of light, and λ taken to be 5500 Å since this is the wavelength used by Hill. Rather than compute the intensity for the ambient HSRA and again with the small temperature perturbations, the intensity has been expanded as a function of temperature:

$$I(T + \Delta T) \simeq I(T) + \Delta T \frac{\partial I(T)}{\partial T}$$

and calculations were made of the ambient intensity and the change in intensity

$$\Delta I = \frac{I \frac{hc}{\lambda k}\left(\frac{\Delta T}{T^2}\right)\exp\frac{hc/\lambda k}{T}}{\left(\exp\frac{hc/\lambda k}{T} - 1\right)} .$$

Layers below the bottom of the HSRA are assumed to have no contribution to the intensity because of the large negative exponential in the source function. Plots of I and $\Delta I(\omega)$ as functions of vertical distance for upward and downward propagating waves are shown in Figures 36 and 37.

The separate calculation of intensity and change of intensity is convenient in calculating the effect on the FFTD limb position because of the linear character of the Fourier transform. The limb is defined to be the position q which causes the following finite Fourier transform to vanish:

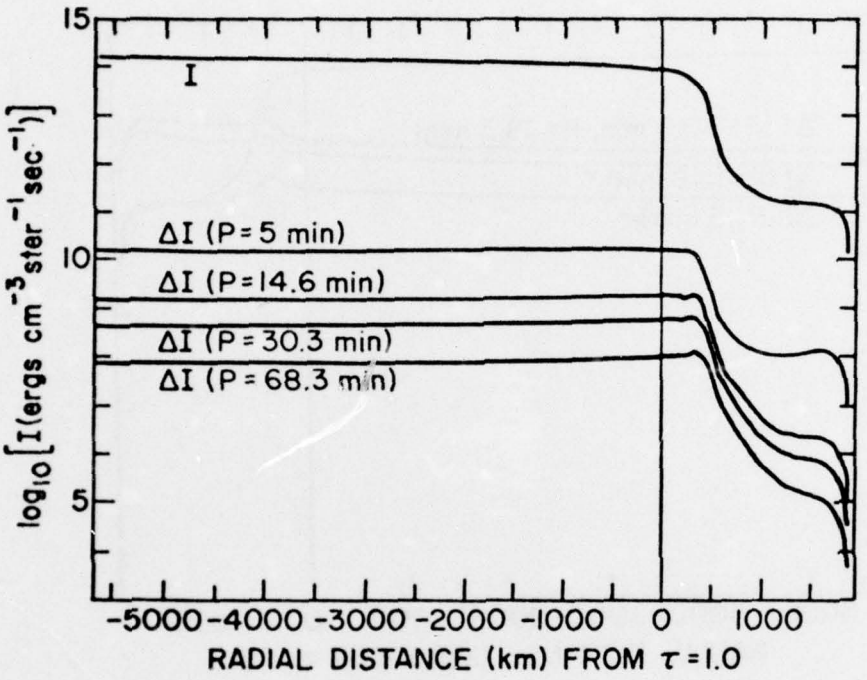

Figure 36. Intensity and change of intensity as a function of radial position (looking at the limb) for the upward propagating solution at periods of 5.0, 14.6, 30.3, and 68.3 minutes.

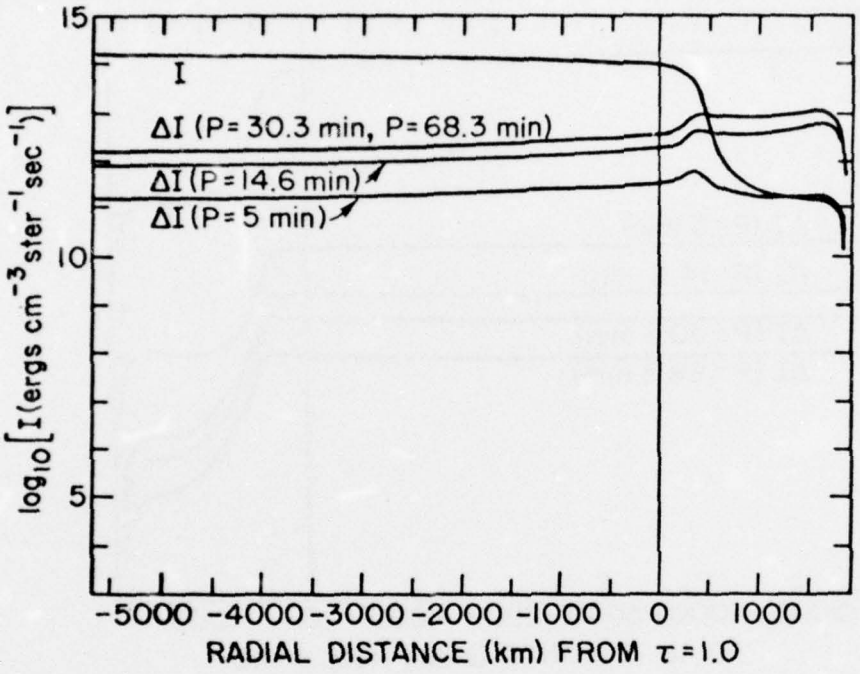

Figure 37. Same as Figure 36 for the downward propagating solution.

$$F(G;q,a) = \int_{-1}^{1} G(q + a \sin \pi s) \cos 2\pi s \, ds ,$$

where G is the intensity, a is the scan amplitude, and s is the integration variable. The Fourier transform of a perturbed intensity $G + \Delta G$ is clearly the sum of the Fourier transforms of the ambient intensity and the intensity perturbation. The substitution $r = a \sin \pi s$ is used to change the transform to

$$\int_{-1}^{1} G(q + a\,t) \frac{1-2t^2}{(1-t^2)^{1/2}} \, dt$$

where $t = r/a$ and r is the radial distance in physical units. Since the integrand is singular at $t = \pm 1$, the intensity is assumed to vary linearly between grid points and the integration is performed explicitly. Defining $G_1 = G(q + a\,t_1)$ and $G_2 = G(q + a\,t_2)$, one performs the integration

$$\int_{t_1}^{t_2} \left\{ \frac{G_2-G_1}{t_2-t_1}\, t + \frac{G_1 t_2 - G_2 t_1}{t_2-t_1} \right\} \frac{1-2t^2}{[1-t^2]^{1/2}} \, dt =$$

$$\frac{G_2-G_1}{t_2-t_1} \left\{ (1-t_2^{\,2})^{1/2} - (1-t_1^{\,2})^{1/2} - \frac{2}{3}(1-t_2^{\,2})^{3/2} + \frac{2}{3}(1-t_1^{\,2})^{3/2} \right\}$$

$$+ \frac{G_1 t_2 - G_2 t_1}{t_2-t_1} \left\{ t_2(1-t_2^{\,2})^{1/2} - t_1(1-t_1^{\,2})^{1/2} \right\}$$

with care taken at $t_1 = -1$ to avoid a singularity. Plots of the finite Fourier transform for the unperturbed intensity profile and for the intensity perturbations produced at the periods used previously are shown in Figures 38 and 39 for upward and downward propagating solutions.

The important feature in these figures is the place where the finite Fourier transform crosses zero. In the unperturbed case, the zero crossing

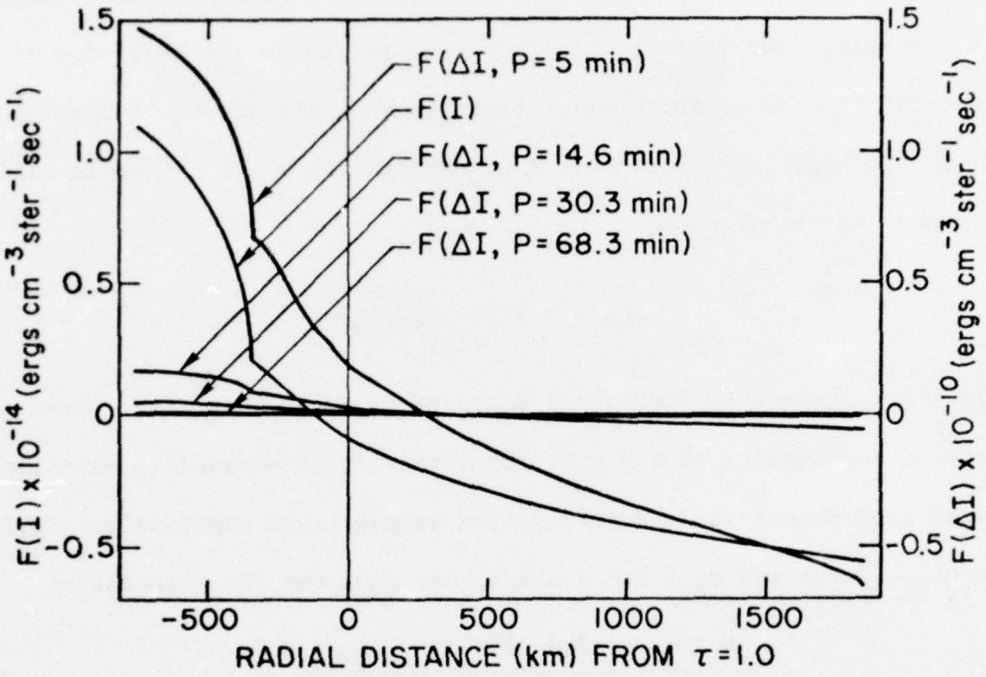

Figure 38. Finite Fourier transform calculated for the intensity and intensity change values calculated for the upward propagating wave as plotted in Figure 36.

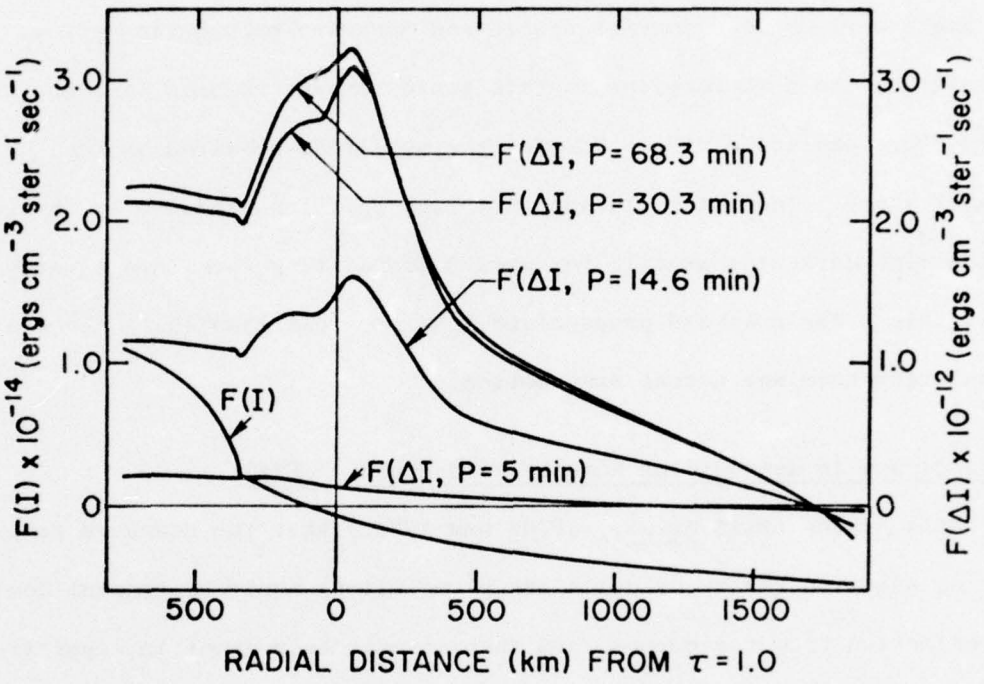

Figure 39. Same as Figure 38 for the downward propagating wave.

is at a level 122.6 + 3.32 km below optical depth unity. In the perturbed case, the limb is defined by the zero crossing of the sum of the finite Fourier transforms of ambient intensity and intensity perturbation. Table 6 shows the calculated shift in limb position for the eight periods used and for upward and downward propagating waves. In calculating the numbers given in this table, it was assumed that the oscillatory amplitude at $\tau = 0.2$ was the amplitude measured in the present study. The shifts in apparent limb position produced by changes in the limb darkening profile for upward propagating waves are clearly negligible. For downward propagation, the apparent limb shift becomes much larger than any actual mass motion.

Difficulties in Reconciling Results With Those of Hill

Hill argues (Hill et al., 1976b and 1977a) that the downward propagating solution (which he calls the β^+ solution) would be present due to reflection from the corona, and that it must be present in significant amounts in order to account for the differences in amplitude observed by his techniques and those reported from the spectral techniques used by other observers, such as Brookes et al., Grec and Fossat, and the present group. However, there is physical reason to believe that the β^+ solution is not present in significant amounts, and that Hill's amplitudes cannot therefore be reconciled with those of other observers. One of those cited by Hill for the suggestion that downward propagating waves may be present due to reflection is Ulrich (1970) whose discussion of reflection is based partly on the work of Souffrin (1966). As shown in Figure 1, the dispersion relation for an isothermal adiabatic atmosphere divides the k-ω plane into regions of propagation ($k_z^2 > 0$ and of

Table 6

Comparison of Equivalent Limb Shift from

Present Work with SCLERA Signal

Period (min)	SCLERA Signal (arc msec)	Present Work V_{rms} (m/s) (ℓ=0 mode)	Real Limb Shift (msec)	Limb Darkening Up Prop	Limb Shift Down Prop
68.3	7.0	1.89 $\pm$ 0.13	3.40	1.13×10^{-3}	104.6
47.9	5.3	1.56 $\pm$ 0.10	1.97	1.79×10^{-3}	82.4
30.3	4.6	1.00 $\pm$ 0.06	0.80	2.62×10^{-3}	46.6
24.8	7.7	0.92 $\pm$ 0.07	0.60	3.41×10^{-3}	38.0
21.0	7.0	0.84 $\pm$ 0.08	0.46	4.15×10^{-3}	30.8
17.1	4.2	0.76 $\pm$ 0.10	0.34	5.33×10^{-3}	23.6
14.6	4.0	0.65 $\pm$ 0.05	0.25	5.96×10^{-3}	17.3
5.0	4.8	100.0 assumed	13.17	6.40	249.7

attenuation ($k_z^2 < 0$). Souffrin showed that with the addition of radiative damping, the wave number is no longer purely real or imaginary but complex, which means that the k-ω plane can only be divided into regions that are predominantly propagating or attenuating regions, with the boundary defined by equating real and imaginary parts of the wavenumber. This gives an equation which Ulrich uses to define a critical horizontal wavenumber for reflection:

$$k_h^2 = \frac{\omega^2}{c^2} \frac{\omega^2 + \gamma\omega_R^2 - \omega_o^2(1 + \omega_R^2/\omega^2)}{\omega^2 + \omega_R^2 - N^2}$$

where ω_R, ω_o, and N are the inverse radiative relaxation time, the acoustic cutoff frequency, and the Väisälä-Brunt gravity-wave frequency and are given by

$$\omega_R = \frac{16\ \sigma T^3 \kappa}{c_p} (1 - \tau_e \cot^{-1} \tau_e),\ \omega_o = c/2H,$$

and

$$N^2 = -\frac{g}{\rho}\left(\frac{\partial \rho}{\partial S}\right)_p \frac{dS}{dz} = \left[(\gamma-1)\frac{g}{c} + \frac{g}{T}\frac{dT}{dz}\right] \text{ (Whitaker, 1963).}$$

Waves with horizontal wavenumber greater than the critical wavenumber will be predominantly propagating--those with smaller wavenumber will be predominantly attenuated. For a spherical harmonic or order $\ell = 2$, the horizontal wavenumber is given by $k_h = \sqrt{\ell(\ell+1)}/R_\odot = 3.87 \times 10^{-11}$ cm^{-1} (Ando and Osaki, 1975), so reflection would be expected at $k_h^2 = 1.50 \times 10^{-21}$ cm^{-2}. Calculations of k_h^2 using the HSRA show this condition not to be met anywhere between $\tau = 25$ and $\tau = 10^{-5}$ for the periods considered in Table 6. For the region between $\tau = 0.5$ and $\tau = 10^{-8}$ at the periods used which are longer than five min, $k_h^2 > 3 \times 10^{-19}$, which means that this is a predominantly attenuating region. For a five-minute

period, the Ulrich reflection criterion is satisfied near $\tau = 2 \times 10^{-6}$. This indicates that for periods longer than five minutes, reflections occur either at the bottom or above the top of the region tabulated in the HSRA. Waves reflected at or below the bottom of the HSRA will not be present in the line-forming region. If waves are totally reflected just above the top of the HSRA (at $\tau = 10^{-8}$) so that the amplitude of upward and downward propagating components is the same at $\tau = 10^{-8}$, the calculations plotted in Figures 31 and 32 may be used to compare the amplitudes present at the height of formation of FeIλ5124 ($\tau = 0.2$). To facilitate comparison, it was assumed that the upward propagating wave was of amplitude 1.0 m/s at $\tau = 0.2$. As Table 7 shows, the downward propagating (β^+) solution is very unimportant.

Further evidence that the downward propagating solution cannot be of large amplitude in this region of the atmosphere comes from a comparison with observations of five-minute oscillations. Since there are differences both in methods and results between the calculations made here and those described in Hill et al. (1977a), both have been used for comparison. Using the results of the present work, a 100 m/s wave is assumed to be present at the height of formation of FeIλ5124 ($\tau = 0.2$) and the amplitude is calculated throughout the HSRA. It has been mentioned above that the amplitude for the upward propagating solution increases to 155-195 m/s at the height of formation of the Na-D_1 line, in reasonable agreement with the measurements of Deubner (1971). The downward solution would give an amplitude of 1000 - 6000 m/s in the same range. In another measurement, Deubner (1969) reported a factor of six increase in amplitude between FeIλ5250 and H_α. This compares with a factor

Table 7

Computed Amplitudes for a 1.0 m/s Wave

Totally Reflected at $\tau = 10^{-8}$

Period (min)	Amplitude (m/s) Upward Propagation $\tau = 0.2$	$\tau = 10^{-8}$	Downward Propagation $\tau = 10^{-8}$	$\tau = 0.2$
68.3	1.00	1.01	1.01	2.99×10^{-6}
47.9	1.00	1.03	1.03	3.07×10^{-6}
30.3	1.00	1.07	1.07	3.31×10^{-6}
24.8	1.00	1.10	1.10	3.52×10^{-6}
21.0	1.00	1.14	1.14	3.80×10^{-6}
17.1	1.00	1.22	1.22	4.33×10^{-6}
14.6	1.00	1.31	1.31	5.02×10^{-6}
5.0	1.00	16.92	16.92	8.32×10^{-4}

of 8.22 calculated for the upward propagating solution and a factor of 1.02×10^4 for the downward solution. This comparison can only be valid as an order of magnitude argument since the assumptions of the theory are not valid for very large amplitudes, line contribution functions are broad, and measured amplitudes are dependent on details both of observational technique and of line formation. For example, Deubner (1971) reported a larger amplitude for MgIλ5173 (b_2) than for NaIλ5896 (D_1), though Athay (1976, p. 170) assigns a lower height of formation to the magnesium line. With these words of caution in mind, this comparison supports the conclusion that the upward propagating solution is predominant in this portion of the atmosphere.

A second comparison was made using the enhancement factors Hill et al. (1976b and 1977a) have calculated for the FFTD technique as compared with spectral velocity measurements. Though the enhancement they calculated is in comparison with a spectral line formed at $\tau = 10^{-3}$, comparison of the results at $\tau = 0.2$ with observations in the line NaIλ5896 mentioned above, and with those of Grec and Fossat (1976) show there to be no important differences. The power spectrum of the present observations converted to Hill's units (Figure 30) has been multiplied by the enhancement factors calculated. It is assumed that the Hill technique will see both the real limb shift and the apparent shift introduced by limb darkening, and that they will agree in phase. The result is shown in Figure 40. For the β^- solution (referred to herein as the upward propagating solution) the amplitude of the signal presently measured is everywhere too low, especially in the 10-40 minute period range. Addition of the 12 $(\text{arc msec})^2$ error bar found by Brown et al. (1976) brings the two

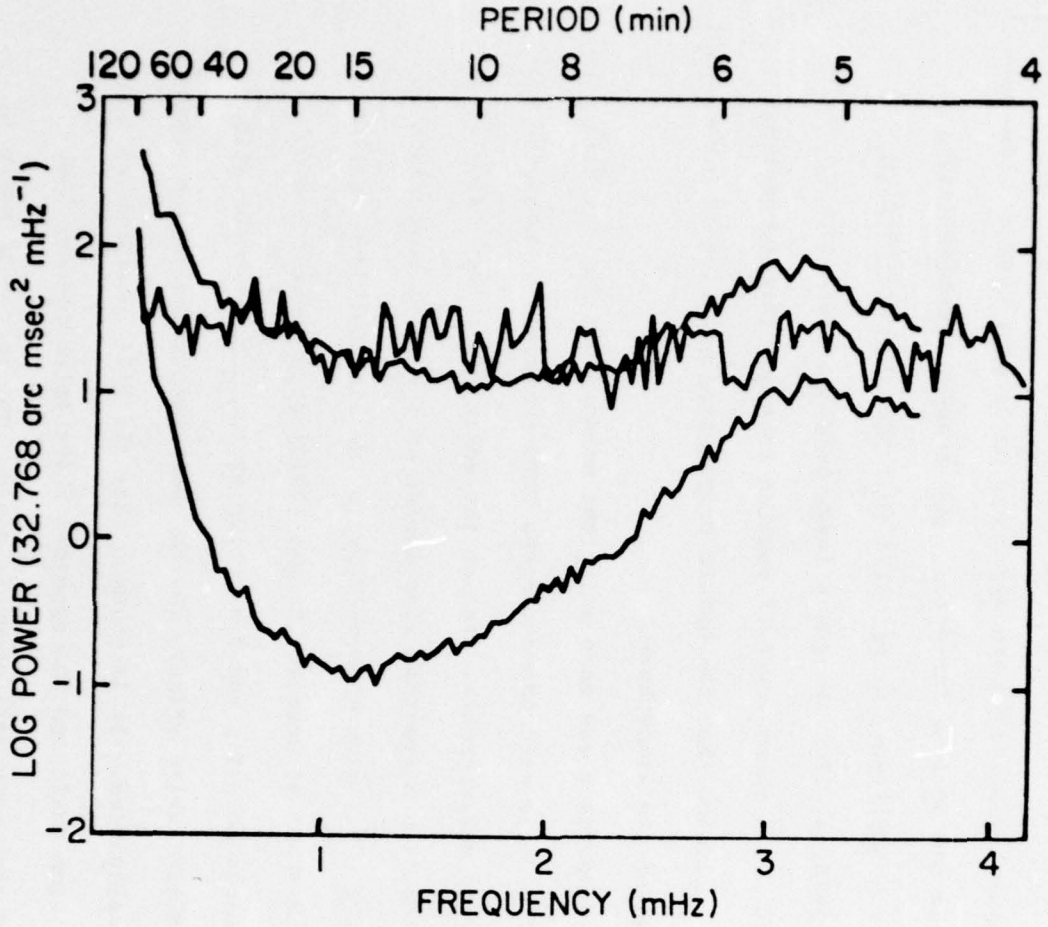

Figure 40. The line with greatest point-to-point fluctuations is the logarithm of the SCLERA power spectrum. The other two lines are the logarithm of the limb shift calculated from the power spectrum presently measured (Figure 29), multiplied by the enhancement factors calculated by Hill et al. (1976b). The lower line is for the β^- (upward propagating) solution, the smoother upper line is for the β^+ (downward propagating) solution.

observations into near agreement at five minutes. On the other hand, if one uses the β^+ (downward propagating) enhancement factors, the two observations nearly agree at 10-40 minute periods but the five-minute power measured in the present experiment becomes too large (and disagreement is substantial because a logarithmic scale is used). Any linear combination of the two solutions encounters the same basic difficulty--using Hill's enhancement factors and geometric scaling corrections that are generous at longer periods and conservative at five minutes, the power measured herein at five minutes is 8 times larger for the β^+ solution and 100 times larger for the β^- solution than the power measured at ten minutes. A calculation was also made to include the effect of the change in amplitude between $\tau = 0.2$ and $\tau = 10^{-3}$, and the result is still a five-minute amplitude 4 times larger for β^+ and 200 times larger for β^- than the ten-minute value. Since Hill et al. report a power spectrum that is flat or if anything lower at five minutes than at ten minutes, the two results cannot be reconciled unless the reflected solution is present in greater proportion at longer periods than at five minutes. As the results of the calculations presented in Table 7 show, the opposite is likely to be the case since waves of five-minute period are more likely to be reflected and are reduced less by radiative damping than those of longer period. The results of the present study and those of Hill et al. are very hard to reconcile, which makes it unlikely that both sets of measurements are entirely of solar origin.

Statistical Significance of the SCLERA Peaks

If the peaks observed in the SCLERA power spectra are not solar pulsations, what are they? Grec and Fossat (1976) have suggested that

the peaks in the power spectrum of Hill et al. (1976a) are no larger than might be expected due to statistical fluctuations. The SCLERA group has responded by publishing a new power spectrum (Brown et al., 1976) with higher resolution and somewhat lower amplitudes, especially at the lowest frequencies. The reduced amplitudes below 0.5 mHz could be in part due to removal of slow drifts in the signal by subtraction of a parabolic fit. Brown gives the following three reasons for arguing that the peaks in the power spectra are significant and of solar origin: (1) Variances computed at a given frequency for eleven independent power spectra are smaller than the signal in the range from 0.2 to 1.0 mHz (see Groth, 1975). (2) The largest peaks are reproducible--when the data are divided in half and the fifteen largest peaks are compared, ten are coincident. (3) The peaks have an average height above the local mean of 9.2 (arc msec)^2 in the frequency range from 0.2 to 2.5 mHz compared with a height of 8.0 $\pm$ 1.2 (arc msec)^2 computed for noise alone.

A critical examination of these arguments leaves some room to doubt the conclusions. First, the comparison of variance and power does provide evidence for signal power in the frequency interval considered (0.2 - 1.0 mHz) but does not give evidence for a concentration of that signal power into discrete peaks. In fact, if one accepts the noise level adopted in this paper (12 arc msec^2/frequency interval) and takes the 28 points in the 0.2 - 1.0 mHz interval, excluding the 7 peaks above the 0.999 confidence level; of the remaining 21 points, 16 have power significant at the 0.950 confidence level. The binomial probability of this being true of noise is only 3.01×19^{-17}, which means either that the power must not be concentrated in the peaks or that some contamination

of the peaks into adjacent frequencies is produced by experimental or analytical techniques.

The third argument mentioned above is advanced to support the concentration of the power into peaks, since the peaks are larger than calculated statistical fluctuations. However, this calculation would be dependent on the assumed level of noise power--the fact that the observed peaks are larger than those calculated would argue just as well for the noise level being larger than adopted as it would for the peaks being of non-statistical origin.

By far the most impressive argument for the concentration of power at discrete frequencies is the second one, their repeatability. It is hard to imagine why background noise of instrumental origin should be concentrated in such repeatable peaks. This argument becomes less persuasive, however, if one compares the most recently published power spectrum (Brown et al., 1976) with the one previously published (Hill et al., 1976a). Figure 41 shows a plot of both power spectra to the same scale. Differences in resolution and smoothing of the earlier power spectrum complicate comparison, as does their complexity, so one might see wonderful agreement or absurd disagreement depending on one's point of view. A more quantitative approach is to compare the five or ten largest peaks in the interval from 0.7 to 6.0 mHz for coincidences. Lower frequency comparison is excluded by the qualitative differences in the two spectra below 0.7 mHz. If one defines a coincidence by having a peak in the higher resolution spectrum (that of Brown) within $\pm$ 1/2 frequency bin ($\pm$ 0.035 mHz) of a peak in the older spectrum (that of Hill), one obtains two coincidences among the five largest peaks and two among

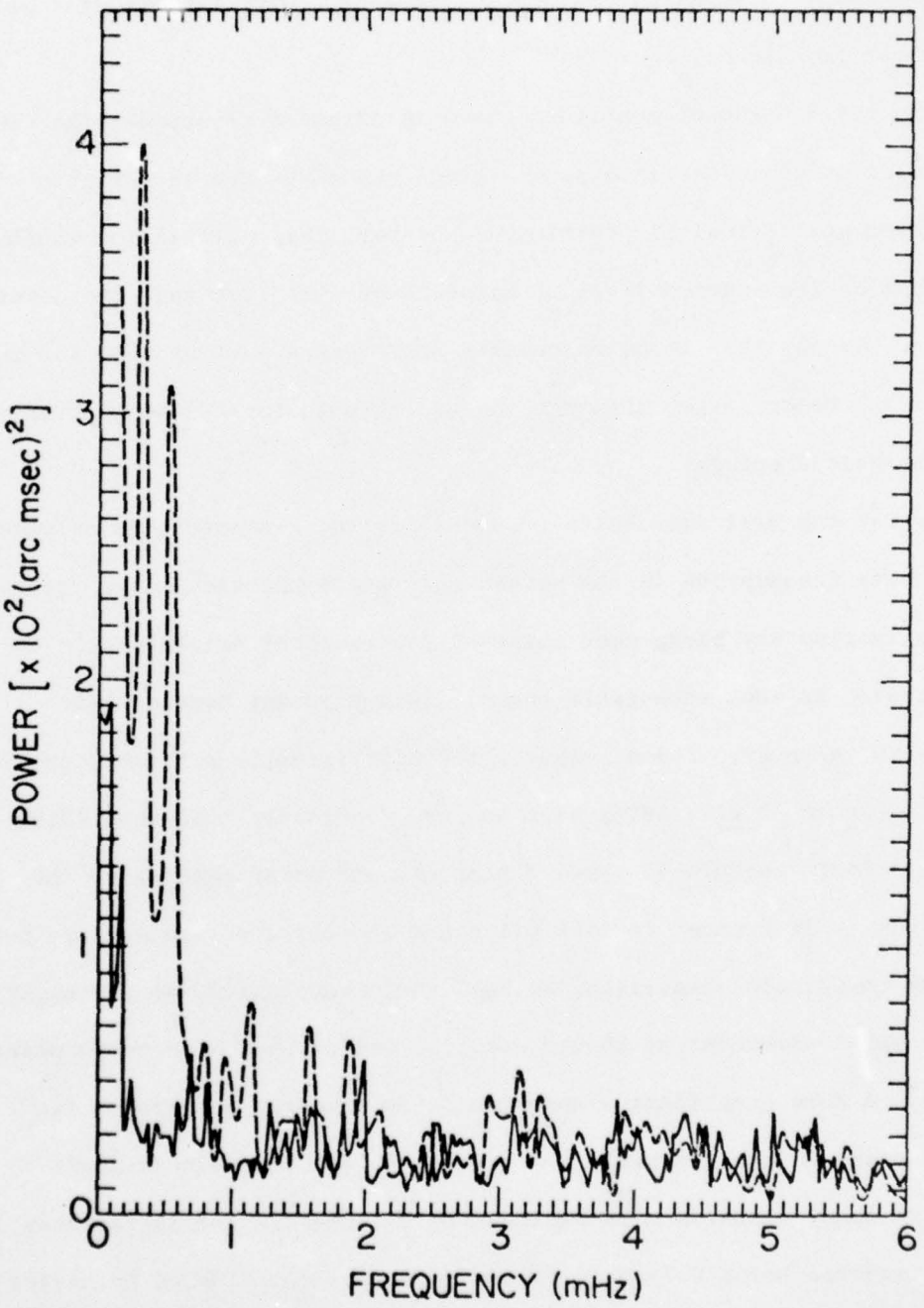

Figure 41. The dashed line is the SCLERA power spectrum reported in Hill et al. (1976a). The solid line is the SCLERA power spectrum reported in Brown et al. (1976).

the ten largest peaks. The most impressive degree of alignment is obtained for the largest peaks, with the two coincidences of five having a 3.2% probability of chance occurrence if one assumes that there are 14.4 frequency bins per mHz (or 76 in the interval from 0.7 mHz to 6.0 mHz). However, closer examination shows the power spectra not to be flat but to be higher at lower frequencies, causing the largest peaks to be concentrated at lower frequencies. If one takes only the interval from 0.7 mHz to 2.0 mHz there are still two coincidences among the five largest peaks, but since there are now only 19 frequency bins, the probability of chance occurrence is raised to 39.7%. Though Brown selects the largest peaks in terms of height with respect to surroundings rather than absolute height, the same preference of peaks for lower frequencies is still apparent from examination of the published power spectra, which would mean the probability estimate of 5×10^{-4} is too low. Whether or not such mistakes were made, the agreement between the two power spectra in Figure 41 is not impressive. Differences in length of observation, in frequency resolution, and in analysis (subtraction of a parabolic fit in the later power spectrum) do complicate this comparison and could explain discrepancies, but if the details of the power spectra are strongly dependent on the observational parameters or techniques of analysis, any information they contain about the sun will be of limited reliability. This discussion does not pretend to prove that the SCLERA signal is purely noise--it would be hard to prove this even if the original data were available. Nor can the strength of the argument concerning repeatability of peaks in the power spectrum be denied. But in view of questions raised herein, the statistical significance of these peaks does not seem well established.

And in view of the negative results of other solar observers at similar frequencies, the solar origin of these peaks would still be open to question even if their statistical significance were well proven.

The Two-Hour Forty-Minute Oscillation

As mentioned previously, it was not possible to completely eliminate slow drifts in the signal which were probably due to shifts in position of the lenses or the polarizing optics (which were caused by the heating effect of the same solar radiation which was being studied). These slow drifts made any general search for oscillations of very small amplitude and long period hazardous. In the present investigation, attention was therefore especially directed at attempts to confirm the oscillation reported by Severny et al. (1976a and b). This specific search could be conducted with greater confidence because not only were the amplitude ($\pm$ 2 m/s) and period (2 hr 40 min $\pm$ 0.5 min) published, but information was also available through private communication regarding the phase of the oscillation and the methods of analysis used.

To limit ambiguity as much as possible in comparing results, data reduction and analysis was performed as nearly as possible in an identical manner to that used in the Crimea. Data were first multiplied by the calibration factor to convert to m/s. In most of the analysis, they were then multiplied by - 1.68 to correct for different aperture geometries and opposite sign conventions. Five-minute averages were then found for intervals centered on UT times multiples of five minutes, for example, the average of measurements between UT 2147:30 and UT 2152:30 was computed and assigned to the time UT 2150. This averaging was performed both for

conformity with the procedure used in the Crimea and to remove most of the effect of five-minute oscillations. Plots of the original observations were used to identify and remove features in the new five-minute average data set which were obviously spurious. Each observation was then fitted by least squares to a parabola and the fit subtracted. Observations shorter than two hours were excluded from further analysis at this point. The data were then superposed about keytimes at intervals of 2 hr 40 min and the result of this superposed epoch is shown in Figure 42. There is no indication of the sinusoid of amplitude $\pm$ 2 m/s which Severny et al. obtained from a similar analysis. The values obtained using the Crimean data for 1975 are plotted for comparison--the 1976 Crimean results were not used because there were appreciable differences between two available copies of the epoch obtained using 1976 Crimean observations. Because of the similarity of methods used, the different result obtained was unexpected and led to a careful re-examination of observations and analysis in search of an explanation.

Instrumental Differences

One experimental detail with potential for error was the calibration factor (see Appendix B). There was some scatter in values obtained in different calibration measurements, and major losses in sensitivity were known to have occurred at times due to a misalignment of polarizing optics. However, the large amplitude of five-minute power observed, in agreement with previous results, makes such a calibration error very unlikely. In efforts to be discussed below taking all periods between 150 and 170 minutes, the largest amplitude sinusoid measured in this range in the present work is still a factor of two smaller than the

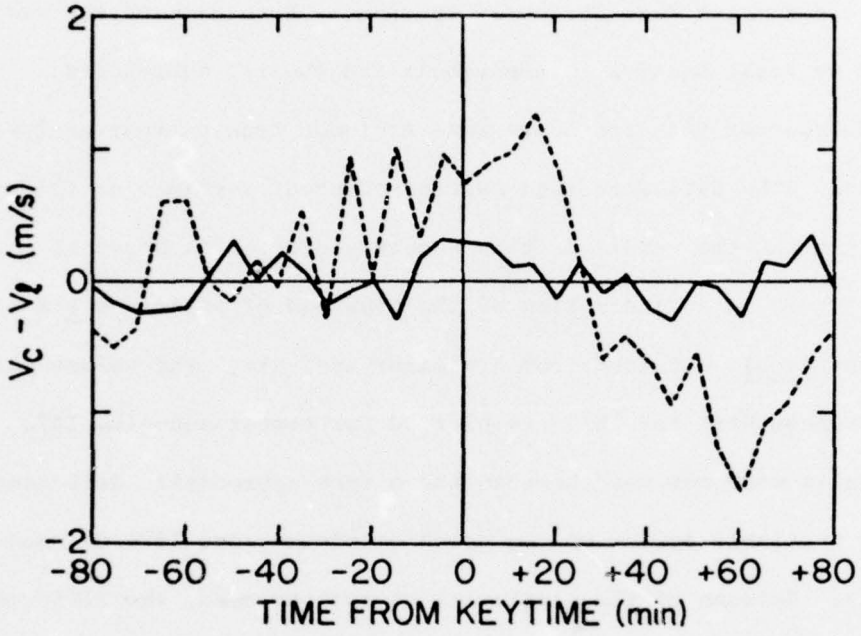

Figure 42. The solid line is the superposed epoch obtained at a period of 2 hr 40 min using the Stanford 1976 data. The dashed line represents the same superposed epoch, with adjustment for phase, sign, and sensitivity, for the Crimean 1975 data.

Crimean result with correction made for different detector geometries, and a multiplication of the calibration factor by two would give a five-minute oscillation amplitude much larger than expected from other observations using small or large apertures.

Another possibility, suggested by Severny, is that the optical arrangement used at Stanford could produce extreme vignetting which would give large amplitude five-minute oscillatory power but would reduce sensitivity to global modes. This suggestion and experiments made to determine the extent of vignetting were discussed above in the chapter describing the instrument, with the conclusion being that such extreme vignetting was not present (see especially Figures 17 and 18). This result was further insured by the adjustment of the iris diaphragm regularly performed in alignment and calibration to insure equal intensity of light from center and limb portions of the solar image. This intensity balance is consistent with essentially uniform transmission of sunlight out to $\sim 0.8\ R_{\odot}$, and would not be possible for transmission limited to a small spot or long sliver on the solar image.

Another possible experimental reason for the detection of a 2 hr 40 min oscillation at the Crimea but not at Stanford is the masking off of the outer 0.20 of the sun's radius to insure equal intensities of center and limb light. Severny has suggested that by so doing, the Stanford apparatus might no longer be sensitive to some non-spherical modes. This masking results in the loss of 0.36 of the area of the solar disk and 0.275 of the total sunlight, and might prove especially critical in reducing sensitivity to the predominantly horizontal motions to be expected for the g-mode oscillations which are theoretically expected at

such long periods. For radial motions having an angular dependence described by spherical harmonics, Table 4 in the previous chapter gives the result of calculations of the sensitivity factors for the different geometries used at Stanford and the Crimea. The Stanford geometry is always less sensitive than that used in the Crimea, with the worst relative loss of sensitivity being 0.596 for the $\ell = 0$ spherical harmonic. In order to make the same comparison for horizontal motion, it was assumed that the displacements were again given by spherical harmonics but that the motions were tangential rather than radial with amplitude and direction given by the negative gradient of the spherical harmonic. The averaged velocity signal was weighted by limb darkening, and an ensemble average was taken for all possible observer orientations, with orientations being limited to the $\theta = \pi/2$ plane for normal orientation calculations (corresponding to the mode being aligned with the ecliptic). The results of these calculations are also given in Table 4, with the Y_{21} mode excluded since it is geometrically equivalent to the Y_{22} mode. The worst relative loss of sensitivity is for the Y_{11n} mode, for which the Stanford geometry is only 0.655 as sensitive. For both radial and tangential motions, calculation of modes only out to $\ell = 2$ appears justified since sensitivities become more nearly comparable for higher order modes. When the 200 m/s shift in baseline was noticed in early July observations, calculations showed that a displacement of the polarizing aperture relative to the solar image capable of producing such a shift would reduce the sensitivity factor for radial oscillations from 0.208 to 0.152. However, when the baseline shift was found to be due to a misalignment of the image slicer, this calculation was redone and the loss of sensitivity was found to be less than 1%.

Examination of Data Analysis Techniques

Since the instrumental differences do not appear to be sufficient to explain the difference in result, the data analysis techniques used were then re-examined to see if a real 2 hr 40 min signal might not have been missed or removed. An easy way such a period could be missed would be if the superposed epoch used to search for the period were not of exactly the right period. Data from April 13 through August 6 span about 1036 periods of 2 hr 40 min, so a period error as small as 1.0 sec would produce a phase slippage $\Delta\emptyset$ of 17 min. The reduction of amplitude for an arbitrary phase slippage may be obtained from:

$$\langle y(x)\rangle = \frac{1}{N}\sum_{i=1}^{N} \cos\left(x + \frac{i\Delta\phi}{N}\right) \simeq \frac{1}{\Delta\phi}\int_{o}^{\Delta\phi} \cos(x + \phi)\,d\phi$$

$$= \frac{\sin(x + \Delta\phi) - \sin x}{\Delta\phi} = \frac{\sin \Delta\phi/2}{\Delta\phi/2} \cos\left(x + \frac{\Delta\phi}{2}\right).$$

So a total phase slippage of $\Delta\phi$ will produce a shift in the average phase of $\Delta\phi/2$ and a decrease in amplitude by $(\sin \Delta\phi/2)/(\Delta\phi/2)$. To be sure of not missing an important period, the superposed epoch was repeated, stepping the period by 0.1 min from 150.0 min to 170.0 min. Any real period could be missed by at most 0.05 min = 3 sec, giving a total phase shift of $\Delta\phi$ = 51.8 min = 2.034 radians and a reduction of amplitude by a factor of 0.836. Rather than plot the 201 resulting epochs, each was fitted to a sinusoid of the same period and the harmonic amplitudes are plotted in Figure 43. No single period is clearly outstanding and the largest amplitude is 0.44 m/s. One of the periods yielding this amplitude is 160.3 min, but it is sufficiently different in amplitude (twice as small) and period (0.3 min gives a phase shift of $\Delta\phi$ = 154.8 min for which $(\sin \Delta\phi/2)/(\Delta\phi/2)$ = 0.034) that it is not likely to correspond to the signal reported by Severny.

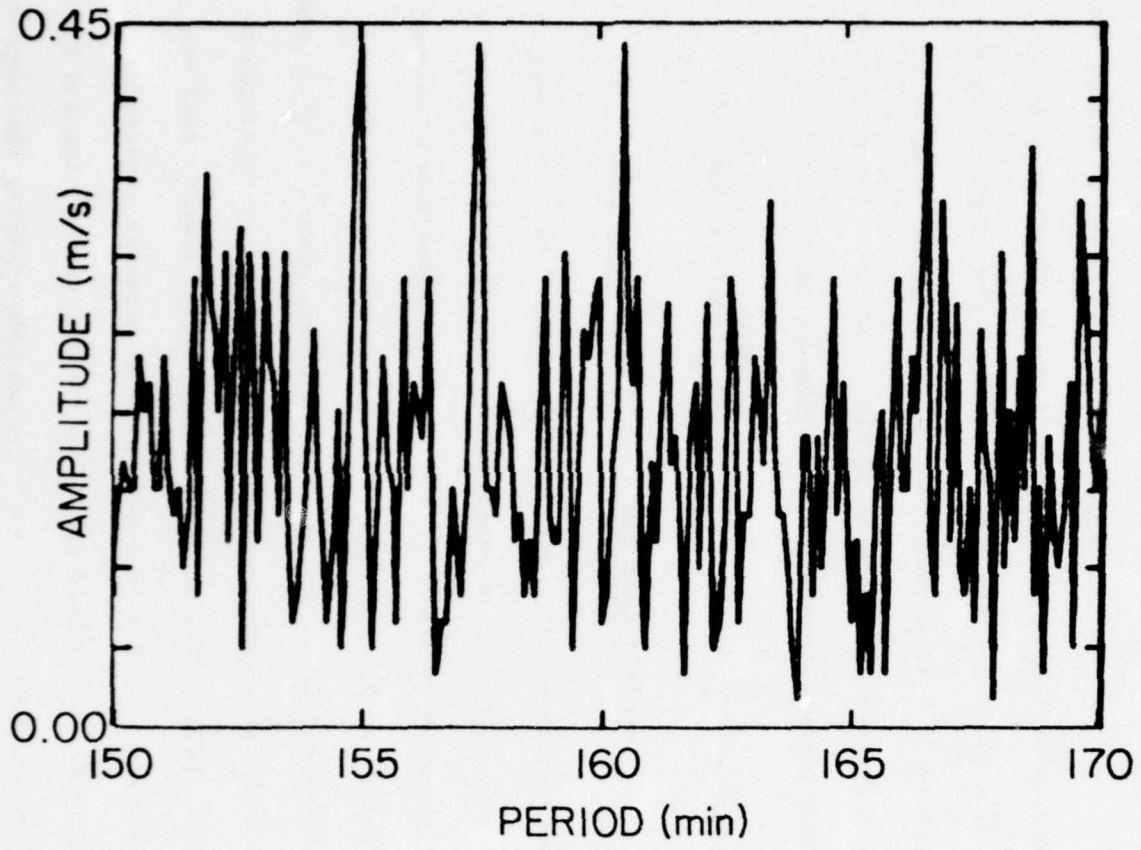

Figure 43. Scan of amplitudes obtained by fitting superposed epochs of 1976 Stanford data at periods from 150.0 min to 170.0 min to sinusoids. Values are multiplied by 1.68 to correct for different polarizer dimensions.

An estimate of the amplitude of the upper limit indicated by each superposed epoch was also calculated. First, for the number of points w in the epoch window (33 points for a 160 min period), the probability of there being n points more than an error bar from a true signal is given by

$$P(n,w) = \frac{n!(w-n)!}{w!} (0.317)^n (0.683)^{w-n}$$

This number was computed and added starting with n = 0 until the sum $\sum_{n=o}^{k} P(n,w)$ became ≥ 0.05, and then k-1 gave the largest number of points in the window that a curve could miss before the probability of the curve matching the data dropped below 5% ($\sim 2\sigma$). At each period between 150.0 min and 170.0 min, sinusoids were stepped in amplitude by 0.01 m/s and in phase by 5 min until the largest sinusoid was found which had 5% probability of matching the curve produced by the superposed epoch. Figure 44 shows a plot of the upper limits thus calculated. The largest value obtained in this interval is 0.81 m/s, which is smaller than the value obtained by fitting an epoch of the Crimean data to a sunusoid and much smaller then the $\pm$ 2.0 m/s amplitude originally reported. This analysis indicates that there is less than a 5% probability that the Stanford data could contain anywhere in the 150 to 170 minute range of periods a signal of the amplitude reported from the Crimea.

Another part of the analysis which could conceivably result in loss of a real 2 hr 40 min signal is the removal of a parabolic fit from each observation. To determine the effect of this fit, a sine curve of amplitude 0.75 m/s was added to the data at a period of 160.25 min. This 0.75 m/s sine curve was added to data which had not been multiplied by

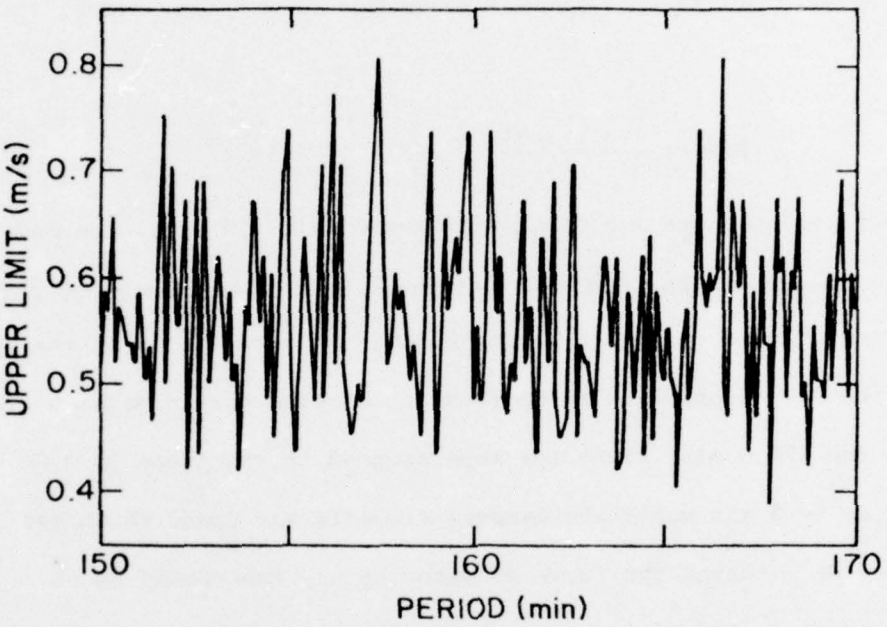

Figure 44. Scan of upper limits calculated for superposed epochs of Stanford 1976 data at periods from 150.0 min to 170.0 min. Values are multiplied by 1.68 to correct for different polarizer dimensions.

the 1.68 sensitivity factor correction, and so would correspond to a 1.26 m/s signal for the Crimean geometry. This period was chosen to be midway between periods used in the epoch analysis so a maximum possible phase slippage would be present, and also was near one of the largest amplitude epochs (at 160.3 min) which gave a stiff test of possible masking of a solar signal by instrumental background. The sine curve was added at four different phases (separated by $\pi/2$) and the fit was then removed and analysis conducted as previously. Figure 45 shows plots of the superposed epoch of the original data and of data plus sinusoid at 160.2 min and 160.3 min. The sine curve shows up clearly for all four phases at 160.2 min, but at the second phase at a period of 160.3 min, it is directly out of phase with the instrumental background and the result is a poor sinusoid of amplitude no larger than the original. It is therefore possible that a solar signal as large as 1.26 m/s could be hidden if its period fell exactly between those used in the scan of epochs and if it was adjacent to and exactly out of phase with the largest instrumental signal in the interval.

As a test to determine if any period in the interval behaved like a real signal persisting over the full period analyzed, the data were next divided into three equal segments and a similar scan of epochs was performed over each segment to see if any period was large over all three segments. The largest twenty epochs, measured by the amplitude of the harmonic fit and separately by the amplitude of the $P = 0.05$ upper limit, were determined for each third of the data and examined for coincidences. It would be expected that any two sets of twenty numbers drawn at random from 200 values would have two in common, and with three independent segments, six double coincidences would be expected. Seven were found

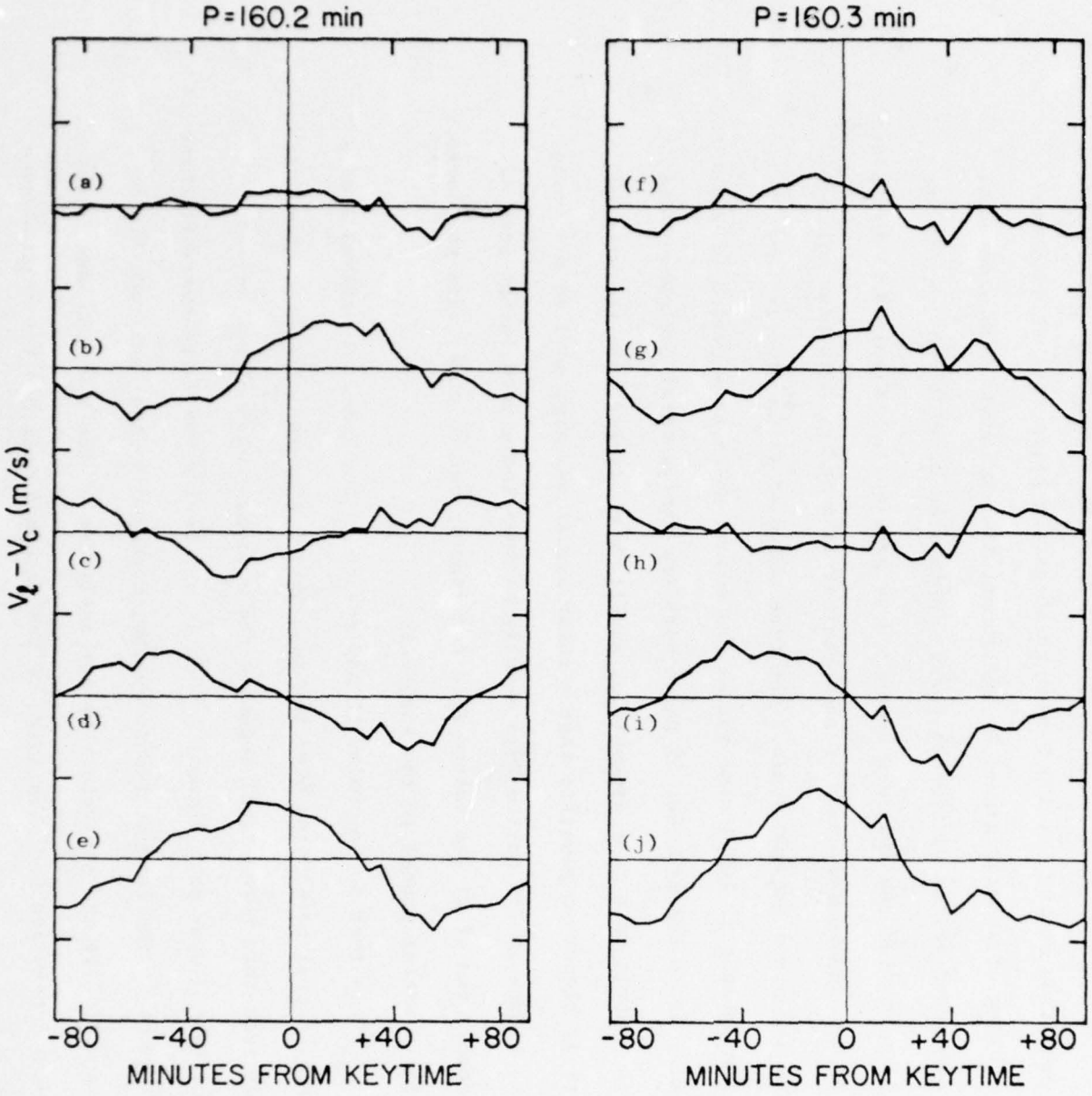

Figure 45. The top two curves are the superposed epochs obtained at periods of 160.2 and 160.3 minutes using the original Stanford data. The bottom eight curves are the same results obtained using data with a 0.75 m/s sinusoid added at a period of 160.25 min at four different phases.

using harmonic amplitudes, and eight using upper limits. No triple coincidences were found--in other words, no period was among the largest twenty for all three data segments. For comparison, if the data with added sinusoid was used, the 160.2 min period was among the largest twenty for all three segments and all four phases using both harmonic amplitudes and upper limits. The 160.3 min period was among the twenty largest in 11 of 12 cases using harmonic amplitudes and 10 or 12 cases using upper limits. This result confirms the above conclusion that a 0.75 m/s signal (1.26 m/s with the Crimean geometry) could have escaped detection only if adjacent to and out of phase with a large instrumental signal. It would not appear that a larger signal, such as the $\pm$ 2 m/s sine curve originally reported by Severny et al. (1976a) could have escaped detection. The publication of smaller amplitude curves for 1975 and 1976 (Severny et al., 1976b) and the use of a different definition of amplitude weaken this conclusion, since the 1975 data fit a sine curve of amplitude only 0.84 m/s, which is only two-thirds of the test signal used and could therefore conceivably be masked by instrumental drifts.

Second Examination of Data Analysis Techniques

An unusual opportunity to compare the Stanford result with that of the Crimea has been afforded by an exchange of data between the two observatories, which was suggested by John M. Wilcox. The resulting correspondence also resulted in a re-examination of the Stanford analysis. The first step in this process was a letter suggesting the exchange sent from Stanford to the Crimea, along with the Stanford data. The first response received was a telegram reporting that the 2 hr 40 min

oscillation was seen clearly in the Stanford data. In order to determine whether this signal could have been missed due to a computer programming error, Philip H. Scherrer wrote independent programs to reproduce the analysis described above. Using the Stanford velocity data with parabola fit subtracted, superposed epochs were produced at periods from 158.5 min to 161.5 min in steps of 0.1 min and the previous results and conclusions were confirmed. In order to investigate the possibility that the parabola fit was somehow removing a real signal, Dr. Scherrer then repeated the analysis, but instead of subtracting a fitted parabola from each observation, he removed only the observational mean. The resulting superposed epoch is shown in Figure 46. There is a roughly sinusoidal signal which fits a sinusoid of amplitude 0.87 m/s. Repeating the superposed epoch at adjacent periods in steps of 0.1 min revealed the highest peak to be of amplitude 1.08 m/s and period 159.9 min. The harmonic amplitudes were computed between 150.0 min and 165.0 min and the spike at 159.9 min was found to be outstanding, with a 4 σ significance estimated by Leif Svalgaard. A solar origin was suggested by the near coincidence with the Crimean period of 160.0 min and by apparent phase agreement in the two results.

This apparent confirmation of the Crimean result did not account for the absence of any significant 2 hr 40 min signal in the Stanford data with parabola removed, especially in view of the ability of an artificial signal inserted at 160.25 min to survive the fit subtraction process. Closer examination also showed the apparent phase agreement to be disagreement since opposite signs were used at the two observatories. Since 160.0 min is exactly one-ninth of a day, an investigation of the

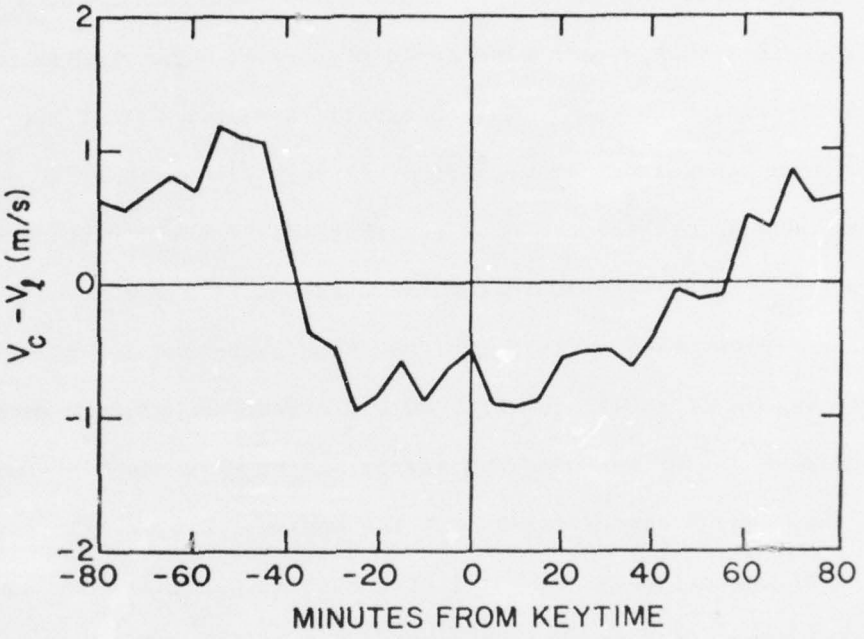

Figure 46. Superposed epoch of Stanford 1976 data at 160 minutes with the mean, rather than a parabola, subtracted from each observation. Values have been multiplied by -1.68 to match the Crimean sign and correct for different polarizer dimension.

relationship between the daily trend, as shown in Figure 20, and the apparent 2 hr 40 min signal led to a convincing alternate explanation. Plotting the daily trend in nine 2 hr 40 min pieces showed most of the data to be in a five-hour section of the afternoon, where the signal is declining. Superposition produces a smoothed sawtooth with 2 hr 40 min period. Proof that such a mechanism could produce the observed result was obtained by replacing the actual observations with a fit of the daily trend to a sinusoid of 12 hr period. A very similar 2 hr 40 min signal was produced. It was demonstrated that this was the responsible mechanism by smoothing the data (using the data set with the mean subtracted from each observation) with four-hour high- and low-pass filters. As Figure 47 shows, the 2 hr 40 min signal was clearly present when the low-pass filter was used and nearly absent when the high-pass filter was used, which demonstrates that the apparent 2 hr 40 min peak was produced by variations in the data of period longer than four hours. A more general conclusion is that any period that is an integer fraction of a day should be regarded with suspicion, especially when daily trends are present and the observations are evenly spaced about a day apart.

Stanford Analysis of 1975 Crimean Data

The second communication received from the Crimea contained the 1975 Crimean velocity data. Examination of the Crimean data showed there to be present baseline shifts of very large amplitude (the recorded raw velocity signal covered a range of 1000 m/s) and slow drifts of variable amplitude and no obvious diurnal pattern. The test described in the Nature article (Severny et al., 1976a) of observing in a telluric line to show that slow signal variations are of solar rather then instrumental

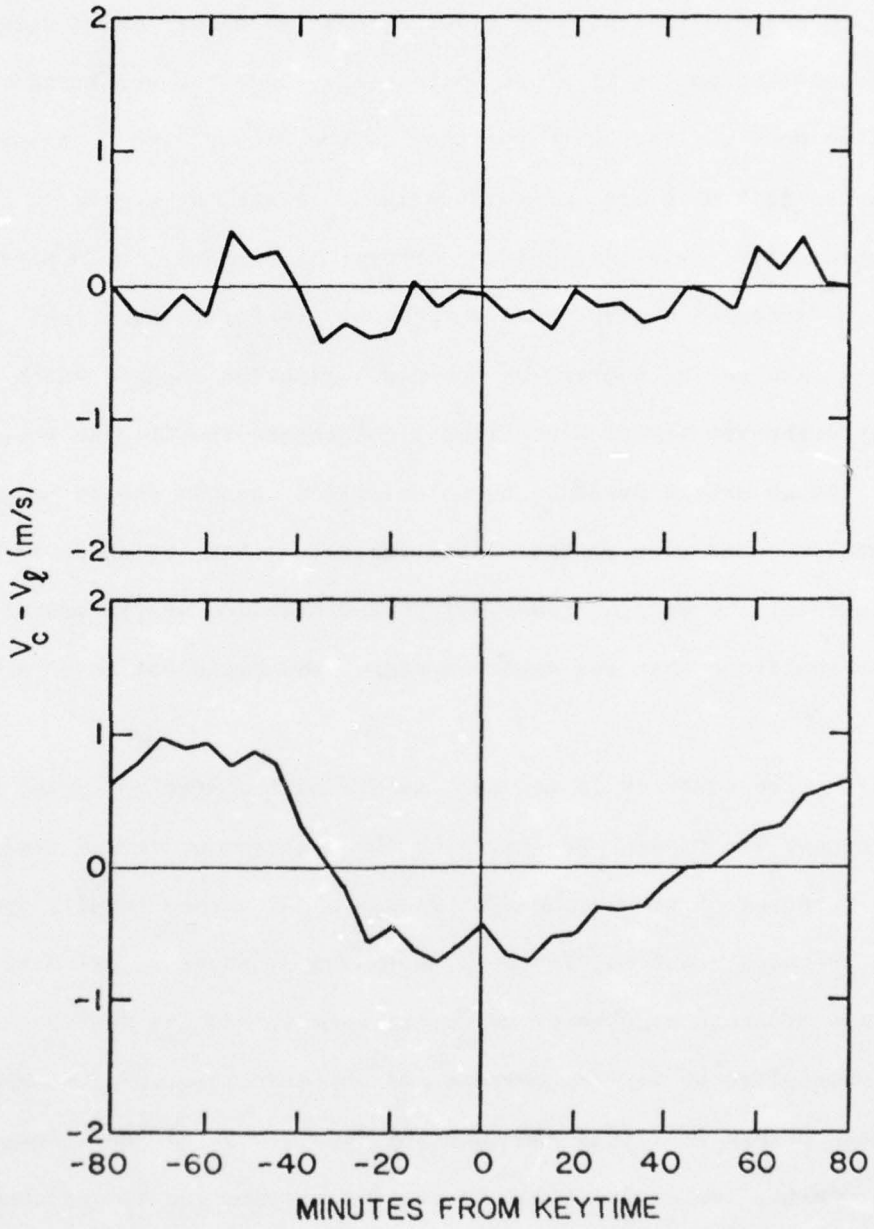

Figure 47. Same as Figure 46 with the data filtered (top) with a four-hour high pass filter, and (bottom) with a four-hour low pass filter.

origin does not preclude an instrumental origin related to guiding errors or atmospheric transparency fluctuations (as described in detail above with relation to the Stanford instrument) since the wavelength of a telluric line does not vary with position on the disk due to rotation as does the wavelength of a line of solar origin. Since the drifts do not show a simple daily variation, guiding errors, if present, would have to be of a very different character from those at Stanford. Electronic drifts could also be the source, as could polarization changes which could more easily enter the signal since limb light enters the Crimean instrument unchanged, though drifts produced by polarization changes should be of smaller amplitude and more regular daily variation than the observed drifts. Whatever the origin, these drifts and baseline shifts are of much larger amplitude than the reported signal and could not be of solar origin.

The data were analyzed in the same manner as the Stanford data, and the 160 min peak was clearly present with the reported phase and amplitude. For purposes of comparison the Crimean and Stanford results are plotted on the same graph in Figure 42, with the UT phase adjusted to be the same, the Stanford sign reversed for agreement, and the Stanford amplitude multiplied by 1.68 to correct for different aperture geometries. The reported Crimean amplitude had been obtained by taking the average of the maximum and two adjacent points and the minimum and two adjacent points from the superposed epoch curve. If the curve is instead fit to a sinusoid, the amplitude is only 0.84 m/s which is small enough to be hidden by instrumental drifts in the Stanford data, judging from the results obtained using the data with 0.75 m/s sinusoid added at a period of 160.25 min.

However the amplitude is defined, it is readily apparent that the Stanford result is negative. As mentioned above, a comparison with the 1976 Crimean result was not made in Figure 42 because there are differences in two available reports of the epoch obtained using 1976 observations, and the data itself was not available for comparison. Both epochs do show a signal at 2 hr 40 min in phase with the 1975 signal. Though the amplitude is smaller for 1976 than for 1975, it is still large enough to make it unlikely that the absence of signal in the 1976 Stanford data could be explained by a secular change in a real solar oscillation.

Further examination of the Crimean data set showed that the 160 min signal was not produced by longer period diurnal drifts. The first indication of this fact was that the plot of the daily pattern of data with parabola removed (Figure 48c) had the character of a noisy and interrupted 2 hr 40 min sinusoid rather than a simple inverted U. Furthermore, if the original data were filtered with a 3 hr 20 min low-pass filter before the parabola was subtracted, the 160 min signal virtually disappeared. However, if fits of polynomial order from zero to three were subtracted and epochs were produced at periods from 115 min to 245 min, it was found that the 160 min period was not exceptional. In addition, it was found that the very process by which data were collected and analyzed could easily result in large signals falling in a certain frequency range, particularly if those periods were integer fractions of a day.

To show how this could occur, refer to Figure 48. Figure 48a shows the superposed epoch of the Crimean data about keytimes at UT1200 with a zeroth order polynomial (the mean) subtracted from each observation. Though daily variations are not as regular or repeatable as with the

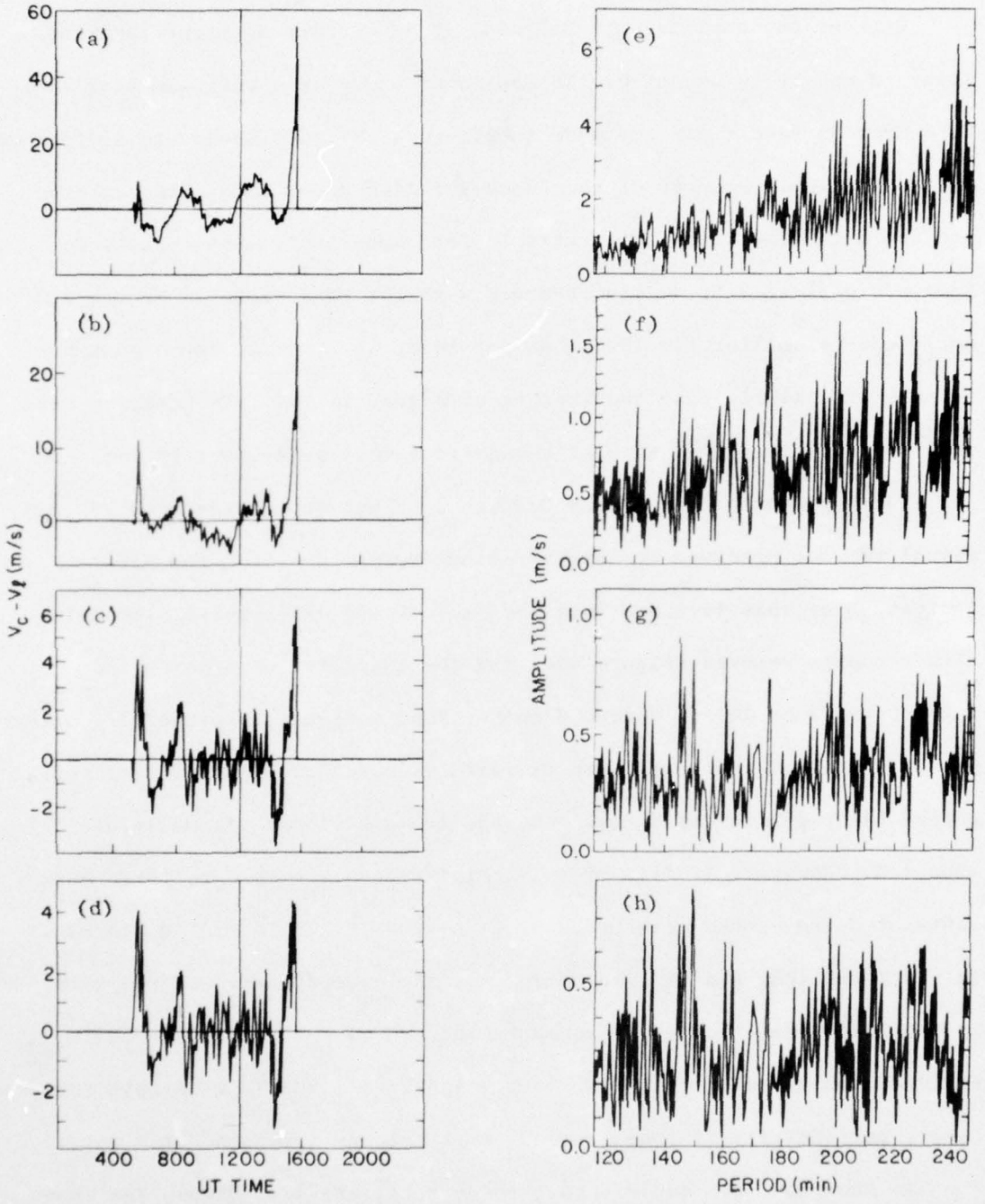

Figure 48. The curves at the left are plots of the 1975 Crimean data as a function of time of day with (a) the mean, (b) a linear fit, (c) a parabolic fit, and (d) a cubic fit subtracted from each observation. The curves at the right are the amplitudes of superposed epochs obtained at periods from 115.0 min to 245.0 min using the same data with corresponding fits subtracted.

Stanford data (see Figure 20), they are of sufficient repeatability for 67.2% of the points to be different from zero by more than an error bar. The daily trend has a sinusoidal character of period near 4 hr 20 min. It is reasonable to expect that if continuous data were available and no mean were removed, the fluctuations would be of indefinitely increasing amplitude for longer periods. Since observations were of average length 260 min (median length = 215 min), longer periods are filtered out by subtracting the mean, and a broadband peak is produced around four hours. In addition, since observations are limited to daylight hours and diurnal variations are somewhat repeatable, periods near four hours that are integer fractions of a day will be especially favored since they will be in phase with the diurnal pattern from one day to the next. The result is that the scan of superposed epochs in period (Figure 48e) has a very prominent peak of amplitude 6.08 m/s at 240 min (one-sixth of a day). If the scan is extended to 295 min, the second and third largest peaks are at 285 min and 288 min, with the latter being exactly one-fifth of a day.

When a first order polynomial fit is removed (Figure 48b) the amplitude of daily variations is reduced with longer periods especially filtered. The scan of epochs (Figure 48f) shows that the 240 min peak is no longer present, and features at 144 min (one-tenth of a day), 160.5 min (near one-ninth of a day) and 179.5 min (near one-eighth of a day) are now locally prominent. When the parabola fit is removed, the daily variation (Figure 48c) has excursions of period near 160 min. The scan of periods (Figure 48g) has its three largest peaks at 200 min, 144 min, and 160 min in that order, with the latter two being at one-tenth and one-ninth of a day respectively. The daily variation with

cubic fit removed (Figure 48d) shows variations of still lower amplitude and higher frequency. The 160 min peak is now the eighth largest out of the 261 surveyed, with six of the seven that are larger falling at periods from 132 min to 149 min.

The picture that emerges is that subtraction of polynomial fits of successively higher order results in low-pass filtering leaving broad-band peaks at successively shorter periods. Some periods stand out because of statistical fluctuations, and periods which are integer fractions of a day are especially likely to be selected because of daily data sampling and recurring daily variations.

Though a statistical explanation exists for the reported 160 min signal, it is difficult to prove on the basis of available information that the observed signal is of statistical origin. The report by the Crimean group of 144 min and 180 min peaks is consistent with the explanation developed above, though it is also true as they suggest that a solar pulsation of 160 min would produce ghost signals at 144 min and 180 min because of the daily observing pattern. One would then be left with the difficulty of determining which period is a ghost and which is real. The 6.08 m/s, P = 240 min signal in the data with mean removed cannot be explained as a ghost of the 0.82 m/s, P = 160 min signal present in the data with parabola removed. The large signal present at 240 min clearly demonstrates that the statistical mechanism outlined above for enhancing integer fractions of a day does operate. The near phase constancy from year to year in the Crimean signal could also be explained by diurnal patterns introduced by the instrument, although if the signal continues to advance in phase by 15 minutes each year

(Severny et al., 1976b) a solar origin would be favored. If the 160 min signal is a statistical artifact, statistical fluctuations should cause it to be absent in some of the data. Examination of the 1976 Crimean epoch (Figure 7 of Severny et al., 1976b) does indeed show the "signal" to be very poorly defined--fully twelve of the sixteen points in the epoch are within an error bar of zero, which is more than the 68.3% one would expect from a normal distribution. One cannot rule out a real decline of a real 160 min solar signal between 1974 and 1976, though the observed decrease of the 160 min signal does favor the statistical explanation. In the absence of a clear test, if a statistical origin for a signal can be found, it should be favored over a physical explanation, though it would be much more satisfying to demonstrate conclusively which explanation is correct.

Crimean Analysis of Stanford Data

Further filtering and fitting is not likely to settle the question of the source of the Crimean signal, which makes the Stanford attempt at confirmation even more crucial. The third correspondence received from the Crimea detailed the report in the earlier telegram that a positive signal had indeed been found in these data. The Stanford data had been correctly multiplied by -1.68 to correct for changes in sign and geometry. More important, the observations were examined critically to determine whether or not they were of smooth parabolic form, and those that were not were either shortened by editing or were fit with two parabolas. In addition, the data was split into three pieces, consisting of the intervals April 13 - May 31, June 1 - June 24, and July 1 - August 6. The result was that the null result obtained at Stanford was also obtained

in the Crimea for the second interval, a marginal signal was present in the first interval, but for the third interval, a large signal was present which agreed in phase with the Crimean result. The importance of this segment was amplified by multiplying the measured velocity by 4/3 since early calculations at Stanford suggested the misalignment in the image slicer present in July would reduce sensitivity to a radial pulsation by 3/4. The third segment was also edited much less extensively than the previous two, since it was felt to be of higher quality. Using the edited data set with data from July 1 onward multiplied by 4/3, an impressive sinusoid was obtained for the full data set with 2 hr 40 min period and phase agreeing well with the Crimean phase.

Since the calculation of a loss of sensitivity by 25% was incorrectly based on the assumption that the observed shift in baseline was due to a displacement of the polarizing aperture relative to the solar image, this calculation was redone assuming a displacement of light off of the Littrow lens, and the result was a loss of sensitivity of less than 1%. The Stanford data were edited to duplicate the Crimean work, and without multiplying the July measurements by 4/3, the result shown in Figure 49 was obtained for a 160 min epoch. Though the amplitude is still less than a third of that obtained with the Crimean data (including correction for aperture geometries) the sinusoidal character and agreement with the Crimean phase are impressive. Epochs were produced at intervals of 0.1 min in period for periods from 150.0 min to 170.0 min, and the peak at 160.0 min was now visible, though only the seventh largest in the interval.

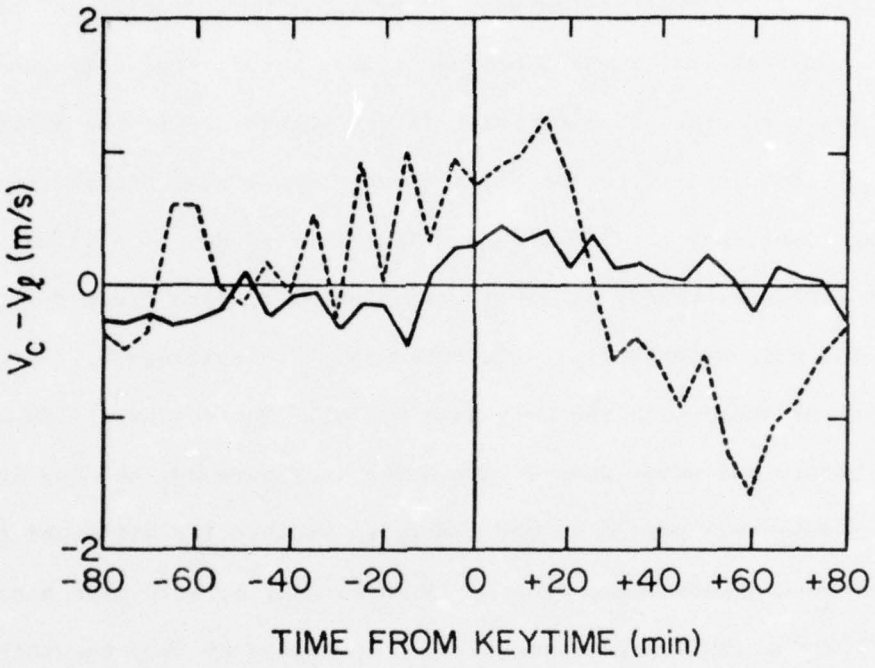

Figure 49. The solid line is the superposed epoch obtained at 160 min with the Stanford 1976 data as edited at the Crimea. The dashed line is the result obtained using the 1975 Crimean data. Correction for sign, phase, and aperture geometry has been made.

The difference in amplitude remains a problem and could not be explained by a calibration error without making the amplitude of five-minute oscillations much too large. There are two other difficulties with this apparent confirmation of the Crimean result--the data subdivision test, and the means by which it was obtained. If the Stanford data are divided into three intervals as was done in the Crimea, it becomes apparent that the 160.0 signal is primarily due to a signal of amplitude 0.57 m/s present in the third interval of data, from July 1 onward. The data before July 1 fit a sinusoid of amplitude 0.11 m/s and are out of phase with the July data by 70°. The epochs at 160.0 min for data before and after June 30 are shown in Figure 50. A real change in the sun over this period is not likely to explain the different result because Crimean observations from April 26 to July 8, 1976 give a positive result. For the 160.0 minute signal to be produced by only one-third of the data makes the reality of this signal very questionable unless there is something about the July observations which makes them superior. Examination shows the opposite to be the case. Mathematically, the average variance of the July epoch using unedited data is 2.854 $(m/s)^2$ compared with 2.062 $(m/s)^2$ for the earlier data, and this comparison becomes worse with editing since the July data was edited much less--its variance becomes 2.395 $(m/s)^2$ compared with 1.254 $(m/s)^2$ for the earlier data. Experimentally, the July data are less trustworthy since they were taken when the image slicer was misaligned, resulting in lost light, uneven weighting of the disk and a sizable baseline offset. In addition, the July data were taken with dangerous regularity, being confined to just over six hours in the afternoon and with only seven days missed out of 36

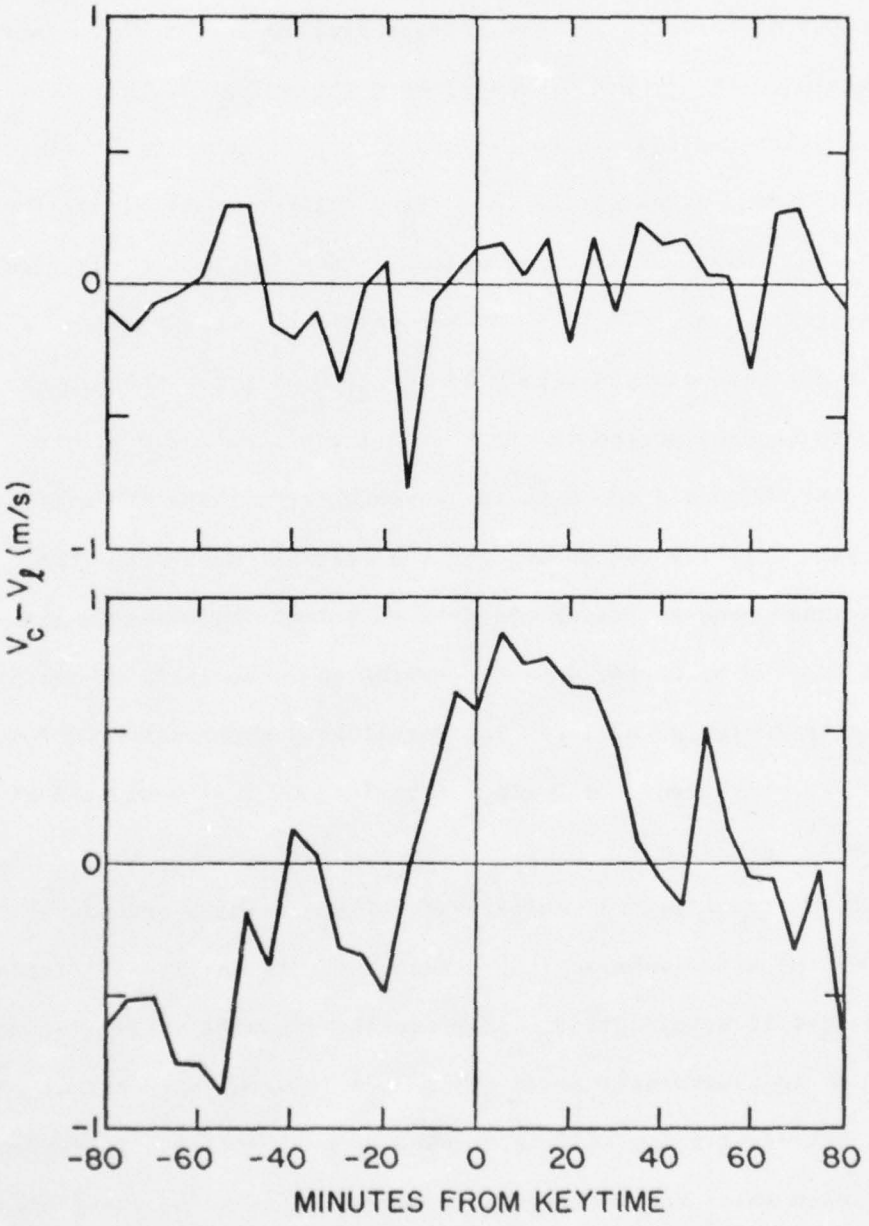

Figure 50. Superposed epochs obtained at 160 min using the Stanford data with Crimean editing. The top curve is for data before June 30, the bottom curve is for data after June 30.

(only 3 of the first 27) which make these data particularly susceptible to enhancement of periods that are integer fractions of a day. In fact, larger signals (0.67 m/s and 0.69 m/s) were present at 120 min (one-twelfth of a day) and 144 min (one-tenth of a day) than at 160 min.

The data are very sensitive to editing changes--only six of the twenty-nine July observations were edited with a net loss of 43 five-minute averages out of 1475 (2.9% of the data) and the amplitude of the 160.0 min signal was changed from 0.24 m/s to 0.57 m/s. When epochs were produced at each period in steps of 0.1 min from 150.0 min to 170.0 min, the 160.0 min epoch is the seventh largest for the edited data set, but ranks 164 out of 201 for the original data set. Two mechanisms would tend to filter the data to select the observed signal. One is the shortening of the data by editing and especially by fitting some data sets to two parabolas. The result is a suppression of lower frequencies which changes the period of variations in the diurnal signal from $\sim$ 4 hr to 120-140 min.

The other effect is the subjectivity of the editing procedure. The advantage of the Kotov subtraction technique is its ability to distinguish between changes in wavelength of solar and instrumental origin, since many kinds of instrumentally produced changes in wavelength affect center and limb light equally and will be removed by subtraction. If differentiation between solar and instrumental changes is based on the judgment of the observer, two factors likely to affect this judgment are the "smoothness" of the data and the regularity of the variation. Selection by smoothness results in broad-band filtering in the frequency domain, and selection by regularity favors enhancement of daily patterns with

AD-A040 653 STANFORD UNIV CALIF INST FOR PLASMA RESEARCH F/G 3/2
LARGE-SCALE PERIODIC SOLAR VELOCITIES: AN OBSERVATIONAL STUDY.(U)
MAR 77 P H DITTMER N00014-76-C-0207
UNCLASSIFIED SU-IPR-686 NL

3 OF 3
AD
A040653

END
DATE
FILMED
7-77

resultant enhancement of integer fractions of a day when observations and patterns are sufficiently regular. The safest approach is to use all data without a known instrumental pecularity, which in this case could have been used to justify exclusion of the July data and consequent elimination of the 2 hr 40 min signal.

It is hoped that someone, somewhere will have the experimental skill and patience to reproduce this observation without the instrumental drifts so that no editing or fitting need be used. Until that time, the Crimean report of a 2 hr 40 min solar pulsation remains unconfirmed but intriguing on theoretical as well as observational grounds, especially by virtue of its coincidence with one-ninth of a day.

CHAPTER IV

SUMMARY AND CONCLUSIONS

The most important results of this investigation can be expressed very simply in terms of the three things which were not observed--large-scale organization of five-minute oscillations was not observed, oscillations at periods from five to seventy minutes were not observed, and two-hour forty-minute oscillations were not observed. Rather than conclude this investigation on such a negative note, some of the positive findings of this study should be mentioned.

First, the velocity subtraction technique developed by Valeri A. Kotov has been found to be a sensitive and useful technique. The subtraction was quite successful both in reducing the deviations in the five-minute period range caused by convection in the spectrograph, and in removing the longer period drifts produced by grating drifts, changes in spectrograph temperature or pressure, and the earth's rotation. The remaining low-frequency drifts could probably be reduced by positioning guiding diodes at the image used for observations and by using a larger Littrow lens or a smaller image to reduce the possibility of losing light off the edge of the Littrow lens. If such adjustments did not succeed in reducing slow drifts, the hypothesis favored herein that these drifts are caused by relative shifts of different optical elements would have to be discarded and another explanation found.

Other measurements might also be performed using similar subtractive techniques. A quarter-wave plate and two semicircular linear polarizers oriented at +45° and -45° could be used to look for $\ell=1$ modes of solar pulsation. Apertures could also be designed to look for other possible pulsational modes or other large-scale motions such as meridional flows. Optical subtraction could be used to produce the filter which Fossat and Martin (1974) designed to select a particular horizonal wavenumber, thus permitting mapping of the oscillatory power in the k-ω plane. The finite Fourier transform used by Hill et al. (1975) to define the position of the solar limb could be calculated directly by optical subtraction, with resultant advantages in light levels and instrumental simplicity over the scanning and minicomputer calculation presently employed.

It is because of the sensitivity of the subtractive technique that it has been possible to confirm the result of Fossat and Ricort (1975a) that five-minute oscillations can be observed over the full disk. The observed amplitude of 2.0 m/s is consistent with a large horizontal scale of over 20000 km, and argues in favor of a global rather than local excitation mechanism. The longer period reported here as compared with previous measurements is an interesting result, though of unknown significance. The suggestion given herein that the longer period is associated with the large aperture used should be confirmed by observations in a single line over a large range of apertures. Until such confirmation exists, this result is not well-established.

The significance of the observed lack of large-scale organization of five-minute oscillations with respect to sector boundaries is somewhat dependent on the establishment of a clear physical connection between the

oscillations and coronal heating. If such a connection exists, it follows from the present study that the high coronal emission observed near sector boundaries (Antonucci and Duvall, 1974) and the high solar wind velocities and coronal holes found in the center of sectors (Sawyer, 1976; Wagner, 1976) are more likely to be the result of different magnetic field geometries than of different energy input. The fact that coronal temperatures and solar wind velocities are organized with relation to sector boundaries while five-minute oscillations are not (to the limits of detection of the present study) does not preclude the possibility that five-minute oscillations are the agent responsible for heating the solar corona. Magnetically determined differences in energy loss from the corona could still explain the observed large-scale structures even if the energy input were uniform (Adams and Sturrock, 1975; Rosner and Vaiana, 1976).

The work described herein on the oscillations at periods from five to seventy minutes reported by Hill and co-workers is not likely to terminate conclusively the discussion of these oscillations. Future discussion should not focus on differences between the eigenfunctions calculated by Hill and those described herein as based on the work of Noyes and Leighton (1963). Both calculations lead to difficulties in attempts to reconcile Hill's measurements with those of observers using spectral techniques--Hill's enhancement factors predict more power at five than at ten minutes, at variance with his observations, and present calculations suggest that a large proportion of the downward propagating solution would produce much greater increases of five-minute amplitude with height than are observed. Though these represent serious discrepancies, Hill and

colleagues have in the past demonstrated great capacity to explain the failure of other observers (Brookes et al., 1976; Grec and Fossat, 1976; Livingston et al., 1977; Musman and Nye, 1976a and b) to confirm his results. Plausible explanations will therefore probably be devised for the lack of a five-minute resonant bump in the SCLERA power spectrum, for the limited growth of five-minute amplitude with height, and the limited agreement in the two power spectra which have been published by the SCLERA group (Hill et al., 1976a; Brown et al., 1976). Ability to explain a lack of confirmation is much less convincing than actual confirmation would be. Future efforts should probably be devoted not only to determining whether or not Hill's explanation can account for the lack of confirmation in past experiments, but also to predicting what future experiments can be made to confirm Hill's observation if his explanation is correct. For example, if his explanation is correct, velocity and temperature fluctuations should have much greater amplitudes for higher than for lower lines, and the enhancement should be substantially greater for longer periods ($\sim$ 40 minutes) than at five minutes. Observations should be able to determine whether or not this is the case.

The analysis described herein at periods longer than two hours shows that daily observing patterns and diurnal variations can produce impressive signals at periods which are integer fractions of a day. There is, of course, no reason why the sun should be prohibited from oscillating at such a period. If Crimean observations are continued in 1977, it will be interesting to see if the amplitude continues to decline as it did from 1974 to 1976, and to see if the phase continues to advance by 14 min per year. The lack of confirmation with the Stanford instrument raises

serious doubts about the solar origin of the reported signal. It would be interesting to analyze the Crimean data for 1974 and 1976 to see if the statistical explanation developed herein can account for the observed signals. If sufficient interest and controversy remain to justify further observations at Stanford, these should be done with identical aperture geometry to that used in the Crimea and over the same time interval so that ambiguities of interpretation could be minimized.

APPENDIX A

DERIVATION OF THE CALIBRATION EXPRESSION

It is convenient for calculations of instrumental sensitivity to assume triangular line profiles and point slits. The slits are referred to as R and B (red and blue) and the circular polarizations are abbreviated by + (rcp) and - (lcp). For convenience, I_c^+ continuum intensity is designated by I_1, with B_1 and R_1 the intensities measured by blue and red slits respectively $I_c^- \equiv I_2$, $I_\ell^- \equiv I_3$, and $I_\ell^+ \equiv I_4$. Using these definitions, the three fundamental signals are:

$$\text{Intensity} = (B_1 + R_1 + B_2 + R_2 + B_3 + R_3 + B_4 + R_4)/2$$

$$\text{DC Difference} = (B_1 + B_2 + B_3 + B_4) - (R_1 + R_2 + R_3 + R_4)$$

$$\text{AC Difference} = \text{Zeeman} = (B_1 + B_4 - R_1 - R_4) - (B_2 + B_3 - R_2 - R_3).$$

The ratio of core to continuum intensity is denoted by I_o, and the slope by mI_{cont}, so the intensity $\Delta\lambda$ from the line core is given by $(I_o + m|\Delta\lambda|)I_{cont}$. Line core for light from the center of the disk is designated by λ_c, for the limb by λ_ℓ, and the slits are at $\lambda_o \pm \Delta\lambda/2$. If $\lambda_\ell > \lambda_o > \lambda_c$ and $\Delta\lambda/2 > \lambda_\ell - \lambda_c$, it follows that

$$B_1 = (I_o - m[\lambda_o - \Delta\lambda/2 - \lambda_c])I_1, \quad B_2 = (I_o - m[\lambda_o - \Delta\lambda/2 - \lambda_c])I_2$$

$$B_3 = (I_o - m[\lambda_o - \Delta\lambda/2 - \lambda_\ell])I_3, \quad B_4 = (I_o - m[\lambda_o - \Delta\lambda/2 - \lambda_\ell])I_4$$

$$R_1 = (I_o + m[\lambda_o + \Delta\lambda/2 - \lambda_c])I_1, \quad R_2 = (I_o + m[\lambda_o + \Delta\lambda/2 - \lambda_c])I_2$$

$$R_3 = (I_o + m[\lambda_o + \Delta\lambda/2 - \lambda_\ell])I_3, \quad R_4 = (I_o + m[\lambda_o + \Delta\lambda/2 - \lambda_\ell])I_4$$

Using these values, the three fundamental quantities become:

$$\text{Intensity} = (2I_o + m\Delta\lambda)(I_1 + I_2 + I_3 + I_4)/2$$

$$\text{DC Difference} = -2m(\lambda_o - \lambda_c)(I_1 + I_2) - 2m(\lambda_o - \lambda_\ell)(I_3 + I_4)$$

$$\text{Zeeman} = 2m(\lambda_o - \lambda_c)(I_2 - I_1) + 2m(\lambda_\ell - \lambda_o)(I_4 - I_3)$$

A fourth useful quantity is the ratio Zeeman/Intensity ≡ ZI, which now becomes:

$$ZI = \frac{4m(\lambda_o - \lambda_c)(I_2 - I_1) + 4m(\lambda_\ell - \lambda_o)(I_4 - I_3)}{(2I_o + m\Delta\lambda)(I_1 + I_2 + I_3 + I_4)}$$

When calibrating the center, the limb is masked off so $I_3 = I_4 = 0$. A known wavelength shift is introduced $(\Delta\lambda_{calib}) = (\lambda_o - \lambda_c)$, and some ZI value K is measured, given by:

$$K = \frac{4m(\Delta\lambda_{calib})(I_2 - I_1)}{(2I_o + m\Delta\lambda)(I_1 + I_2)}$$

This expression can be inverted to give $4m/(2I_o + m\Delta\lambda)$ in terms of measurable quantities, which changes the expression for ZI to:

$$ZI = \frac{K(I_1 + I_2)}{\Delta\lambda_{calib}(I_2 - I_1)} \left\{ \frac{(\lambda_o - \lambda_c)(I_2 - I_1) + (\lambda_\ell - \lambda_0)(I_4 - I_3)}{I_1 + I_2 + I_3 + I_4} \right\}$$

In normal operation, the servo nulls the DC Difference signal, so it follows that

$$(\lambda_\ell - \lambda_o) = \frac{(I_1 + I_2)}{(I_3 + I_4)} \quad (\lambda_o - \lambda_c)$$

Substitution and manipulation yields the expression

$$(\lambda_\ell - \lambda_c) = \frac{ZI(\Delta\lambda_{calib})}{K} \frac{(I_2 - I_1)(I_1 + I_2 + I_3 + I_4)^2}{2(I_1 + I_2)(I_4 I_2 - I_3 I_1)}$$

For limb calibration, I_1 and I_4 are interchanged as are I_2 and I_3, and the expression remains the same with the exception of replacing

$$\frac{(I_2 - I_1)}{(I_2 + I_1)} \quad \text{with} \quad \frac{(I_3 - I_4)}{(I_3 + I_4)}$$

For perfect polarizers and perfect alignment, $I_2 = I_4 = 0$ and $I_3 = I_1$ and both expressions reduce to:

$$(\lambda_\ell - \lambda_c) = \frac{ZI(\Delta\lambda_{calib})}{K} \times 2$$

APPENDIX B

THE SEPTEMBER 13, 1976 ALIGNMENT AND CALIBRATION

Calibration of the instrument requires a knowledge of the dispersion of the spectrograph at 5124 Å. This was measured on July 21, 1976, and was not repeated since the measurement showed good internal agreement and since routine measurement of the dispersion at 5250 Å had previously demonstrated that variations are small. The dispersion was measured by allowing the exit slit servo to lock on different lines near FeIλ5123.730 and recording the encoder position. The values obtained (averages of two readings) were:

λ(Å)	Encoder Position
5123.730	398940
5126.199	447855.5
5127.368	471096.5
5123.730	398937
5121.649	357410
5123.730	398295

From these measurements, the Doppler encoder was calibrated in terms of wavelength, which in turn was converted to velocity in m/s using the classical Doppler shift expression, $v/c = \Delta\lambda/\lambda$.

Line Pair	$\Delta\lambda$(Å)	Encoder Shift	Velocity (m/s) (Encoder Unit)$^{-1}$
5123.730 - 5126.199	2.469	48915.5	2.9533
5123.730 - 5127.368	3.638	72159.5	2.9499
5123.730 - 5121.649	2.081	41527	2.9321
5123.730 - 5121.649	2.081	41519.5	2.9326
		average =	2.9436

Hence the value 2.94 m/s (encoder unit)$^{-1}$ was used for the dispersion.

The standard calibration procedure was followed on September 13, 1976, which included measurement of the calibration constant, realignment of polarizers and iris diaphragm, and a second measurement of the calibration constant. To measure the calibration constant, it was first necessary to measure the intensity of right and left circularly polarized light passing through center and limb. Intensity measurements were made with the exit slits 24400 encoder units (1.228 Å) to the blue from 5123.730 line center. Because of difficultes in directly separating center and limb light due to the bevelled edge of the half-wave plate, this separation was done mathematically as explained below.

First, the full aperture intensity was measured (here + means right circularly polarized and - means left circularly polarized)

$$(I_c + I_\ell)^- = 643, \quad (I_c + I_\ell)^+ = 585$$

Next, masks were used to allow light to pass only through first the center, then the limb. In order to insure that only center or limb light was passed, the masks were made smaller than the full center or limb aperture:

$$i_c^- = 7,\ i_c^+ = 292,\ \text{so}\ I_c^-/I_c^+ = i_c^-/i_c^+ = 7/292$$

$$i_\ell^- = 370,\ i_\ell^+ = 3,\ \text{so}\ I_\ell^-/I_\ell^+ = i_\ell^-/i_\ell^+ = 370/3.$$

So the lcp equation above becomes:

$$I_c^- + I_\ell^- = 7/292\ I_c^+ + 370/3\ I_\ell^+ = 643.$$

This may be solved with the rcp equation to obtain:

$$I_c^+ = 579.9,\ I_\ell^+ = 5.1.$$

Substitution then yields

$$I_c^- = 7/292\ I_c^+ = 13.9,\ I_\ell^- = 370/3\ I_\ell^+ = 629.1$$

It follows that the intensity factor in the equation derived in Appendix A has the value 1.970 for the center, and 2.034 for the limb.

The effective slope of the absorption line was next measured by moving the exit slit a known number of encoder units off of line center and recording the ZI signal, then repeating symmetrically in the opposite direction. The values obtained were as follows:

	Encoder Shift	ZI Value
center	100	10.507
	200	20.314
	500	47.329
limb	100	10.458
	200	20.521
	500	47.975

Using the values obtained for an encoder shift of 100 units, it follows that for the center, 1 ZI unit = 0.0952 encoder units =

28.015 m/s x (1.970) = 55.20 m/s, and for the limb, 1 ZI unit = 0.0956 encoder units = 28.02 m/s x (2.034) = 55.20 m/s.

To perform the realignment, the aperture is first centered on the solar image. The mask is next inserted to pass only center light, and the KDP voltage is set to pass only lcp light. The linear polarizer is then rotated to minimize the transmitted light as read on an oscilloscope, which insures that the center passes rcp light and the limb passes lcp light. The mask is then removed, the KDP modulation turned on, and the iris diaphragm is adjusted to eliminate the square wave in intensity, again read on an oscilloscope, thus insuring equal intensities of rcp and lcp light, and hence of center and limb light. After the realignment performed on September 13, 1976, the calibration constant was remeasured as follows:

$$(I_c + I_\ell)^+ = 569 \qquad (I_c + I_\ell)^- = 569$$

$$I_c^+/I_c^- = 287/2 \qquad I_\ell^-/I_\ell^+ = 355/4$$

So $I_c^+ = 562.633$, $I_c^- = 3.921$, $I_\ell^+ = 6.367$, and $I_\ell^- = 565.079$.

The intensity factors are 2.0086 for the center and 1.9914 for the limb. The ZI values for displacements of 100 encoder units were 11.166 for the center and 11.403 for the limb. It follows that 1 ZI unit is equivalent to 52.950 m/s for the center and 51.408 m/s for the limb. The calibration factor generally showed good agreement from one measurement to the next, and an overall average value of 54.4 m/s was used in the analysis.

REFERENCES

Adams, W. M., and Sturrock, P. A. 1975, Astrophys. J., 202, 259.

Aleshin, V. I. 1974, Sov. Astron., 18, 263 (translated from Astron. Zh., 51, 445).

Allen, C. W. 1973, Astrophysical Quantities (3d ed.; London: Athlone Press).

Altschuler, M. D., Trotter, D. E., and Orrall, F. Q. 1972, Solar Phys., 26, 354.

Ando, H., and Osaki, Y. 1975, Pub. Astr. Soc. Japan, 27, 581.

Antonucci, E., and Duvall, T. L., Jr. 1974, Solar Phys., 38, 439.

Athay, R. G. 1976, The Solar Chromosphere and Corona: Quiet Sun (Dordrecht, Holland: D. Reidel), pp. 29, 30, 170.

Athay, R. G., White, O. R., Bruner, E. C., Jr., Chipman, E. G., Lites, B. W., Shine, R. A., and Orrall, F. Q. 1976, Bull. Amer. Astr. Soc., 8, 312.

Babcock, H. W. 1961, Astrophys. J., 133, 572.

Bahcall, J. N., and Davis, R., Jr. 1976, Science, 191, 264.

Bahng, J., and Schwarzschild, M. 1963, Astrophys. J., 137, 901.

Baluteau, J. P., Bussoletti, E., and Epchstein, N. 1973, Nature, 244, 562.

Beckers, J. M., and Schultz, R. B. 1972, Solar Phys., 27, 61.

Beckers, J. M., and Tallant, P. E. 1969, Solar Phys., 7, 351.

Bevington, P. R. 1969, Data Reduction and Error Analysis for the Physical Sciences (New York: McGraw-Hill), p. 122.

Bhatnagar, A., Livingston, W. C., and Harvey, J. W. 1972, Solar Phys., 27, 80.

Bhatnagar, A., and Tanaka, K. 1972, Solar Phys., 24, 87.

Bhattacharyya, J. C. 1972, Solar Phys., 24, 274.

Billings, D. E. 1959, Astrophys. J., 130, 215.

Blackman, R. B., and Tukey, J. W. 1958, The Measurement of Power Spectra (New York: Dover Publications, Inc.), pp. 34-36, 120, 121.

Boury, A., Gabriel, M., Noels, A., Scuflaire, R., and Ledoux, P. 1975, Astron. Astrophys., 41, 279.

Bray, R. J., and Loughhead, R. E. 1967, The Solar Granulation (London: Chapman and Hall).

Brookes, J. R., Isaak, G. R., and van der Raay, H. B. 1976, Nature, 259, 92.

Brown, T. M., Stebbins, R. T., and Hill, H. A. 1976, The Proceedings of the Solar and Stellar Pulsation Conference, Los Alamos, New Mexico, ed. A. N. Cox and R. G. Deupree, Los Alamos Report No. LA-6544-C.

Bruner, E. C., Jr., Chipman, E. G., Shine, R. A., Lites, B. W., Rottman, G. J., Orrall, F. Q., Athay, R. G., and White, O. R. 1976, Bull. Amer. Astr. Soc., 8, 313.

Bumba, V. 1970, Solar Phys., 14, 80.

Bumba, V., and Howard, R. 1965, Astrophys. J., 141, 1502.

Busse, F. H. 1970, Astrophys. J., 159, 629.

Canfield, R. C., and Musman, S. 1973, Astrophys. J. (Letters), 184, L131.

Cha, M. Y., and Orrall, F. Q. 1973, Solar Phys., 28, 333.

Cha, M. Y., and White, O. R. 1973, Solar Phys., 31, 23.

Chapman, R. D., Jordan, S. D., Neupert, W. M., and Thomas, R. J. 1972, Astrophys. J. (Letters), 174, L97.

Chipman, E. G., Bruner, E. C., Jr., Shine, R. A., Lites, B. W., Rottman, G. J., Orrall, F. Q., White, O. R., and Athay, R. G. 1976, Bull. Amer. Astr. Soc., 8, 312.

Christensen-Dalsgaard, J., Dilke, F. W. W., and Gough, D. O. 1974, Mon. Not. R. Astr. Soc., 169, 429.

Christensen-Dalsgaard, J., and Gough, D. O. 1976, Nature, 259, 89.

Cooley, J. W., and Tukey, J. W. 1965, Math. Comput., 19, 297.

Cowling, T. G. 1941, Mon. Not. R. Astr. Soc., 101, 367.

Cox, J. P. 1976, Ann. Rev. Astron. Astrophys., 14, 247.

Cox, J. P., and Giuli, R. T. 1968, Principles of Stellar Structure (New York: Gordon and Breach), Vol. 1, ch. 9.

Deubner, F.-L. 1967, Solar Phys., 2, 133.

Deubner, F.-L. 1969, Solar Phys., 9, 343.

Deubner, F.-L. 1971, Solar Phys., 17, 6.

Deubner, F.-L. 1972a, Solar Phys., 22, 263.

Deubner, F.-L. 1972b, Solar Phys., 23, 304.

Deubner, F.-L. 1974, Solar Phys., 39, 31.

Deubner, F.-L. 1975, Astron. Astrophys., 44, 371.

Deubner, F.-L., and Hayashi, N. 1973, Solar Phys., 30, 39.

Dhanju, M. S., and Sarabhai, V. 1970, J. Geophys. Res., 75, 1795.

Dicke, R. H., and Goldenberg, H. M. 1967, Phys. Rev. Lett., 18, 313.

Dilke, F. W. W., and Gough, D. O. 1972, Nature, 240, 262.

Durasova, M. S., Dobrin, M. M., and Yudin, O. I. 1971, Nature Phys. Sci., 229, 82.

Durney, B. 1970, Astrophys. J., 161, 1115.

Eddy, J. A. 1976, preprint.

Edmonds, F. N. 1966, Astrophys. J., 144, 754.

Evans, J. W. 1963, Astron. J., 68, 750.

Evans, J. W., Main, P., Michard, R., and Servajean, R. 1962, Astrophys. J., 136, 862.

Evans, J. W., and Michard, R. 1962a, Astrophys. J., 135, 812.

Evans, J. W., and Michard, R. 1962b, Astrophys. J., 136, 493.

Evans, J. W., Michard, R., and Servajean, R. 1963, Ann. d'Astrophys., 26, 368.

Evans, J. W., Michard, R., and Servajean, R. 1965, Ann. d'Astrophys., 28, 534.

Fisher, R. P., and Hill, R. C., II 1971, Solar Phys., 18, 211.

Fossat, E. 1974, Astron. Astrophys. Suppl., 15, 475.

Fossat, E. 1975, "Etude des Oscillations dans l'Atmosphère Solaire par Resonance Optique" (unpublished dissertation, Docteur es Sciences Physiques, Institut de Mathématiques et Sciences Physiques, Université de Nice), Annexe à l'article IV.

Fossat, E., and Martin, R. 1974, Nouvelle Revue d'Optique, 4, 5.

Fossat, E., and Ricort, G. 1973, Solar Phys., 28, 311.

Fossat, E., and Ricort, G. 1975a, Astron. Astrophys., 43, 243.

Fossat, E., and Ricort, G. 1975b, Astron. Astrophys., 43, 253.

Fossat, E., Ricort, G., Aime, C., and Roddier, F. 1974, Astrophys. J. (Letters), 193, L97.

Fossat, E., and Roddier, F. 1971, Solar Phys., 18, 204.

Frazier, E. N. 1966, Pub. Astr. Soc. Pacific, 78, 424.

Frazier, E. N. 1968a, Astrophys. J., 152, 557.

Frazier, E. N. 1968b, Z. Astrophys., 68, 345.

Gebbie, H. A., Emery, R. J., Bohlander, R. A., and Gimmestad, G. G. 1974, Nature, 244, 562.

Gibson, E. G. 1973, The Quiet Sun (Washington, D. C.: Technical Information Office, National Aeronautics and Space Administration), p. 100.

Gingerich, O., and de Jager, C. 1968, Solar Phys., 3, 5.

Gingerich, O., Noyes, R. W., Kalkofen, W., and Cuny, Y. 1971, Solar Phys., 18, 347.

Glencross, W. M., and Craig, I. J. D. 1972, Nature Phys. Sci., 238, 50.

Gonczi, G., and Roddier, R. 1969, Solar Phys., 8, 255.

Gopasyuk, S. I., and Tsap, T. T. 1973, Sov. Astron., 16, 870 (translated from Astron. Zh., 49, 1066).

Grec, G., and Fossat, E. 1976, submitted to Astron. Astrophys.

Grec, G., Fossat, E., and Vernin, J. 1976, Astron. Astrophys., 50, 221.

Groth, E. J. 1975, Astrophys. J. Suppl., 29, 285.

Halm, J. 1922, Mon. Not. R. Astr. Soc., 82, 479.

Hart, A. B. 1954, Mon. Not. R. Astr. Soc., 114, 17.

Hart, A. B. 1956, Mon. Not. R. Astr. Soc., 116, 38.

Hill, H. A., Caudell, T. P., and Rosenwald, R. D. 1976b, The Proceedings of the Solar and Stellar Pulsation Conference, Los Alamos, New Mexico, ed. A. N. Cox and R. G. Deupree, Los Alamos Report No. LA-6544-C.

Hill, H. A., Caudell, T. P., and Rosenwald, R. D. 1977a, submitted to Astrophys. J. (Letters).

Hill, H. A., Caudell, T. P., and Rosenwald, R. D. 1977b, submitted to Astrophys. J.

Hill, H. A., Stebbins, R. T., and Brown, T. M. 1976a, Proceedings of the Fifth International Conference on Atomic Masses and Fundamental Constants, ed. J. H. Sanders and A. H. Wapstra (New York: Plenum Press), pp. 622-628.

Hill, H. A., Stebbins, R. T., and Oleson, J. R. 1975, Astrophys. J., 200, 484.

Hines, C. O. 1960, Can. J. Phys., 38, 1441.

Holweger, H., and Testerman, L. 1975, Solar Phys., 43, 271.

Howard, R. 1962, Astrophys. J., 136, 211.

Howard, R. 1967, Solar Phys., 2, 3.

Howard, R. 1971, Solar Phys., 16, 21.

Howard, R., and Harvey, J. 1970, Solar Phys., 12, 23.

Howard, R., Tanenbaum, A. S., and Wilcox, J. M. 1968, Solar Phys., 4, 286.

Huber, M. C. E., Dupree, A. K., Goldberg, L., Noyes, R. W., Parkinson, W. H., Reeves, E. M., and Withbroe, G. L. 1973, Astrophys. J., 183, 291.

Hudson, H. S., and Lindsey, C. A. 1974, Astrophys. J. (Letters), 187, L35.

Iben, I., and Mahaffy, J. 1976, Astrophys. J. (Letters), 200, L39.

Jensen, E., and Orrall, F. Q. 1963, Astrophys. J., 138, 252.

Jones, R. A., and Rense, W. A. 1970, Solar Phys., 15, 317.

Jones, W. L. 1969, Solar Phys., 7, 204.

Kahn, F. D. 1961, Astrophys. J., 134, 343.

Kahn, F. D. 1962, Astrophys. J., 135, 547.

Kalinjak, A. A., and Vassilyeva, G. J. 1971, Solar Phys., 16, 37.

Kato, S. 1966a, Astrophys. J., 143, 372.

Kato, S. 1966b, Astrophys. J., 143, 893.

Kato, S. 1966c, Astrophys. J., 144, 326.

Kato, S. 1969, Astrophys. J., 157, 827.

Kaufmann, P. 1972, Solar Phys., 23, 178.

Kleczek, J., and Kuperus, M. 1969, Solar Phys., 6, 72.

Kobrin, M. M., and Korshunov, A. I. 1972, Solar Phys., 25, 339.

Kobrin, M. M., Korshunov, A. I., and Pakhomov, V. V. 1973, Sov.-Phys. Usp., 16, 287 (translated from Usp. Fiz. Nauk, 109, 774).

Lamb, H. 1945, Hydrodynamics (New York: Dover Publications, Inc.), p. 541.

Ledoux, P. 1965, "Stellar Stability," in Stellar Structure, ed. L. H. Aller and D. B. McLaughlin, Vol. 8 of Stars and Stellar Systems, ed. G. P. Kuiper and G. M. Middlehurst (Chicago: University of Chicago Press), pp. 499-574.

Ledoux, P., and Walraven, Th. 1958, "Variable Stars," in Handbuch der Physik, Vol. 51, ed. S. Flugge (Berlin: Springer-Verlag), pp. 353-604.

Leibacher, J. 1973, paper presented at joint meeting of Commissions 12 and 36 at XVth General Assembly of the International Astronomical Union in Sydney, Australia, August, 1973.

Leibacher, J., and Stein, R. F. 1971, Astrophys. Letters, 7, 191.

Leibacher, J., and Stein, R. F. 1974, Ann. Rev. Astron. Astrophys., 12, 407.

Leighton, R. B. 1964, Astrophys. J., 140, 1547.

Leighton, R. B., Noyes, R., and Simon, G. 1962, Astrophys. J., 135, 474.

Liu, S.-Y. 1974, Astrophys. J., 189, 359.

Livingston, W., Milkey, R., and Slaughter, C. 1977, Astrophys. J., 211, 281.

Lynch, D. K. 1975, Astrophys. Letters, 16, 77.

Lynch, D. K., and Chapman, G. A. 1975, Astrophys. J., 197, 241.

McKenzie, J. F. 1971, Astron. Astrophys., 15, 450.

Meadows, A. J. 1970, Early Solar Physics (Oxford: Pergamon Press), p. 28.

Mehltretter, J. P. 1971, Solar Phys., 16, 253.

Mein, P. 1965, Comptes Rendus, 260, 1867.

Mel'nikov, O. A., Salman-Zade, R. Kh., Solonskii, Yu. A., and Khilov, E. D. 1973, Sov. Astron., 16, 1019 (translated from Astron. Zh., 49, 1275).

Monaghan, J. J. 1973, Aust. J. Phys., 26, 597.

Monaghan, J. J. 1974, Aust. J. Phys., 27, 667.

Moore, D. W., and Spiegel, E. A. 1964, Astrophys. J., 139, 48.

Moore, D. W., and Spiegel, E. A. 1966, Astrophys. J., 143, 871.

Moore, R. L. 1974, Solar Phys., 36, 321.

Moore, R. L., and Tang, F. 1975, Solar Phys., 41, 81.

Mullan, D. J. 1973, Astrophys. J., 185, 353.

Munro, R. H., and Withbroe, G. L. 1972, Astrophys. J., 176, 511.

Musman, S. 1974, Solar Phys., 36, 313.

Musman, S., and Nye, A. H. 1976a, Bull. Amer. Astr. Soc., 8, 299.

Musman, S., and Nye, A. H. 1976b, Bull. Amer. Phys. Soc., 21, 1228.

Musman, S., and Rust, D. 1970, Solar Phys., 13, 261.

Ness, N. F., Searce, C. S., and Cantarano, S. 1966, J. Geophys. Res., 71, 3305.

Noxon, J. F. 1966, Astrophys. J., 145, 400.

Noyes, R. W. 1967, in Aerodynamic Phenomena in Stellar Atmospheres, ed. R. N. Thomas, IAU Symp. No. 28, 293.

Noyes, R. W., and Hall, D. N. B. 1972, Astrophys. J. (Letters), 176, L89.

Noyes, R. W., and Leighton, R. B. 1963, Astrophys. J., 138, 631.

Oleson, J. R., Zanoni, C. A., Hill, H. A., Healy, A. W., Clayton, P. D., and Patz, D. L. 1974, Appl. Optics, 13, 206.

Orrall, F. Q. 1965, Astrophys. J., 141, 1131.

Orrall, F. Q. 1966, Astrophys. J., 143, 917.

Plaskett, H. H. 1954, Mon. Not. R. Astr. Soc., 114, 251.

Plaskett, J. S 1915, Astrophys. J., 42, 373.

Reif, R. J., and Musman, S. 1971, Solar Phys., 20, 257.

Rhodes, E. J., Jr., Ulrich, R. K., and Simon, G. W. 1976, Bull. Amer. Astr. Soc., 8, 310.

Roddier, F. 1965, Ann. d'Astrophys., 28, 463.

Roddier, F. 1966, Ann. d'Astrophys., 29, 639.

Roddier, F. 1967, Astrophys. J., 147, 1113.

Rose, W. K. 1968, Astrophys. J., 152, 245.

Rosner, R., and Vaiana, G. S. 1976, submitted to Astrophys. J.

Sawyer, C. 1974, Solar Phys., 35, 63.

Sawyer, C. 1976, J. Geophys. Res., 81, 2437.

Schatzman, E., and Souffrin, P. 1967, Ann. Rev. Astron. Astrophys., 5, 67.

Scherrer, P. H. 1976, private communication.

Scherrer, P. H. 1977, in preparation.

Schmidt, H. U., and Zirker, J. B. 1963, Astrophys. J., 138, 1310.

Scuflaire, R., Gabriel, M., Noels, A., and Boury, A. 1975, Astron. Astrophys., 45, 15.

Sentman, D. D., and Shawhan, S. D. 1974, Solar Phys., 35, 83.

Severny, A. B. 1967, Sov. Astron., 11, 383 (translated from Astron. Zh., 44, 481).

Severny, A. B., Kotov, V. A., and Tsap, T. T. 1976a, Nature, 259, 87.

Severny, A. B., Kotov, V. A., and Tsap, T. T. 1976b, paper given at IAU Meeting, Grenoble, France, Aug. 24 to Sept. 2, 1976.

Sheeley, N. R., Jr., and Bhatnagar, A. 1971a, Solar Phys., 18, 195.

Sheeley, N. R., Jr., and Bhatnagar, A. 1971b, Solar Phys., 18, 379.

Sheeley, N. R., Jr., Harvey, J. W., and Feldman, W. C. 1976, preprint.

Shibahashi, H., Osaki, Y., and Unno, W. 1975, Pub. Astr. Soc. Japan, 27, 401.

Shuter, W. L. H., and McCutcheon, W. H. 1973, Nature Phys. Sci., 241, 140.

Simon, G. W., and Leighton, R. B. 1964, Astrophys. J., 140, 1120.

Simon, M., and Shimabukuro, F. I. 1971, Astrophys. J., 168, 525.

Singleton, R. C. 1969, IEEE Trans. AU-17, p. 93.

Sivaraman, K. R. 1973, Solar Phys., 33, 333.

Snider, J. L., Eisenstein, J. P., and Otten, G. R. 1974, Solar Phys., 36, 303.

Souffrin, P. 1966, Ann. d'Astrophys., 29, 55.

Souffrin, P. 1972, Astron. Astrophys., 17, 458.

Souffrin, P., and Spiegel, E. A. 1967, Ann. d'Astrophys., 30, 985.

Spiegel, E. A. 1957, Astrophys. J., 126, 202.

Spiegel, E. A. 1964, Astrophys. J., 139, 959.

Starr, B. P., and Gilman, P. A. 1965, Astrophys. J., 141, 1119.

Stein, R. F. 1967, Solar Phys., 2, 385.

Stein, R. F., and Leibacher, J. 1969, Astrophys. Letters, 3, 95.

Stix, M. 1970, Astron. Astrophys., 4, 189.

Stix, M., and Wöhl, H. 1974, Solar Phys., 37, 63.

Tanenbaum, A. S. 1971, "A Study of the Five-Minute Oscillations, Supergranulation, and Related Phenomena in the Solar Atmosphere" (unpublished Ph.D. dissertation, Department of Physics, University of California, Berkeley).

Tanenbaum, A. S., Wilcox, J. M., Frazier, E. N., and Howard, R. 1969, Solar Phys., 9, 328.

Tanenbaum, A. S., Wilcox, J. M., and Howard, R. 1971, in Solar Magnetic Fields, ed. R. Howard, IAU Symp. No. 43, 348.

Thomas, J. H. 1972, Solar Phys., 24, 262.

Thomas, J. H., Clark, P. A., and Clark, A., Jr. 1971, Solar Phys., 16, 51.

Uchida, Y. 1965, Astrophys. J., 142, 335.

Uchida, Y. 1967, Astrophys. J., 147, 181.

Ulrich, R. K. 1970, Astrophys. J., 162, 993.

Ulrich, R. K. 1973, Nature Phys. Sci., 241, 111.

Wagner, W. J. 1976, Astrophys. J., 206, 583.

Whitaker, W. A. 1963, Astrophys. J., 137, 914.

White, O. R., and Cha, M. Y. 1973, Solar Phys., 31, 23.

Wilcox, J. M. 1968, Space Sci. Rev., 8, 255.

Wilcox, J. M., and Howard, R. 1968, Solar Phys., 5, 564.

Wolff, C. L. 1972a, Astrophys. J., 176, 833.

Wolff, C. L. 1972b, Astrophys. J. (Letters), 177, L89.

Wolff, C. L. 1973, Solar Phys., 32, 31.

Wolff, C. L. 1974a, Astrophys. J., 193, 721.

Wolff, C. L. 1974b, Astrophys. J., 194, 489.

Worden, S. P., and Simon, G. W. 1976, Astrophys. J. (Letters), 210, L163.

Worrall, G. 1972, Astrophys. J., 172, 749.

Yoshimura, H. 1971, Solar Phys., 18, 417.

Yoshimura, H., and Kato, S. 1971, Pub. Astr. Soc. Japan, 23, 57.

Yudin, O. I. 1968, Sov.-Phys. Dokl., 13, 503 (translated from Dokl. Akad. Nauk SSSR, 180, 821).

Zhugzhda, Y. D. 1972, Solar Phys., 25, 329.